THE BIOMECHANICS OF INTERMEDIATE FILAMENT-BASED MATERIALS: INSIGHTS FROM HAGFISH SLIME THREADS

by

DOUGLAS STEVEN FUDGE

B.A., Cornell University, 1991
M.A.T., Cornell University, 1992
M.Sc., The University of Guelph, 1996

A THESIS SUBMITTED IN PARTIAL FULFILMENT OF THE REQUIREMENTS FOR THE DEGREE OF

DOCTOR OF PHILOSOPHY

in

THE FACULTY OF GRADUATE STUDIES

(Department of Zoology; Faculty of Science)

We accept his thesis as conforming
to the required standard

THE UNIVERSITY OF BRITISH COLUMBIA

November 4, 2002

ABSTRACT

Intermediate filaments (IFs) provide mechanical integrity to a wide range of biomaterials, from soft epithelia to hard keratins such as nail and horn. Although much is known about the mechanical properties of IF-rich materials such as hair, the mechanical properties of individual IFs are unknown. In this thesis, I employed hagfish slime threads, which are composed almost exclusively of highly aligned IFs, as a model for exploring the mechanics of IFs both in living cells and keratinized tissues.

Experiments with hydrated slime threads suggest that IFs in cells are extremely soft, extensible, strong, and tough when compared to actin filaments and microtubules. These data support the view that the main role of IFs in cells is to provide mechanical integrity and strength. The data also suggest that IFs are likely to provide the primary passive mechanism by which cells recover from large deformations. Structural data suggest that post-yield deformation of IFs leads to an irreversible $\alpha \rightarrow \beta$ transition, which may be used by cells as a mechanosensory cue.

Tensile tests in air revealed that dehydrated IFs behave similarly to hard α-keratins in water, suggesting that one role of the hard α-keratin matrix is to maintain IFs in a dehydrated state, even when immersed in water. Recovery tests suggest that an additional role of the matrix is to permit full recovery from post-yield deformations by both inhibiting β-sheet formation and providing a restoring force in parallel to the IFs. The dramatic difference in properties between wet and dry slime threads suggests that hydrated IFs consist of soft and rigid components arranged in series. These components correspond to the terminal and coiled coil domains of the IF protein dimers, respectively. This arrangement of components is the key to understanding the remarkable mechanical versatility of IFs.

Experiments on hagfish slime revealed aspects of the slime's mechanical properties, its mechanism of formation, and some behavioral aspects of its release. Results from these experiments suggest that hagfish slime does not behave as a fibre-reinforced composite, but as an extremely dilute assemblage of protein threads and mucins that functions to protect hagfishes from gill-breathing predators.

TABLE OF CONTENTS

LIST OF TABLES

LIST OF FIGURES

ACKNOWLEDGEMENTS

I would first like to thank John Gosline for his unswerving support and enthusiasm over the past five years. John has been incredibly generous with his time and wisdom, and many of the most important ideas in this thesis came directly out of conversations with him. I feel incredibly fortunate to have been his student. I also owe a great debt to members of the Gosline Lab, who helped in numerous ways by teaching me new techniques, critiquing manuscripts, troubleshooting equipment, and even collecting animals. So special thanks go to Margo Lillie, Paul Guerette, Ken Savage, Chris Ortlepp, William Megill, Tara Law, Marvin Braun, and Mario Kasapi. I'd also like to thank the various faculty members who served on my research committee over the years and helped to shape the direction of my research: David Jones, Bill Milsom, Tom Carefoot, Bob Blake, Trish Schulte, and especially Wayne Vogl, who introduced me to the wonders of cell biology. Thanks are also in order to Elaine Humphrey and Garnet Martens for helping with all issues microscopical. Thanks to the staff of the Bamfield Marine Station who helped me collect the animals for this study, especially Joelle Harris and Nathan Webb. Thanks to Ken Chan and Agnes Lacombe from whom I always seemed to be borrowing equipment. Thanks to Kenn Gardner, who convinced me to put my thesis writing on hold to go to Grenoble with him for the x-ray diffraction experiments. Thanks also to Trevor Forsyth for helping organize the Grenoble experiments and to Christian Riekel and Manfred Burghammer for their incredible technical prowess. Thanks to the Canadian Society of Zoologists for helping to get me to Grenoble. A huge thanks goes to the Killam Foundation for supporting me financially for four years. I was fortunate to work with several undergraduate and high school students over the past five years. Scott Chiu, Nimrod Levy, Peter Harpur, and Sarah Ong all made their own contributions to this project. J.B. Heiser and Ric Martini of the Shoals Marine Lab deserve much credit and blame for introducing me to hagfish and hagfish slime. Anne Todgham, Todd Gillis, and Bev Wicks deserve huge thanks for helping collect animals at Bamfield, but especially for being great friends. Gina Ogilvie and Ian Scott also were incredibly supportive and endured countless updates on the latest exciting developments in the world of hagfish slime. I would like to thank my family, especially my parents, Ron and Marilyn Fudge, for unconditional love and support over the years. I would also like to thank my wife Esta's family, especially Linda Spalding and Michael Ondaatje for their support and generosity. Finally, I would like to thank my loving wife and friend Esta Spalding for always being there for me, and for putting up with so much. Esta deserves credit for any narrative thread that exists in this thesis, and for that matter, in my life.

If it is love that makes the world go round, then it is surely mucus and slime that facilitate its translational motion.

-Roger H. Pain (1980)

CHAPTER 1: GENERAL INTRODUCTION

Introduction to Intermediate Filaments

Since the advent of the electron microscope, cell biologists have known that the cytoplasm of eukaryotic cells is permeated by a complex network of filaments known as the cytoskeleton. Though the structure and composition of the cytoskeleton varies among cell types, most animal cells possess three types of cytoskeletal filaments: actin filaments (F-actin), microtubules, and intermediate filaments. F-actin has a diameter of about 6-7 nm and is typically most abundant near the cell cortex. Microtubules are cylindrical structures with an outer diameter of about 25 nm and typically radiate out from the nucleus toward the cell periphery. The third class of cytoskeletal filaments is intermediate in size to F-actin and microtubules, and are therefore referred to as intermediate filaments (IFs). IFs are about 10 nm in diameter, and in living cells are typically clustered around the nucleus, with filaments radiating peripherally to connect with desmosomes and hemidesmosomes (Alberts et al., 1994).

Whereas the sequences of actin and tubulin (the protein monomers for F-actin and microtubules, respectively) are highly conserved among taxa, IF proteins exhibit a rich diversity, with almost 300 IF proteins characterized to date (Weber, 1999). The human genome alone contains at least 67 IF genes (Hesse et al., 2001), and the number of unique filament types is likely far higher than this due to the ability of certain pairs (and even trios) of IF proteins to co-polymerize into competent IFs both in vitro and in vivo. At present, IF proteins are grouped into six types according to their amino acid sequence (Table 1.1). Types I and II are the acidic and basic keratin IF proteins, respectively, which form heteropolymer IFs in epithelial cells, with type I and II chains present in a 1:1 ratio. Type III IF proteins are expressed in cells of mesenchymal origin and make up vimentin, desmin, glial fibrillary acidic protein (GFAP), and peripherin IFs. Type IV IF proteins form the neurofilaments, which are abundant components of the cytoskeleton in neurons. Type V IFs, the nuclear lamins, are the only IFs that occur within the nucleus. Filaments such as nestin, synemin, and paranemin make up the Type VI IFs (Parry and Steinert, 1999).

Table 1.1. The six classes of intermediate filaments, their constituent polypeptides and tissues in which they are found.

IF Type	Component Polypeptides	Cell Types
I	acidic keratins	epithelial cells and their derivatives
II	basic keratins	epithelial cells and their derivatives
III	vimentin, desmin, GFAP, peripherin	mesenchymal cells, muscle, glial cells, peripheral neurons
IV	Neurofilaments NF-L, NF-M, and NF-H	neurons
V	Nuclear lamins A, B, and C	eukaryotic cell nuclear envelopes
VI	Nestin, synemin, paranemin	neuroepithelial stem cells

GFAP = glial fibrillary acidic protein.
NF-L, NF-M, and NF-H are the three types of neurofilaments which are classified according to their molecular weights (light, medium, and heavy).

Although the study of IF evolution is still in its infancy, some interesting patterns have begun to emerge from the deluge of sequence data that has become available in the past few years. From sequence homology, it is clear that all IF proteins evolved from a single ancestral protein. Based on the sequence of IF proteins from the most primitive animals in which they have been identified (annelids, nematodes, and mollusks), it is now believed that the ancestral IF protein resembled modern day nuclear lamins. IF proteins possess a tripartite structure, with a linear central rod domain dominated by α-helical structure flanked on either side by globular terminal domains. The sequence of the rod domain can be broken down into heptads, with hydrophobic residues occurring in positions 1 and 4 of each heptad. Like the nuclear lamins, these invertebrate IFs possess 45 heptads in their rod domain, unlike the 39 heptads found in the non-lamin IF proteins (Bovenschulte et al., 1995). These data suggest that the so-called "short-rod" IFs (i.e. types I-IV) evolved more recently. The keratin IFs (type I and II) are believed to have first appeared in the chordates, with subsequent gene duplications and divergence occurring after the separation of the vertebrates from the cephalochordates. It also appears that type III and IV IFs underwent duplication and divergence within the vertebrate lineage (Luke and Holland, 1999).

While our knowledge of IF genetics, expression, structure, and evolution has increased greatly in the past two decades, our understanding of IF function in vivo remains incomplete. Most researchers agree that the primary function of IFs is to impart mechanical integrity to cells. A mechanical role for IFs is supported by the fact that IF-rich structures (such as skin and nail) tend to be mechanically robust (Lazarides, 1980). Mouse knockout studies provide more direct evidence for a mechanical role for IFs. Deletion of some epidermal IFs has obvious effects on the structural integrity of skin, often resulting in extensive blistering (Fuchs and Cleveland, 1998). Knockout of IF genes expressed by internal epithelia result in a range of disorders, from colorectal hyperplasia to mid-gestational lethality (Baribault et al., 1994; Baribault et al., 1993). Desmin knockouts exhibit cardiomyopathy (Li et al., 1996), and neurons lacking one or more neurofilament genes exhibit reduced axonal caliber (Elder et al., 1998). While it was first reported that vimentin knockout mice display no overt pathologies (Colucci-Guyon et al., 1994), subsequent studies have demonstrated that these mice exhibit vascular (Henrion et al., 1997) and possible renal defects (Terzi et al., 1997), as well as impaired motor function believed to be caused by poor glial development in the cerebellum (Magin et al., 2000).

In spite of the all the evidence that IFs perform a mechanical role in cells and tissues, very little is known about the mechanical properties of IFs. It is tempting to assume that the properties of IF-rich structures such as nail and hair approximate the properties of individual IFs (Howard, 2001). Under this assumption, IFs would have an elastic modulus (or stiffness) of about 2 GPa, which is similar to the stiffness of both F-actin (about 2.6 GPa) (Gittes et al., 1993; Kishino and Yanagida, 1988; Tsuda et al., 1996) and microtubules (about 1.2 GPa) (Gittes et al., 1993). The only mechanical measurements that have been performed on IFs not embedded in keratinous structures have been on suspensions of IFs in vitro. Light scattering experiments have shown that desmin filaments (an IF characteristic of muscle cells) prepared in this way are surprisingly flexible in bending (Hohenadl et al., 1999), a result that is not consistent with the assumption that IFs are as stiff as F-actin or microtubules. Mechanical measurements have also been performed on entangled suspensions of IFs. These experiments demonstrate that IFs in suspension can form soft viscoelastic gels - an attribute that may have relevance for the behavior of IFs in living cells (Janmey et al., 1991; Ma et al., 1999). While knowledge of the behavior of IF gels in vitro is certainly useful, we still lack knowledge of basic IF mechanical parameters such as stiffness, strength, extensibility and toughness. One of the main goals of this thesis is to fill in these gaps in our knowledge so

that we may better understand exactly how IFs impart mechanical integrity to cells and structures such as skin, hair, and nail.

It is unavoidable that the mechanical characterization of filaments only 10 nm in diameter (or about 370 hydrogen atoms wide!) will lead to speculation about the mechanical contribution of individual proteins or even protein domains. It is therefore useful at this point to provide an overview of the proteins that make up IFs, with emphasis on their structure and assembly. All IF proteins exhibit a tripartite structure, with a central α-helical "rod" domain flanked by "head" and "tail" terminal domains (N- and C- termini, respectively). The rod domain is characterized by about 39 heptad repeats (45 in nuclear lamins and most invertebrate IF proteins), in which hydrophobic residues generally occur in positions 1 and 4 of each heptad. Such a configuration results in a stripe of hydrophobic residues that gently spirals around the α-helix. Two α-helices with heptad repeats can minimize contact of their hydrophobic residues with water by wrapping around each other in a left-handed helix known as a coiled coil. In this way IF central rod domains form coiled coil-stabilized dimers either with themselves (homodimers) or with other IF proteins (heterodimers). Consecutive heptad repeats in the rod domain occur in four regions (called 1A, 1B, 2A, 2B) interrupted by three short linker sequences (called L1, L12, L2). All IF proteins also exhibit a unique "stutter" in region 2B, in which three residues are deleted from a heptad (Parry and Steinert, 1995). See Fig. 1.1 for an illustration of the major features of IF protein primary structure.

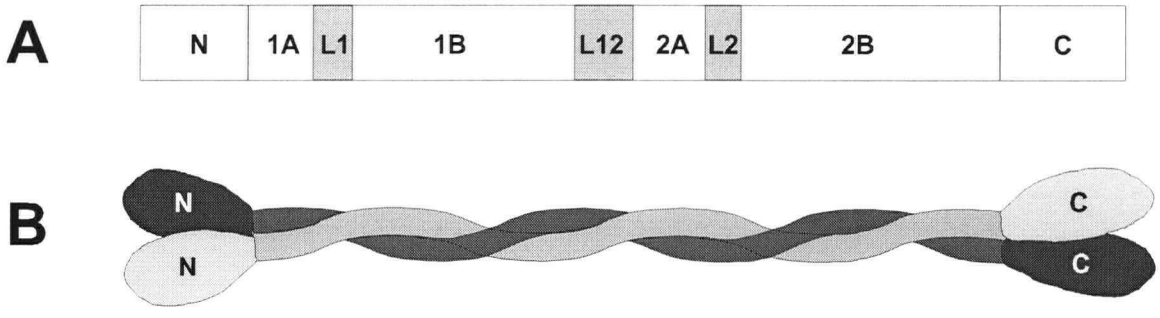

Fig. 1.1. Primary and secondary structure of intermediate filament proteins. A) All IF proteins share a tripartite structure, with an α-helical central rod domain flanked by globular N- and C-terminal domains. The rod domain consists of four regions of heptad repeats (regions 1A, 1B, 2A, and 2B) interrupted by three "linker" sequences (L1, L12, and L2). B) All IF proteins form coiled coil dimers either with themselves (homodimers) or with other IF proteins (heterodimers). In these dimers, the proteins are in axial register and parallel.

The terminal domains that flank the central rod are far less conserved in both size and in sequence, and their structure remains elusive. Terminal domains from keratin (Type I/II) IFs are best studied, and their sequences have been partitioned into three regions on each terminal domain, regions H, V, and R. Regions H1 and H2 flank the central rod domain and show the most conservation In contrast, the adjacent V1 and V2 regions are highly variable, even within individuals in a population. The structure of regions V1 and V2 are thought to consist of glycine and serine loops stabilized by stacking of tyrosine and phenylalanine R groups. Regions E1 and E2 are short basic regions that occur at the N and C termini, respectively (Parry and North, 1998).

One of the defining characteristics of IF proteins is their ability to form filaments in vitro and in vivo on the order of 10 nm in diameter (Fig. 1.2). Whereas the molecular structure of F-actin (Holmes et al., 1990) and microtubules (Nogales et al., 1999) have been worked out via x-ray crystallography, the structure of IFs is still not fully understood. It is believed that the IF cross-section corresponds to sixteen IF protein dimers (or 32 chains) oriented parallel to the filament axis. During assembly, dimers are believed to associate in an antiparallel arrangement with other dimers to form tetramers that can link end-to-end to form protofilaments. Pairs of protofilaments wrap around each other to form protofibrils, and four protofibrils are wrapped together to form an IF (Geisler et al., 1998; Heins et al., 1993; Parry and Steinert, 1995) (Fig. 1.3). One consequence of the anti-parallel arrangement of dimers into tetramers is that IFs lack polarity, in contrast to F-actin and microtubules, which have unique ends.

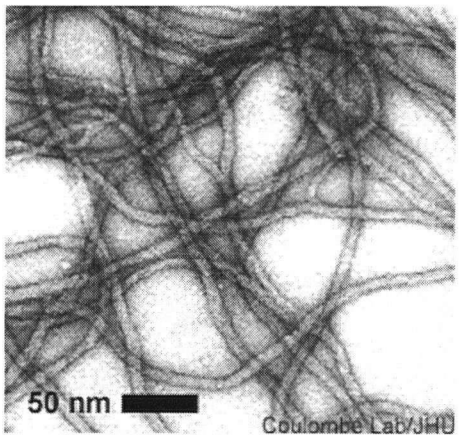

Fig. 1.2. Solubilized IF proteins spontaneously form 10 nm filaments in vitro under appropriate assembly conditions (with permission from Pierre Coulombe).

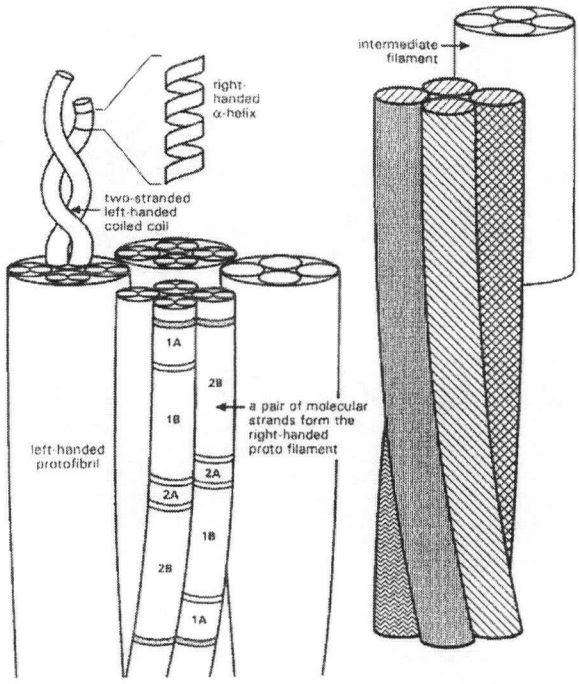

Fig. 1.3. Schematic of the possible structural hierarchy of intermediate filaments. According to this model, right handed α-helices within the rod domains of IF chains wind around each other to form left-handed, parallel coiled coil dimers. The dimers associate into anti-parallel tetramers that link end-to-end to form "protofilaments." Two protofilaments are believed to wind around each other in a left-handed helix to form a "protofibril." Finally, four protofibrils may wrap around each other in a left-handed helix to form an intact IF. From Parry and Steinert (1995), with permission.

Introduction of the model: hagfish slime threads

Although the mechanical properties of IF-based materials such as α-keratins are well described, the mechanical properties of individual IFs are not. Knowledge of the mechanical properties of IFs is essential in order to explain how IFs impart mechanical integrity to the structures in which they are found. The most obvious way to measure IF mechanical properties is to conduct a tensile test on an individual IF. Pulling on a filament only 10 nm in diameter and measuring the forces that develop is a technical challenge, but is not impossible. Indeed, tensile tests have been conducted on individual actin filaments, which are even smaller than IFs (Tsuda et al., 1996). Fortunately, a convenient model – hagfish slime threads - exists for measuring IF mechanics that does not rely on nanomanipulation and measurement of forces in the picoNewton range.

The hagfishes (class Agnatha order Cyclostomata) possess cells in their slime glands that assemble keratin-like IFs into bundles whose tensile properties can be readily measured using techniques developed for the mechanical testing of micron-sized fibers such as spider silks (Gosline et al., 1994). These bundles (hereafter referred to as "slime threads") are manufactured in cells known as gland thread cells (GTCs) (Fig. 1.4) and when unraveled from the cell are 1 to 3 μm in diameter, and several centimetres long (Downing et al., 1981b; Fernholm, 1981). The slime threads are used by the hagfish as part of their defensive strategy (Koch et al., 1991b), and are the only IFs known that are produced specifically for export (Koch et al., 1994). Slime threads are an ideal model for exploring IF mechanics, not only because of their relatively large size, but also because they consist almost exclusively of IFs (Spitzer et al., 1988) (Fig. 1.5). Indeed, no other IF-based material has such a low percentage of non-IF components. Furthermore, TEM images suggest that the IFs within slime threads exhibit high axial alignment, which appears to depend upon a scaffolding of microtubules that is present during GTC development (Downing et al., 1984).

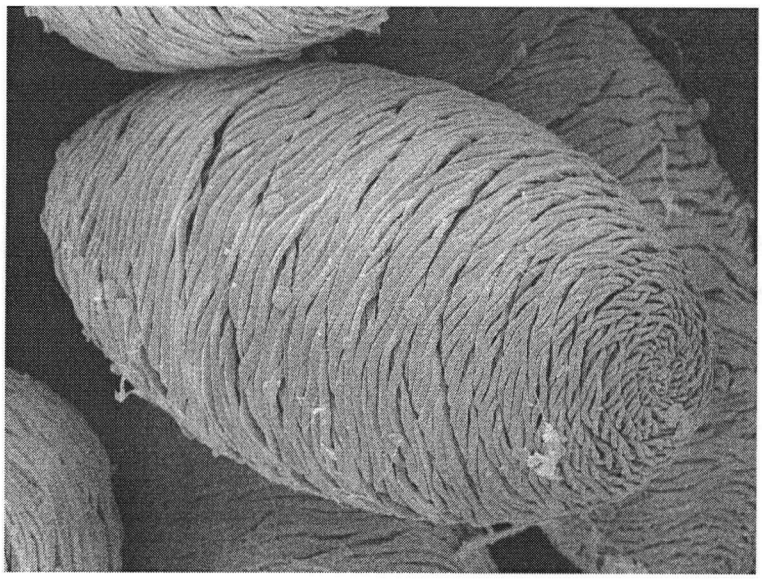

Fig. 1.4. Slime thread skeins (i.e. mature gland thread cells without their plasma membranes) from *Eptatretus stoutii*. Gland thread cells manufacture a single, continuous bundle of keratin-like IFs that eventually occupies the vast majority of the cell volume. When mature, the cell may be ejected into seawater, at which time it loses its plasma membrane, and the skein unravels and interacts with the hydrated mucin component of the slime.

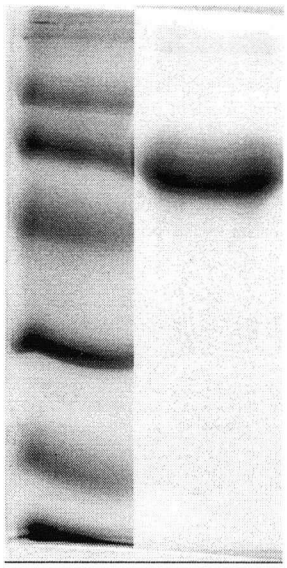

Fig. 1.5. SDS-PAGE of isolated slime thread skeins solubilized in 10 M urea (right lane). These data demonstrate that thread cells are composed almost exclusively of 67 kDa IF proteins, with very little contamination from other proteins. Left lane is molecular weight markers.

Hagfish slime IFs

The validity of using hagfish slime threads as a model for measuring the mechanical properties of intermediate filaments rests on the assumption that slime thread IFs are not exceptional in any way. Koch et al. (Koch et al., 1995; Koch et al., 1994) characterized the two proteins that make up slime thread IFs and demonstrated that they qualify for inclusion in the intermediate filament gene family as homologues of keratin (Type I and II) IF proteins. Like keratin IFs, slime thread IFs are composed of two IF proteins (named α and γ) that form coiled coil heterodimers that assemble into IFs as described above. α and γ both exhibit the characteristic tripartite IF structure, with a central α-helical heptad repeat domain flanked by two non-helical domains. Their central rod domains exhibit definable subdomains (1A, 1B, 2A, and 2B) as in other IF proteins, and region 2B possesses the distinctive "stutter" in the heptad repeat sequence that is seen in all other IF proteins. α and γ both possess high glycine and serine contents in their terminal domains - a trait they share with keratin IF proteins. Lastly, when present in equal concentrations in vitro, α and γ assemble into ~10 nm filaments that are indistinguishable from other IFs.

While it is clear that slime thread IFs resemble other IFs enough to warrant their use as an IF model, it is useful to keep in mind the differences that set them apart. IF proteins within each class of IFs tend to exhibit central rod amino acid

sequence identity of 50-90% (Koch et al., 1994), whereas identity between classes tends to be 30-35% or less (Albers and Fuchs, 1992). The central rod domains of α and γ show low sequence identity with all classes of IF proteins (~20-30%) except (curiously) the keratin IFs, with which they share no particular homology. Sequence identity between α and γ is also low (~23%), but this is not unusual between IF heteropolymers. The central rod domains of α and γ both contain unusually high amounts of threonine (13 and 10%, respectively, vs. 3-5% for other IF), although the functional significance of this is unclear. The linker segment L12 in both α and γ is 21 residues long, whereas in keratin IFs it is 16 or 17 residues (Koch et al., 1995).

In this thesis, I define the mechanical properties of slime threads under a variety of conditions that can be extrapolated to help understand the mechanics of other IF-based materials. In Chapter 2 I provide mechanical results for hydrated slime threads that illuminate the function of cytoplasmic IFs in living cells. Chapter 3 is concerned with the mechanical properties of IFs within both hard α-keratins (such as hair and nail) and soft α-keratins (such as stratum corneum - the outer layer of epidermis in vertebrates). Mechanical tests of hagfish slime fibres in air as well as slime thread swelling data provide insight into the role that IFs play in these materials. Chapter 4 provides some basic information on gland thread cells and the mechanical function of the slime threads within hagfish slime. In Chapter 5, I develop a mechanical model that elucidates how IFs can function in materials with such a huge range of mechanical properties, from soft slime to hard nails.

CHAPTER 2: MECHANICS OF HYDRATED HAGFISH SLIME THREADS: A MODEL FOR IFs IN LIVING CELLS

INTRODUCTION

While IF knockout studies have provided definitive evidence that IFs impart mechanical integrity to cells (Magin et al., 2000), exactly how they do this is unknown. Indeed, the mechanical behavior of individual IFs in vivo is poorly described, especially when compared with F-actin and microtubules, whose mechanics are relatively well studied. The mechanical properties of α-keratins such as wool have been extensively characterized (Hearle, 2000), and because IFs are the major component in these materials, it is assumed that the properties of IFs are about the same. This assumption has been accepted as reasonable because hard α-keratins have an initial stiffness ($E \approx 2$ GPa) that is similar to the other two cytoskeletal filaments, F-actin ($E = 2.5$ GPa) (Gittes et al., 1993; Kojima et al., 1994) and microtubules ($E = 1.2$ GPa) (Felgner et al., 1996; Gittes et al., 1993; Kurachi et al., 1995). In addition, the most salient feature of IF protein dimers is a coiled coil, which is a motif believed to have a stiffness of about 2 GPa (Howard, 2001). Quite simply, the mechanics of individual IFs have not been investigated because it was believed that the answers were already known. In this chapter, I use hagfish slime threads as a model for investigating the mechanical properties and function of IFs in living cells.

IFs are flexible in bending

While the above evidence suggests that IFs are as stiff as α-keratins, IFs exhibit a high flexibility in bending that is difficult to reconcile with this assumption, since bending is essentially a special case of tension and compression (on the outside and inside of the neutral axis, respectively). The evidence for the great flexibility of IFs comes from light scattering experiments (Hohenadl et al., 1999), TEM imaging (Howard, 2001), and atomic force microscopy (AFM) (Muecke and Aebi, 2002). These kinds of experiments suggest that IFs exhibit persistence lengths (L_p) on the order of 1 μm. L_p is a useful measure of a filament's flexibility, and is roughly the minimum length at which the filament ends are uncorrelated due to Brownian motion (Gittes et al., 1993). L_p can be calculated from the following parameters:

$$L_p = \frac{EI}{kT} \tag{2.1}$$

where E is the Young's modulus or stiffness, I is the second moment of area (proportional to the square of the cross-sectional area), k is Boltzmann's constant, and T is temperature. To put the low L_p of IFs in perspective, the L_p for microtubules and F-actin are about 5000 μm and 18 μm, respectively (Felgner et al., 1996; Gittes et al., 1993; Kojima et al., 1994; Kurachi et al., 1995). Note that the IF L_p is considerably smaller than F-actin's in spite of the fact that IFs have a larger radius, and L_p is proportional to the radius to the fourth power. If IFs truly have a stiffness of 2 GPa as is assumed, then Eq. 2.1 predicts that they should have an L_p of about 230 μm, or more than two orders of magnitude higher than the L_p obtained via light scattering or TEM. This paradox (i.e. IFs are stiff in tension but flexible in bending) has been explained by invoking a mechanism whereby the subfilaments within IFs are allowed to slide freely past one another during bending, much like the filaments within a rope (Bray, 2001; Hohenadl et al., 1999; Howard, 2001).

I hypothesized that the great flexibility of IFs is due simply to an inherently low tensile stiffness. Specifically, this hypothesis predicts that IFs have a tensile modulus of about 8 MPa rather than the 2 GPa assumed in the literature. While a modulus of 8 MPa is dramatically lower than the stiffness of hard α-keratins, it is quite similar to the modulus of soft keratins such as stratum corneum, which is 3 to 4 MPa. This value is remarkably close to the 8 MPa value if one considers that the IFs in soft keratins are not oriented in one direction. I tested the hypothesis that hydrated IFs have a low initial stiffness by measuring the tensile properties of hagfish slime threads, which (as I've argued in Chapter 1) are an ideal model for investigating IF mechanics.

Three models of cytoskeletal structure and function

While great strides have been made in recent years toward an understanding of how the cytoskeleton contributes to the mechanical properties of cells (Bray, 2001; Howard, 2001), a comprehensive model of cytoskeletal function continues to elude cell biologists and biophysicists. Currently three models compete for supremacy, although none of them alone can account for all the mechanical properties of living cells.

The simplest model is the Elastic Cortex/Viscous Cytosol model, in which cells are likened to rubber balloons filled with viscous fluid (Heidemann et al., 1999; Heidemann et al., 2000). In this model, a network of elastic cortical F-actin is held in tension by osmotic pressure exerted by the cytosol, which behaves essentially as a viscous fluid and possesses no solid or gel-like characteristics. The strengths

of this model are its simplicity and the fact that cortical actin does appear to behave as an elastic pre-stressed network in tension. The major weakness of this model is its assertion that the cytosol can be modeled as a fluid without any elastic properties, and its denial of cytoskeletal structure other than the F-actin cortex. Micromanipulation studies and in vivo imaging of cytoskeletal filaments suggest that cytosolic structure and mechanics are far more complex than assumed by this model (Alberts et al., 1994; Wang et al., 2001).

The Entropic Gel Network model asserts that the cytosol is a mostly elastic (as opposed to viscous) structure in which the cytoskeletal filaments form an entropic gel network. An entropic gel network is a suspension of filaments that are sufficiently long, flexible, and dynamic enough to form transient entanglements with their neighbors. These entanglements hold the network together (Maniotis et al., 1997), and deformations are resisted via an entropic mechanism whereby elongation decreases the conformational entropy of the filaments. The Entropic Gel Network model is supported by the fact that purified suspensions of cytoskeletal filaments will set into entropic gels with properties not unlike the viscoelastic properties of cytosol (Janmey et al., 1991). The main weaknesses of the model are that it denies the cytoskeletal structure suggested by TEM and in vivo confocal imaging, and is based mainly on experiments using macroscopic samples of cytoskeletal gels in vitro, which may not be relevant within the confines of a cell.

The most powerful yet controversial model is the Tensegrity model put forward by Ingber and colleagues (Ingber, 1993; Ingber and Jamieson, 1985). In this model, cells are likened to the "tensegrity" structures popularized by the architect Buckminster Fuller. In these structures, compressive struts are suspended in and opposed by a continuum of tensile filaments, an arrangement that is both stable and flexible. Tensegrity claims that in cells, F-actin and IFs form the continuum of tensile filaments, whereas microtubules act as the rigid compressive struts that keep the network from collapsing in on itself. Selective ablation of cytoskeletal filaments with optical probes or drugs support the claim that F-actin is generally loaded in tension, and microtubules in compression (Pickett-Heaps et al., 1997). Furthermore, the high stiffness of microtubules, their hollow, cylindrical structure and their long L_P suggest that microtubules have evolved to act as efficient compression-resistant struts in cells.

While tensegrity can explain an impressive suite of cell phenomena, two major weaknesses keep it from completely displacing the other two competing theories. Tensegrity's claim of integrated cytoskeletal structure predicts that cells should

exhibit "action-at-a-distance," in which a perturbation on one side of the cell has discernable consequences at the other (Heidemann et al., 2000). While certain studies have demonstrated action-at-a-distance in living cells (Helmke et al., 2000; Maniotis et al., 1997), others have not (Heidemann et al., 1999). The only way that local mechanical effects (i.e. the opposite of action-at-a-distance) could occur in cellular tensegrity structures is if cells possessed a highly compliant element, and no such element has been identified to date.

Proponents of Tensegrity are fond of building macroscopic tensegrity structures from wooden dowels (compressive struts) and rubber bands (tensile network) that they claim share many similarities with living cells. Unfortunately, no cytoskeletal filament has been identified to date with either the stiffness or extensibility of a rubber band (excluding titin molecules which only occur in muscle cells). Tensegrity models built from materials with properties akin to microtubules and F-actin (e.g. rods and filaments made from hard plastics) are not nearly as impressive, and bear no resemblance to cells. Given the prevalence of IFs in animal cells and the widespread assumptions that have been made about their mechanical properties, I reasoned that a detailed study of IF mechanics (using slime threads as a model) may explain some of the anomalous data that plague current theories of cytoskeletal mechanics.

The keratin $\alpha \leftrightarrow \beta$ transition

One of the major findings that came out of efforts to understand the molecular basis of wool mechanics is a phenomenon known as the alpha-to-beta transition (or $\alpha \leftrightarrow \beta$ transition). From x-ray diffraction data it was shown that fibrous proteins within wool exist primarily as α-helices aligned with the fiber axis (Fraser et al., 1972). X-ray data also show that stretching the fibres in steam results in a loss of α-helical structure and the creation of a new extended conformation known as a β-pleated sheet (Fig. 2.1) (Bendit, 1960). We now know that the fibrous proteins responsible for these x-ray diffraction patterns in wool are keratin IF proteins. It is interesting to note that cell biologists discovered IFs in living cells independently of researchers in the textile industry studying wool structure and mechanics. It wasn't until the late 1970s that both groups acknowledged that cytoplasmic IFs and the "microfilaments" in wool are essentially the same (Parry and Steinert, 1999). In spite of this synthesis, however, cell biologists have never investigated the possibility that cytoplasmic IFs also undergo an $\alpha \leftrightarrow \beta$ transition. Using hagfish slime threads as a model for cytoplasmic IFs, I hypothesized that IFs within cells also undergo an $\alpha \rightarrow \beta$ transition as they do in keratins. I tested this hypothesis using congo red staining

and x-ray diffraction of slime threads strained in water.

In this chapter, I provide evidence from experiments with hagfish slime threads that hydrated IFs are soft not only in bending, but also in tension. This assertion has important implications for both the mechanical function of IFs in living cells, as well as current theories of cytoskeletal mechanics. In addition I demonstrate that hydrated IFs undergo an $\alpha \leftrightarrow \beta$ transition at large strains that may serve as an important mechanosensory cue in cells.

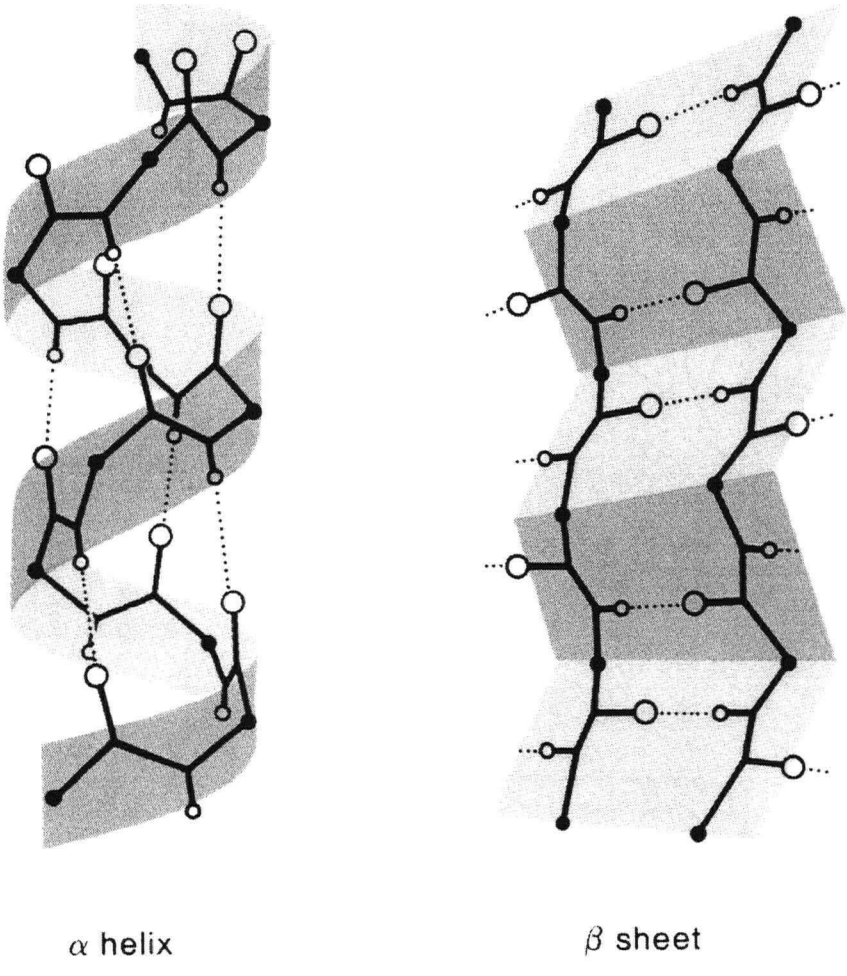

Fig. 2.1. α-helices dominate the secondary structure of intermediate filaments. When α-keratins are stretched in steam, the α-helices are disrupted, resulting in a more extended conformation known as a β-sheet, in which adjacent chains are held together via hydrogen bonds (dashed lines). From (Zubay, 1998).

MATERIALS AND METHODS

Experimental animals

Pacific hagfish (*Eptatretus stoutii*) were obtained with assistance of staff at the Bamfield Marine Station in Bamfield, British Columbia. Traps were baited with herring and set in Barkley Sound on the bottom at a depth of approximately 100 m and left overnight. Hagfish were transported back to the University of British Columbia where they were held in a 200 L aquarium of chilled seawater (34 ‰, 9 °C) in accordance with the regulations of the UBC Committee on Animal Care (protocol A2-0003).

Slime collection

Slime exudate was collected using techniques modified from Ferry (1941) and Downing et al. (1981). Hagfish were anaesthetized in a 5 L bucket of buffered anaesthetic (250 mg/ml MS-222, 500 mg/ml sodium bicarbonate) in seawater until they became unresponsive to touch. They were then placed on a dissection tray nested in ice, and a small portion of their skin was rinsed with distilled water and blotted dry. Slime exudate was expressed from slime glands in the rinsed area using mild electrical stimulation (8V, 80 Hz), which caused contraction of the skeletal muscle that encapsulates each gland (Fig. 2.2). Exudate was collected with a small spatula and transferred to a high osmolarity citrate buffer (0.9 M sodium citrate, 0.1 M PIPES, pH 6.7) modified from Downing et al. (1981). To safeguard against proteolysis, 1 mL of protease inhibitor cocktail (Sigma Aldrich product number P2714) was added to every 100 mL of stabilization buffer.

Micromechanical apparatus

Tensile properties of slime threads were measured using a modification of a glass microbeam force transducer apparatus described in (Pollak, 1991). The technique is based on the premise that extremely small tensile forces can be measured by attaching a test sample to a fine glass microbeam and monitoring the bending of the beam under a microscope as the sample is deformed. Deflections of the beam can be converted to force values using an equation derived from beam theory:

$$F = \frac{3dEI}{l^3} \qquad (2.2)$$

where F is the force, d is the deflection of the beam, E is the Young's modulus of

glass, I is the second moment of area of the beam[1], and l is the length of the beam. The linear relationship between force and deflection holds for beam deflections up to about 10% of the length, and for this reason glass microbeams were chosen so that the maximum deflection during a test was typically only 1% of the length (200 μm deflection for a 20 mm beam).

The Young's modulus of the microbeams was not measured directly, but rather using larger glass rods from which the microbeams were pulled. Glass rods of diameter 3 mm and length 50 cm were mounted horizontally in the jaws of a vise, masses hung from their ends, and the deflection measured using a mounted ruler. From the glass rod radius, length, and deflection under a given load, the elastic modulus was calculated from beam theory (Eq. 2.2) to be $5.72 \pm 0.06 \times 10^{10}$ N/m^2.

The length of the glass microbeams (i.e. the from its base to the point of attachment of the slime thread) were measured after each test to the nearest 0.02 mm using calipers. Microbeam diameter was measured to the nearest μm at the base and point of thread attachment eight times using a 15x filar micrometer eyepiece and 10x objective on a Wild compound microscope.

Individual stabilized thread cells were transferred to a seawater-filled glass-bottomed micromechanical chamber (Fig. 2.3) using a sharpened toothpick. Thread cells were allowed to partially unravel, and a 10 mm segment was mounted at one end to the glass microbeam (diameter = 50-125 μm (depending on the nature of the mechanical test), length ≈ 15 mm), and at the other to a sliding glass platform that could be moved in either direction by turning a micrometer knob. To secure threads to the microbeam, they were first wrapped around it approximately 10 times, and then fixed in place using a small amount of Cenco Softseal TackiWax (Central Scientific Company, Chicago, IL) applied with a fine needle. At the other end, threads were embedded in a 1 mm slab of TackiWax mounted on the sliding glass platform. Threads were extended (strain rate = $0.017\ s^{-1} \pm 0.0006$ (SE)) by coupling the micrometer knob to a 72-rpm motor via a flexible belt. Force was measured by monitoring the bending of the glass microbeam with a video camera mounted on a Wild light microscope using a low power (4x) objective. Deflection of the microbeam was quantified using a video dimension analyzer (VDA model 303, Instrumentation for Physiology and

[1] The diameters of the glass beams used as transducers were often not perfectly constant along their length, but rather were slightly tapered. For a uniformly tapered cylinder with radii r_1 and r_2 (where r_1 is the radius at the point where the beam is fixed, and r_2 is the radius where the sample is attached), $I = \pi/4\ (r_1^3 r_2)$ (Pollak, 1991).

Medicine, San Diego), and voltage output from the VDA was collected at 20 Hz using a National Instruments DaqPad 4060E input/output board and LabView v. 5 data collection software. Strain (change in length/resting length) was calculated from the time field using a calibration of the translation speed of the micrometer/motor set up and the resting length of the mounted thread, which was measured with calipers. The strain value inferred from the time field was corrected for the deflection of the microbeam by subtracting the deflection from the distance traveled by the traveler arm. The voltage output of the VDA was calibrated against a Bausch and Lomb calibration slide with 0.1 mm increments. The slope of the voltage vs. length calibration curve was 10.68 V/mm, with an r^2 value of 0.9998.

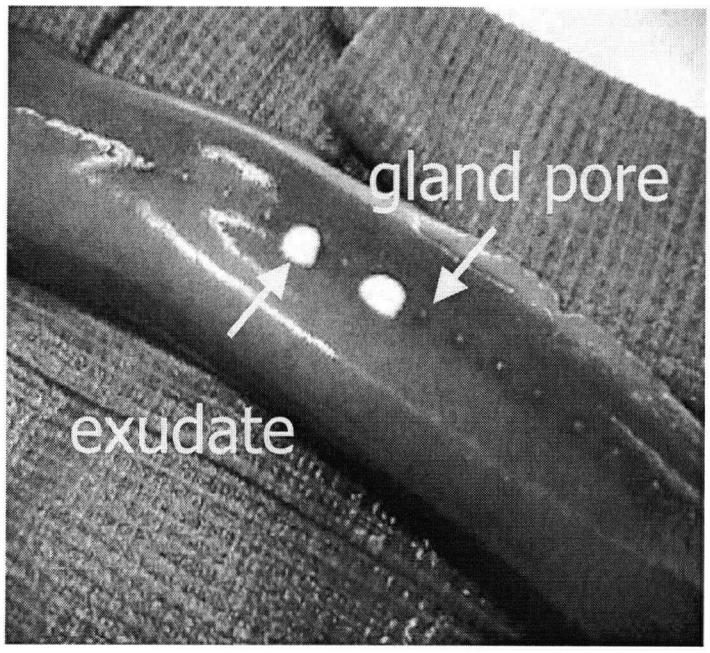

Fig. 2.2. Slime gland exudate can be collected from anaesthetized hagfish via mild electrical stimulation of the slime gland. Here two slime glands have been stimulated, resulting in expression of their contents onto the skin.

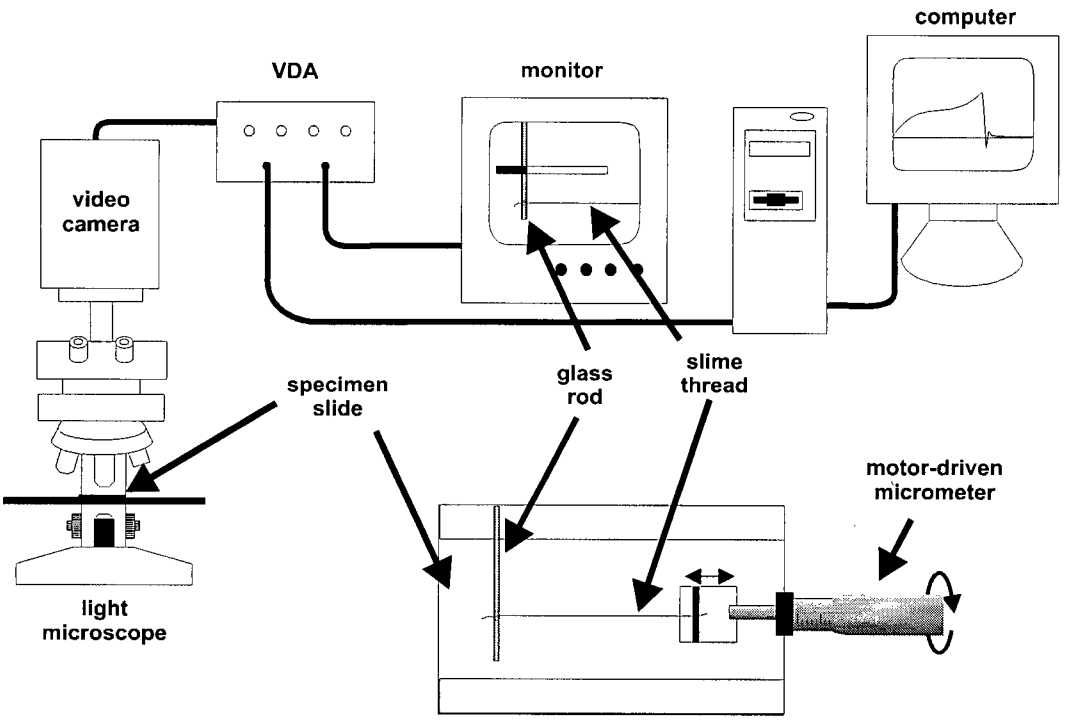

Fig. 2.3. Micromechanical testing apparatus used to measure the tensile properties of isolated lengths of hagfish slime threads in seawater. VDA = video dimension analyzer.

Thread diameter

Thread diameter was obtained for stress calculations in one of two ways depending on the nature of the tensile test. For tests in which the thread returned to its original dimensions after the test (see Fig. 2.6C), the test thread was used for the diameter measurement. At the conclusion of a test, threads were returned to their original length and mounted under a cover glass in seawater while still attached to both the glass microbeam and the sliding glass platform. For tests in which thread diameter may have been altered by the test, an adjacent piece of slime thread was snipped off the test piece before testing and stuck to the glass of the chamber using stopcock grease so that its diameter could be measured after the mechanical test was complete. Diameter was measured under high power (100x interference contrast oil immersion objective) on a Leitz orthoplan polarizing microscope (Ernst Leitz Canada, Midland, Ontario) using a 15x Filar-micrometer eyepiece. For each sample, diameter was measured six times with typical SD values of 0.15 μm for each thread.

Degree of uncertainty in force, stress, and modulus measurements

Four variables were used to calculate force generation by the slime threads during tensile tests: namely the deflection of the microbeam (measured using the VDA), the Young's modulus of glass, the radius of the microbeam (used to calculate its second moment of area (I), and measured using a filar eyepiece micrometer), and the length of the microbeam (measured using vernier calipers). From the uncertainty of each of these measurements, and the exponents to which each variable is raised, it is possible to calculate a combined uncertainty of the force measurements from the following equation (Beckwith et al., 1993):

$$\frac{uF}{F} = \sqrt{\left(\frac{3u_l}{l}\right)^2 + \left(\frac{4u_r}{r}\right)^2 + \left(\frac{u_E}{E}\right)^2 + \left(\frac{u_d}{d}\right)^2} \qquad (2.3)$$

where u_F, u_l, u_r, u_E, and u_d are the uncertainties of the force, beam length, beam radius, Young's modulus of glass, and beam deflection, respectively. The values for each of the four uncertainty terms on the right side of the equation expressed as percentages are about 2%. These combine to give an error estimate for the force measurements of about 10%. The same strategy can be applied to calculate the uncertainty in stress measurements, which were calculated from the force measurements, and the radius of the slime threads used for each test. The error in the thread radius measurements was about 10%, so using an equation analogous to Eq. 2.3 yields an estimate of the stress error of about 22%. Stiffness was calculated from stress and strain measurements, and the error for the latter was about 2%, so the combined error for thread stiffness measurements is still about 22%.

IF bending strain and persistence length

L_p was calculated using Eq. 2.1 assuming an IF diameter of 10 nm and a packing efficiency of IFs within slime threads of 90.7% (hexagonal arrangement of cylinders), with the remaining space occupied by non-load-bearing water. L_p was calculated for a temperature of 20 °C. Because the slime thread stress-strain curve is not linear (Fig. 2.5), it was necessary to gauge the range of strains that are relevant to IF bending. I accomplished this by measuring the radius of curvature from several TEM images of IFs in the literature (Hofmann et al., 1991; Porter et al., 1998; Wang et al., 2000a; Wang et al., 2000b) and estimating maximum strain from the circumference at the outer edge (i.e. the strained length), and the

circumference at the neutral axis (i.e. the unstrained length) using the following equation:

$$\varepsilon = \frac{2\pi r_o - 2\pi r_n}{2\pi r_n} \tag{2.4}$$

where r_o is the radius of curvature at the outer edge, and r_n is the radius of curvature at the neutral axis. From this analysis, I determined that the IF bends usually have a radius of curvature no smaller than 0.1 μm, which corresponds to a maximum strain of about 0.05 in a filament with a diameter of 10 nm. Because most bends had a radius of curvature considerably greater than 0.1 μm, and because 0.05 represents the strain experienced by only a small portion of a bending IF (material closer to the neutral axis experiences less strain), I chose to estimate the Young's modulus over the first 0.02 strain units. The effect of subfilament sliding on L_p was estimated using a modification of Eq. 2.1 in which the 2nd moment of area was calculated as the sum of the 2nd moments of all subfilaments, and assuming a constant total filament cross-sectional area ($A = \pi (5\text{ nm})^2$).

$$L_p = \frac{E\sum_{i=1}^{n} I}{kT} \tag{2.5}$$

where n is the number of subfilaments.

Recovery trials

For recovery trials in which the ability of slime threads to return to their original length was quantified, threads were mounted in the micromechanical testing chamber as described above with one modification. Because force data were not required for these tests, threads were mounted at both ends in a slab of TackiWax. Recovery as a function of strain was quantified by deforming threads to a set strain, holding at that strain for one minute and then slacking them off for ten minutes before the new resting length was measured.

Congo Red staining

To test for the presence of β-sheets in stretched slime threads, threads were stained with congo red (CR). CR is a dye used for the detection of amyloid fibers that creates an apple-green birefringence when it interacts with amyloid β-sheets (Puchtler et al., 1985). Threads were strained in seawater as described above, slackened and allowed to recover for one hour, after which the seawater was removed, and the threads dried onto the glass of the chamber. Threads were

rinsed with distilled water (x2) and dried before 2 hr of staining in a 1% CR in 10% ethanol solution (Knight et al., 2000). Threads were de-stained with distilled water, dried, and mounted in immersion oil for visualization under the polarizing microscope.

X-ray diffraction

X-ray diffraction of slime threads was performed at the microfocus beamline (ID13) of the European Synchrotron Radiation Facility (ESRF) in Grenoble (Riekel et al., 2000). Preliminary attempts with single slime threads using a protein crystallography microdiffractometer with a 5 μm beam (Cusack et al., 1998) revealed that the signal to noise ratio for single threads was prohibitively low, necessitating the use of thread bundles. The thread bundle experiments were performed using the scanning set-up at the ID13 beamline with a glass capillary optics providing a 3 μm beam (λ=0.976Å). No apparent radiation damage was observed at room temperature for average exposure times of 3 minutes per bundle. Bundles of approximately 50 threads at three strain levels (ε = 0, 0.6, 1.0) were mounted across 300 μm copper TEM grids from which the central 200 μm was excised, leaving only the outer rim. Bundles were secured with a small beam of 5-minute epoxy. The TEM grids were mounted on a glass tip attached to a Huber goniometer head and optically prealigned. A motorized x/y/z gantry allowed precise placement of the sample in the beam. Diffraction patterns were collected using a slow-scan MAR CCD detector.

Birefringence

Birefringence of slime threads in seawater was measured to quantify changes in molecular order and alignment induced by straining. Optical retardation (Γ) was measured using a 100x oil immersion lens on a Wild polarizing microscope with a Senarmont 1/4λ compensator. Birefringence was calculated as (Γ/d) where d is the thread diameter, which was measured using the same microscope as described above. Optical data were collected for five threads at each strain level (ε = 0, 0.25, 0.5, 1.0, 1.5).

RESULTS

Slime threads possess low initial stiffness

Tensile tests of slime threads using the most sensitive microbeam force transducer (50 μm diameter) revealed that slime threads possess a startlingly low initial stiffness of only 6.4 ± 0.9 MPa (Fig. 2.4, Table 2.1). In light of the uncertainty calculated for the initial stiffness, most if not all of the variability can be accounted for the measurement process, suggesting that there is little variation among samples. If one assumes ideal hexagonal packing of IFs in the slime threads, these initial stiffness values translates into an IF E_i of 7.0 ± 1.0 MPa. Calculation of the persistence length based on this stiffness (Eq. 2.1) yields an L_p of 0.85 ± 0.12 μm for the IFs that make up the slime threads.

Table 2.1 Mechanical properties of hagfish slime threads tested in seawater.

E_i (MPa)	Yield ε ($\Delta L/L_o$)	Yield σ (MPa)	Extensibility ($\Delta L/L_o$)	Strength (MPa)	Toughness (MJ/m^3)
6.4 ± 0.9	0.34 ± 0.01	3.2 ± 0.4	2.2 ± 0.2	180 ± 20	130 ± 20
(8)	(12)	(12)	(14)	(9)	(9)

Values are mean ± SE. Sample sizes are in parentheses.

The slime thread stress-strain curve is complex

Ultimate tests of slime threads in water revealed complex mechanical behavior, with the low initial stiffness described above giving way to extreme strain hardening (Fig. 2.5A). Fig. 2.5B is a plot of the instantaneous stiffness of a typical slime thread as a function of strain. From this analysis, at least four distinct mechanical regions can be identified. Region I is a low-stiffness initial region that terminates with a yield point at a strain of $\varepsilon \approx 0.34$. Region II is a low stiffness plateau that terminates at a strain of $\varepsilon \approx 0.7$. In region III, stiffness rises dramatically until a strain of $\varepsilon \approx 1.6$. Region IV begins with a gradual drop in stiffness at a strain of about 1.6 and continues to drop until a strain of about 2.0, after which it remains approximately constant until failure.

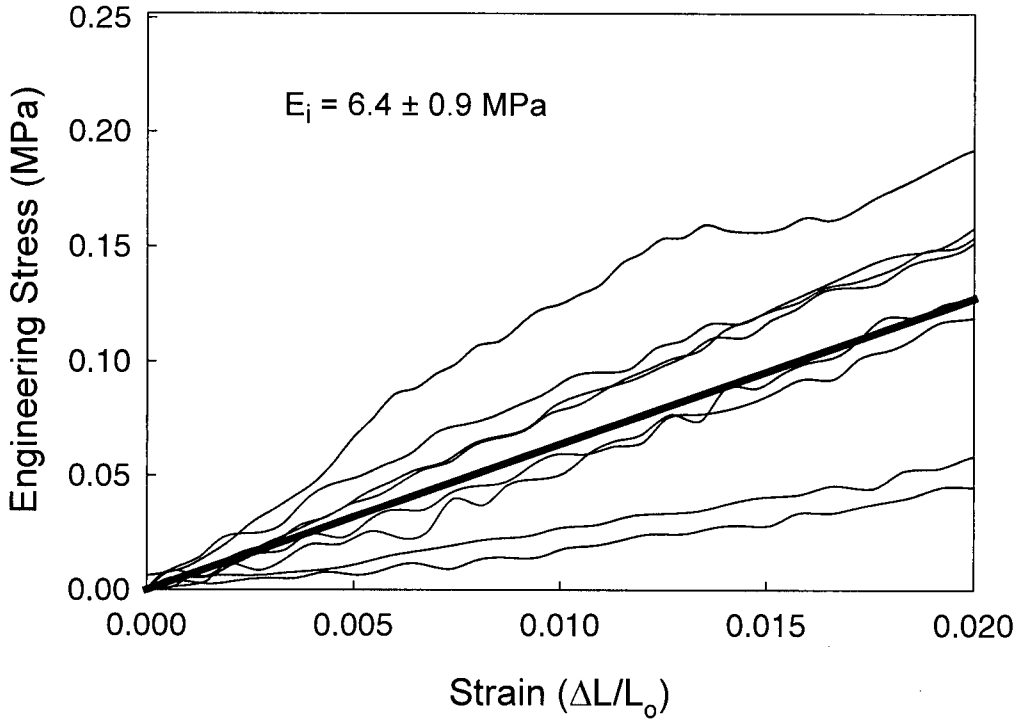

Fig. 2.4. Stress-strain curves for the eight slime threads used to measure the initial tensile stiffness (E_i). The heavy dark line is the average stiffness calculated from these data (E_i = 6.4 ± 0.9 MPa).

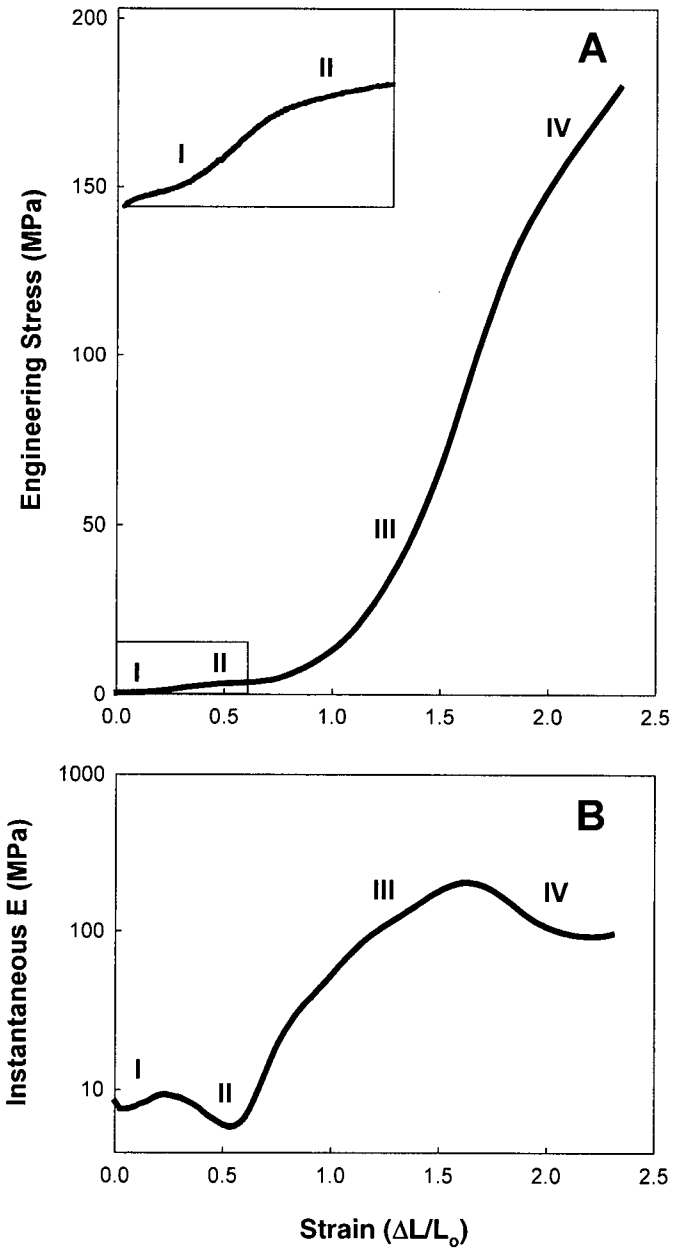

Fig. 2.5. Ultimate tensile behavior of slime threads in seawater. A) Typical stress-strain curve for slime threads strained to failure. Inset at top left is detail of stress-strain curve within box at lower left. B) Plot of the instantaneous stiffness as a function of strain. Roman numerals denote the four distinct regions of the stress-strain curve.

Deformation is elastic in region I and plastic in regions II-IV

Load cycles revealed that deformation in region I is elastic, i.e. the threads returned to their original length (Fig. 2.6A). Resilience values for load cycles in region I were typically 65%. In contrast, load cycles into region II showed much lower resilience, and did not return to their original length (Fig. 2.6B). Recovery experiments confirmed that deformation is primarily elastic in region I, and plastic in regions II-IV (Fig. 2.6C).

Slime threads undergo an $\alpha \rightarrow \beta$ transition at strains greater than 0.34

Threads strained into region I and then stained with congo red (CR) exhibited no CR birefringence. In fact CR had a chaeotropic effect on these threads, causing them to swell to several times their original diameter (Fig. 2.7A). Slime threads strained into region II displayed distinctive apple green CR-birefringence (Fig. 2.7C) and did not appear swollen. Interestingly, the degree of CR metachromasia varied strongly with the strain. In region II, threads ranged from orange-yellow to green (Fig. 2.7B, C), while in region III, threads appeared blue to blue-violet (Fig. 2.7E). Threads strained into region IV appeared faint magenta to colorless (Fig. 2.7F). High angle x-ray diffraction data also support a strain-induced $\alpha \rightarrow \beta$ transition in slime thread proteins. Bundles of unstretched threads yielded a typical "α-pattern", with a meridional reflection at 5.15 Å, and an equatorial reflection at 9.8 Å (Fig. 2.8A). Bundles of threads stretched to a strain of 1.0 yielded a typical "β-pattern," with strong equatorial reflections at 9.7 Å and 4.7 Å, and a meridional reflection at 3.3 Å (Fig. 2.8C). Bundles of threads stretched to a strain of 0.60 yielded a mixed diffraction pattern, with all of the above reflections present (Fig 2.7B). See Fig. 3.1 for examples of α and β diffraction patterns exhibited by keratins.

Slime threads are strong and tough

Ultimate tests revealed that slime threads in seawater fail at a stress of 180 ± 20 MPa and a strain of 2.2 ± 0.2 (Fig. 2.5, Table 2.1). Their modest failure stress combined with their high ultimate strain combine to give them an extremely high energy to break (or toughness) of 130 ± 20 MJ/m^3 (Table 2.1).

Slime thread birefringence increases linearly with strain

Birefringence of slime threads increased linearly with strain ($B = 0.0074\varepsilon + 0.0043$, $r^2 = 0.96$), and showed no correspondence with any of the four mechanical regimes described above (Fig. 2.9).

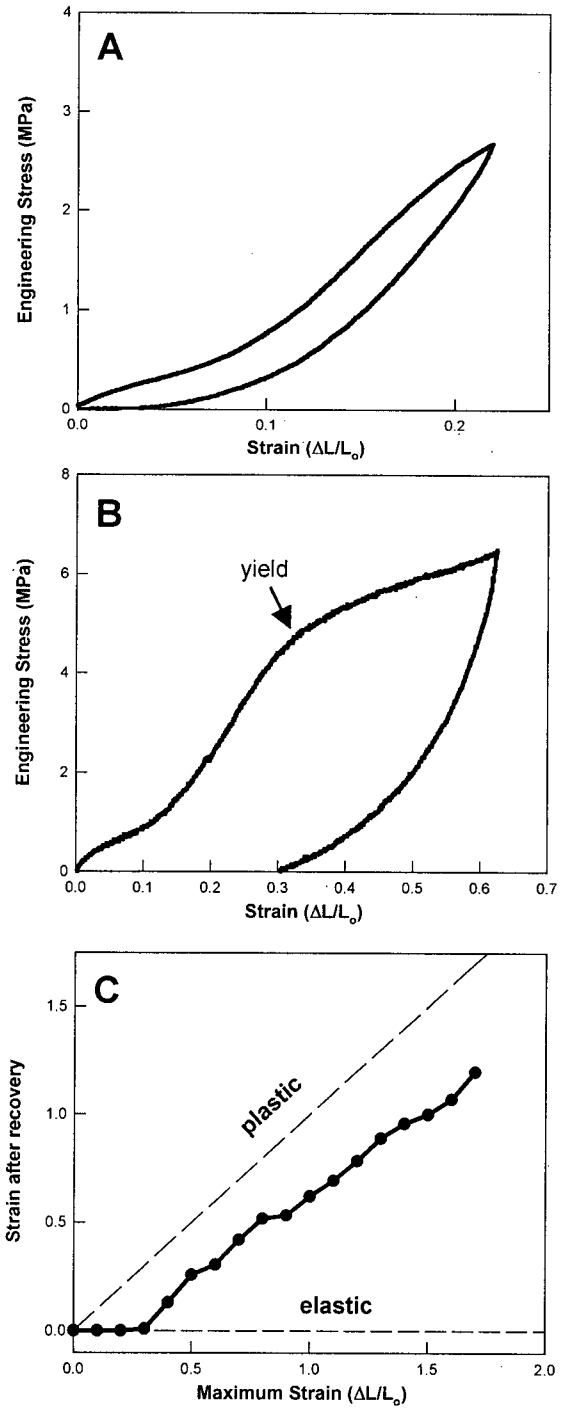

Fig. 2.6. Recovery behavior of slime threads in seawater. A) Load cycle in region I, showing completely reversible deformation. B) Load cycle into region II, showing that deformation past the yield point is mostly plastic. C) Results from trials in which threads were extended to a given strain, held, and allowed to recover. Note that deformation is elastic up to a strain of 0.35, and plastic thereafter.

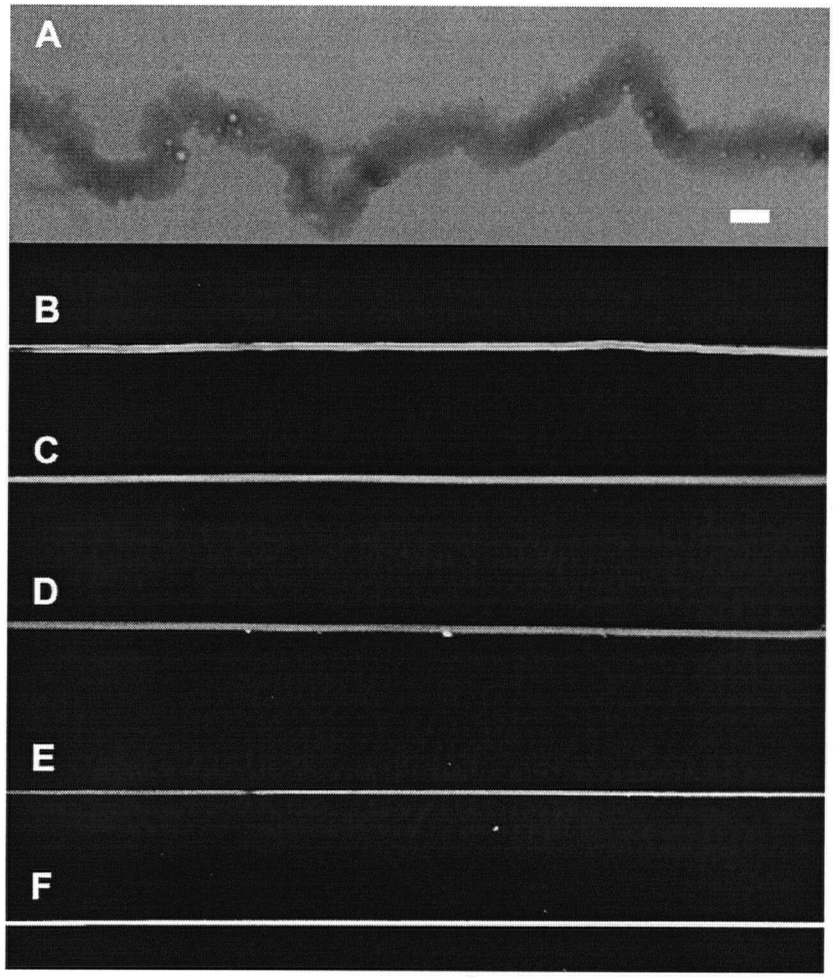

Fig. 2.7. CR staining of slime threads after straining in seawater. A) Unstrained threads and threads extended to $\varepsilon < 0.35$ appeared grossly swollen after CR staining and lost their mechanical integrity. B-F). Threads stained with CR after extension to $\varepsilon > 0.35$ retained their mechanical integrity, and displayed increasing metachromasia as strain increased. Threads appeared orange-yellow when strained to $\varepsilon = 0.35$ (B), green when strained to $\varepsilon = 0.50$, blue at $\varepsilon = 0.75$ (D), blue-violet at $\varepsilon = 1.0$ (E), and pale magenta to colorless at $\varepsilon = 1.50$ (F). Scale bar = 10 μm.

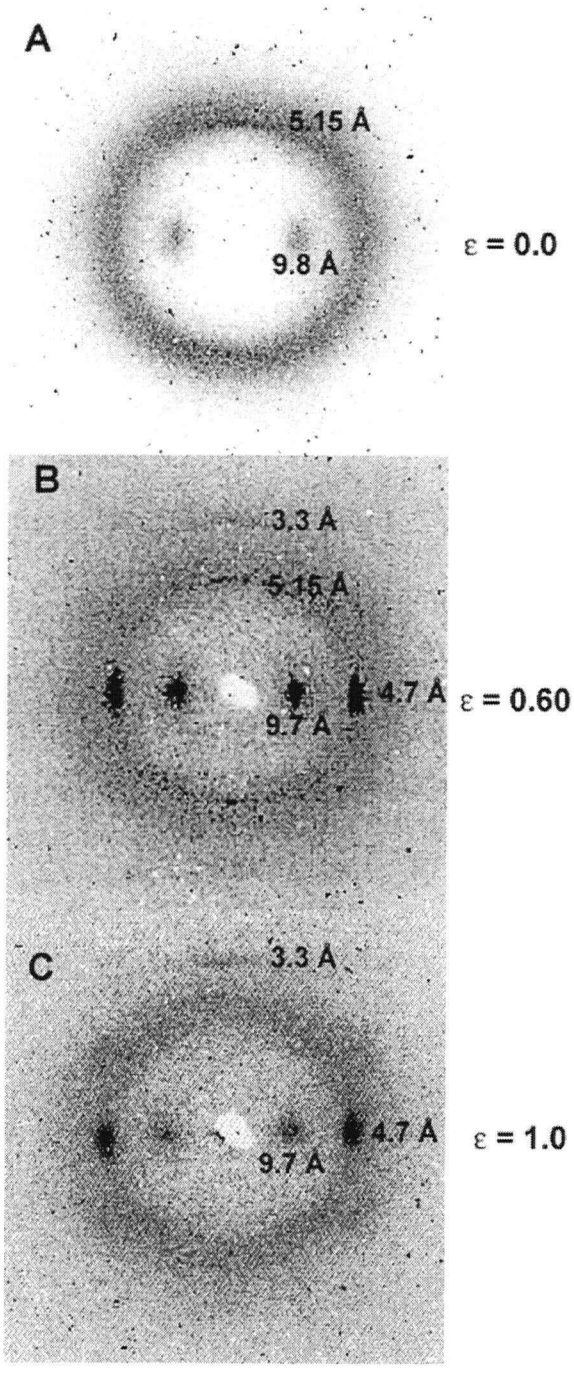

Fig. 2.8. X-ray diffraction patterns for slime thread bundles strained in seawater. A) Unstrained threads exhibited a typical "α-pattern," whereas threads extended to a strain of 1.0 exhibited a typical "β-pattern" (C). Thread extended to a strain of 0.60 exhibited a mixed pattern, suggesting the presence of both α-helix and β-sheet structure (B). Diffraction maxima (dark spots) are labeled according to the molecular spacings (in Angstroms, Å) to which they correspond.

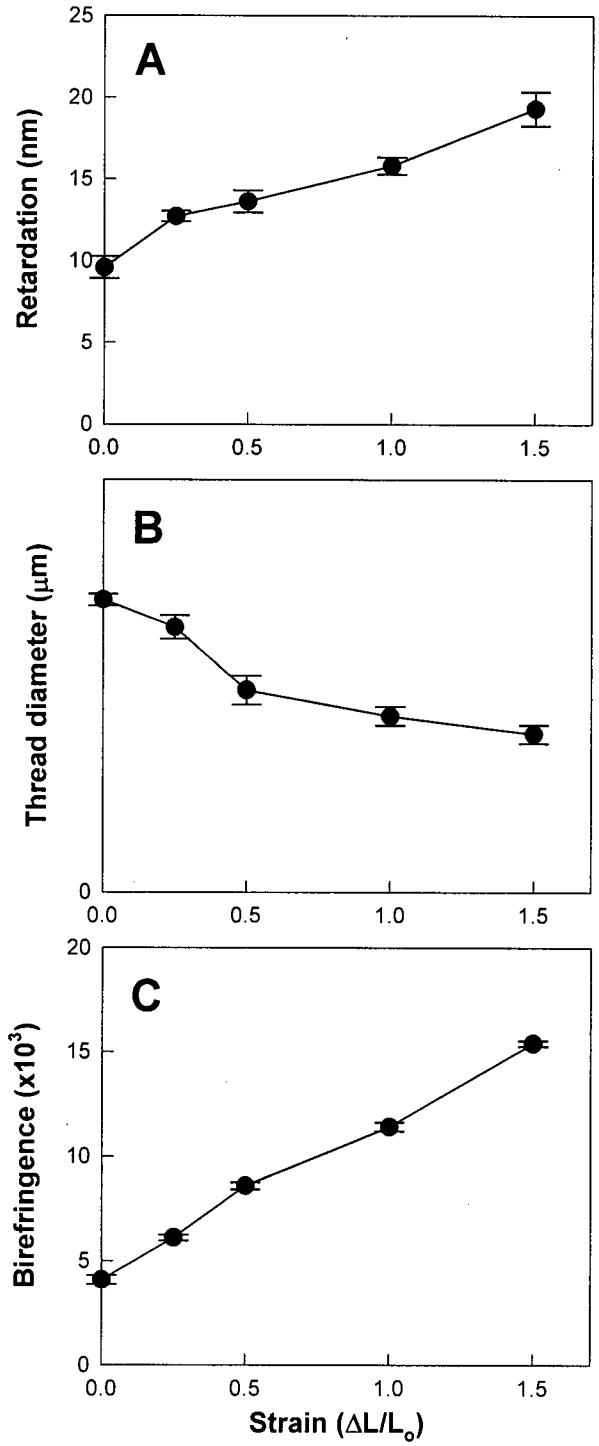

Fig. 2.9. Optical properties of slime threads in seawater as a function of strain. A) Optical retardation vs. strain. B) Average thread diameter vs. strain. C) Thread birefringence vs. strain.

DISCUSSION

The results presented in this chapter support both hypotheses regarding IF structure and mechanics. The low initial stiffness of slime threads is consistent with the hypothesis that IFs are flexible not only in bending, but also in tension. In addition, congo red and x-ray diffraction data from stretched slime threads are consistent with the hypothesis that IFs in cells undergo an $\alpha \leftrightarrow \beta$ transition.

Hagfish slime threads are a good model for investigating IF mechanics

One of the major assumptions of this thesis is that the tensile properties of hagfish slime threads are indistinguishable from the properties of their constituent IFs (with small differences due to the fact that about 10% of thread volume is taken up by water between the IFs). Because IFs within the thread are not continuous from end to end (Downing et al., 1984), this assumption is only valid if stress-transfer among IFs within the threads is effective (so that straining of the threads results in straining of the IFs), and the IFs are long enough that stress transfer occurs over only a small fraction of IF length. If straining of the threads merely results in frictional sliding of the IFs past one another, then the model is clearly invalid. The elastic nature of deformation in region I (depicted in Figs. 2.6A, B) rules out the possibility of inter-IF frictional sliding, at least at these strains. In regions II and III, deformation is not reversible, but most of the plastic deformation can be accounted for by an $\alpha \rightarrow \beta$ transition rather than inter-IF sliding. Furthermore, if IFs within slime threads are as long as IFs in cells, then they have an aspect ratio of about 10^3 (10 μm long/10 nm wide). Such a high aspect ratio should insure that stress transfer occurs over a small fraction of IF length, so that the properties of the threads will reasonably approximate the properties of the IFs.

IFs are flexible because of their low elastic modulus

Previous researchers have invoked the sliding of subfilaments within IFs to explain how IFs could be flexible in bending yet stiff in tension. My data indicate that IFs are over 200 times less stiff in tension than previously assumed, which simply abolishes the need to invoke subfilament sliding. Fig. 2.10 provides a more quantitative illustration of this point, in which L_p is plotted as a function of the number of freely sliding subfilaments within an IF. Using my measured value for the elastic modulus of IFs, and assuming no subfilament sliding within IFs during bending, the predicted L_p is 0.85 μm (Fig. 2.10A), which is consistent with values based on light scattering and TEM measurements (Hohenadl et al.,

1999; Howard, 2001). As the number of freely sliding subfilaments increases, L_p departs more and more from measured values. Furthermore, if L_p is calculated assuming that IFs are as stiff as keratins (Fig. 2.10B), even the most extreme case of subfilament sliding (16 independent filaments composed of dimers joined end to end) predicts an L_p of about 15 μm, which is more than an order of magnitude larger than measured values. The most parsimonious explanation therefore is that IFs are flexible in bending because of their low elastic modulus, and not because of subfilament sliding.

IFs are mechanically distinct from F-actin and microtubules

The initial tensile modulus I report here for IFs is dramatically lower than for the other two cytoskeletal filaments, F-actin (about 300 times lower) and microtubules (about 150 times lower). My results also suggest that IFs are far more extensible, with strains up to 0.34 being fully recoverable (i.e. the thread returns to its original length). This kind of extensibility is exceptional compared to F-actin and microtubules, which will break or yield at strains on the order of 0.01 (Kishino and Yanagida, 1988; Tsuda et al., 1996). High IF extensibility is consistent with TEM images of IFs exhibiting tight bends that simply would not be possible in F-actin or microtubules. In one particularly tight turn (radius of curvature of neutral axis = 17 nm) made by a vimentin filament (Hofmann et al., 1991), the material on the outside of the IF experiences a strain of about 0.30. These results suggest that IFs perform a mechanical role in cells that is distinct from F-actin, the other tension-bearing element in the cytoskeleton (Ingber, 1993). Namely, IFs can stretch to accommodate large cell deformations brought on by external or internal loads and passively return the cell to its original shape when the load is removed.

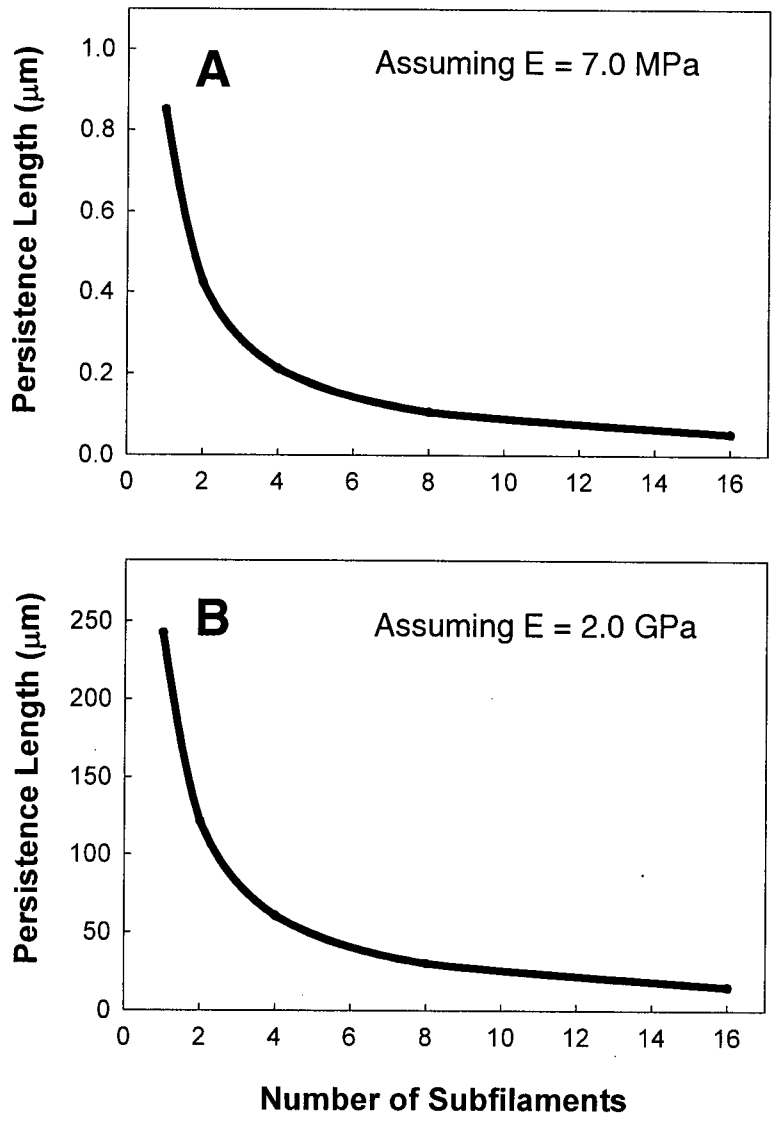

Fig. 2.10. The effect of subfilament sliding on the persistence length of IFs assuming a Young's modulus of 7.0 MPa (A) and 2 GPa (B). Persistence length was calculated assuming an IF diameter of 10 nm for the case of 1 subfilament, and holding the total cross-sectional area constant for all other cases. Note that under the assumption that IFs are as stiff as keratins, even the maximum amount of subfilament sliding predicts a persistence length an order of magnitude higher than measured values.

IFs may form entropic gels in cells

The low IF L_p (0.85 μm) relative to their typical length in cells (10-20 μm) suggests that networks of cytoplasmic IFs are capable of forming entropic gels within the confines of a cell (Gittes et al., 1993). If IFs do indeed form entropic gel networks in the cytoplasm, their overall contribution to cell mechanics will be extremely strain dependent. At low cell strains, IFs may form a soft entropic gel. As strain increases, the stiffness of the IF network will increase due to progressive alignment of IFs in the gel. At higher strains, more IFs will be pulled taut and will contribute to cell stiffness via direct longitudinal straining. Stiffness will continue to rise due to the recruitment of more and more IFs into tension, and because of the approximate J-shape of the IF stress-strain curve in region I (Fig. 2.6B). In this way, cytoplasmic IFs may be responsible for both strain hardening and elasticity in IF-reinforced cells and tissues.

It is of course possible that IFs in cells are held in significant tension, which would make the gel entropy component of their contribution to cell mechanics less significant. Following this line of reasoning leads to the possibility that cells modulate their stiffness by changing the degree of pre-strain in the IF network. Another factor that will affect the ability of IFs to form competent gels in the cytoplasm is their degree of bundling. Bundling of IFs into a cable could increase the persistence length of the cables to the point that they no longer form entropic gels. In the case of keratin IFs, bundling is promoted in physiological solutions, and may represent the natural state of keratin IFs in vivo (Bousquet and Coulombe, 1996; Bousquet et al., 2001; Yamada et al., 2002). Keratin IFs may therefore impart stiffness to epidermal cells less by entropic mechanisms, and more via direct longitudinal straining of IF bundles.

IFs bridge the gap between Tensegrity and Gel Entropy theories

The properties of cytoplasmic IFs described above remarkably strengthen both the Entropic Gel Network and Tensegrity theories of cytoskeletal mechanics. One of the major weaknesses of the former is that in order to make a competent gel, filaments must generally be longer than their persistence length (Gittes et al., 1993). It is therefore unlikely that F-actin (typical length = 1 μm, L_p = 18 μm, length:L_p ratio = 0.05) or microtubules (typical length 10-20 μm, L_p = 5000 mm, length:L_p ratio = 0.003) could form competent gels within cells. IFs, however, with their length:L_p ratio of about 15 (typical length = 10-20, L_p = 0.85 μm), can behave as entropic gels in cells. Thus, if the cytosol behaves as an entropic gel, IFs are likely to be the most important contributors.

As indicated in the Introduction, the survival of Tensegrity theory as a viable model of cell structure and mechanics hinges on the discovery of a compliant (i.e. low stiffness) structural element within cells. Without a compliant element, cellular tensegrity structures would exhibit only limited deformability, and certainly would not allow for local deformations. The mechanical data presented in this chapter suggest that IFs may be the compliant element predicted by Tensegrity. With an initial stiffness about 200 times lower than the other major cytoskeletal filaments, and an ability to deform elastically to relatively large strains, IFs would not only lend considerable deformability to cellular tensegrity structures, but could also allow for local effects. In light of the above analysis, cells may be best described as lying somewhere in the middle on a Gel Entropy to Tensegrity continuum, with IFs behaving as entropic gels at low strains, and tensegrity structures at higher strains.

Elastomeric IF terminal domains dominate the low strain behavior of IFs

The low initial tensile modulus and high elasticity of hagfish slime threads strongly suggest that entropic mechanisms govern their low strain mechanical behavior. Entropic elasticity requires conformational freedom, but it is not at first obvious where within the threads this conformational freedom resides. From the analysis in the above sections, it is clear that IFs themselves can generate entropic elasticity within entangled gel networks. However, it is unlikely that this attribute of IFs can account for the 6.4 MPa initial stiffness of slime threads. IF networks with an IF concentration of 1-2 mg/mL are capable of generating shear moduli on the order of 1 Pa (Janmey et al., 1991). If the concentration of IFs within slime threads is about 1000 times greater, then such a concentrated IF gel could generate a shear modulus on the order of 1 kPa, which is still more than three orders of magnitude lower than the modulus of slime threads. Such a mechanism is also unlikely given the fact that TEM data suggest that the IFs within slime threads are highly axially aligned (Downing et al., 1984), and do not appear to possess conformational freedom.

Another possibility is that protofibrils, protofilaments, or coiled coils within the IFs give rise to the entropic elasticity. According to this hypothesis, these structures within the IF possess conformational freedom, and the initial modulus is governed by the decrease in entropy caused by straightening them out. Such a mechanism predicts that IF sub-filaments, and therefore coiled coils within unstretched slime threads should exhibit a wide range of orientations as a result of their conformational freedom. The x-ray diffraction data contradict this prediction, however, and demonstrate that the coiled coils within unstretched

slime threads exhibit high axial alignment (Fig. 2.8A).

If the IFs themselves nor the subfilaments are the source of the entropic elasticity, this leaves the terminal domains as the last place where the entropic elasticity can reside. According to this model, the terminal domain protein chains behave as elastomers in series with much stiffer coiled coils. If we assume that the dimer is the functional unit of IF mechanics and has the same mechanical behavior as the IFs, it is possible to develop a model that allows us to estimate the average tensile modulus of the terminal domains in region I (Fig. 2.11). First we assume reasonable values for the coiled coil stiffness (2 GPa) (Howard, 2001), and the linear dimensions of the coiled coil (46.2 nm) (Parry and Steinert, 1999) and terminal domains (10.5 nm for sum of head and tail length)[2]. We can then impose a hypothetical stress on the dimer – in this case the stress at the end of the region I, or the yield stress (σ_{yield} = 3.5 MPa). By assuming that the coiled coil and terminal domains are in series and possess similar cross-sectional areas, we can calculate the strain that this stress will cause in the coiled coil (ε_{cc} = 0.002). From the stress-strain behavior of slime threads in water, we also know the yield strain of the dimers (ε_{IF} = 0.34). Using the relative linear proportions of the coiled coil and terminal domains, we can calculate the strain that must occur in the terminal domains in order to give an overall IF strain of 0.34, which is ε_{TD} = 1.8. Knowing the stress and strain for the terminal domains allows us to calculate the average stiffness of these regions, $E_{TD} = \sigma_{TD}/\varepsilon_{TD}$ = 3.5 MPa/1.8 ≈ 2 MPa.

Such low stiffness and high extensibility are consistent with the terminal domains behaving elastomerically. This conclusion is supported by the approximate J-shape of the stress-strain curve in region I (Fig. 2.6B) as well as the reversible nature of deformation in this region (Fig. 2.6A, C). Furthermore, in spite of significant effort, the structure of IF terminal domains remains elusive (Parry and Steinert, 1999; Strelkov et al., 2001). The inability to define the structure of these domains may be due to the fact that they are elastomeric and therefore not confined to one conformation.

[2]These dimensions were calculated by assuming that the terminal domains are ellipsoid in shape, with a length that is twice the width and depth. Terminal domain volume was calculated by inferring their mass from published hagfish slime IF sequence (Koch et al. 1995) and assuming a density of 1.38 g/cm^3.

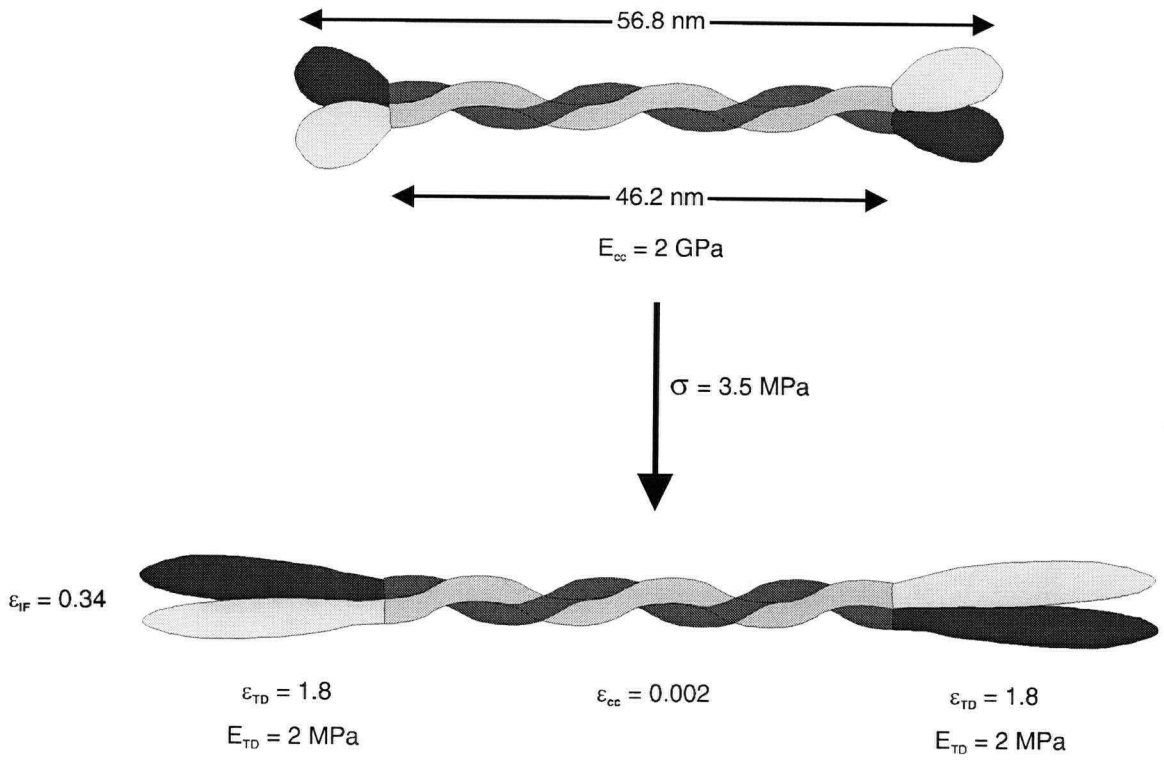

Fig. 2.11. Proposed mechanical behavior of IF dimers in mechanical region I. Assumptions of the model and flow of logic for the analysis are described in the text. The model suggests that in region I, the vast majority of the deformation occurs in highly extensible and low-stiffness terminal domains in series with stiff coiled coils.

IF diversity may reflect mechanical diversity

Compared with the proteins that make up F-actin and microtubules, IF proteins are a diverse group, with the terminal domains accounting for most of the sequence diversity (Weber, 1999). While the differences among terminal domains may correspond to differences in the assembly properties of IFs, or their ability to interact with each other or other proteins (Fuchs and Cleveland, 1998), my results suggest that differences among terminal domains may correspond to differences in the intrinsic mechanical properties of IFs, namely their elastic modulus (and therefore L_P) and extensibility. Indeed, differences in the viscoelastic properties of gels made from various IFs have been demonstrated (Bousquet et al., 2001; Hofmann and Franke, 1997; Janmey et al., 1991). If IF diversity corresponds to mechanical diversity, then tissue- and development-dependent IF expression

may represent a tuning of the mechanical properties of cells to the loads they are likely to experience.

The α→β transition in cytoplasmic IFs is irreversible

In α-keratins, the α↔β transition is a reversible process, with β-sheets reverting to α-helices viscoelastically after a load is removed. In contrast, the α→β transition in slime threads (and therefore cytoplasmic IFs) is not reversible (Figs. 2.6B, C). One implication of this fact is that the protein matrix in α-keratins likely provides a restoring force that acts mechanically in parallel with the IFs in these structures. This concept will be explored in more detail in Chapter 3. In living cells, the implication is that IFs extended past the yield strain will not return to their original length. If IFs are primarily responsible for cell elasticity at high strains, then it follows that the cell also will not return to its original shape after the load is removed. Cell deformations large enough to plastically deform IFs may be rare, but if such an event did occur, the conformational change that IFs undergo could be used by cells as a cue that cytoskeletal integrity has been compromised. Specifically, the appearance of stable β-sheets within IFs may trigger cellular programs of cytoskeletal repair or even apoptosis, depending on the severity of the damage.

Molecular mechanics of cytoplasmic IFs

By synthesizing mechanical, congo red staining, and x-ray diffraction data with knowledge of IF protein and subfilament architecture, it is possible to provide a reasonable account of the molecular events that underlie the mechanical behavior of cytoplasmic IFs described in this chapter (Fig. 2.12). The following model is given under the assumption that coiled coil IF protein dimers are the functional units of IFs and possess the same properties as all higher order structures up to the IFs themselves. I) The low-modulus elastic behavior of region I can be attributed to the presence of elastomeric terminal domains in series with much stiffer coiled coils. By the end of region I, terminal domain strain is approximately 1.8. II) In region II the stress is high enough to begin to extend α-helical domains in the coiled coils into β-strands. α-helices are extended in this region at a fairly constant stress, as they are in the α-keratin "yield region" (Feughelman, 1987) By the end of region II, coiled coils have been extended to a strain of about 0.4. III) In region III, α-helices become more and more difficult to disrupt, causing a rise of both the stress and stiffness in this region. This result is consistent with so-called "series-zone" models of IF mechanics developed by

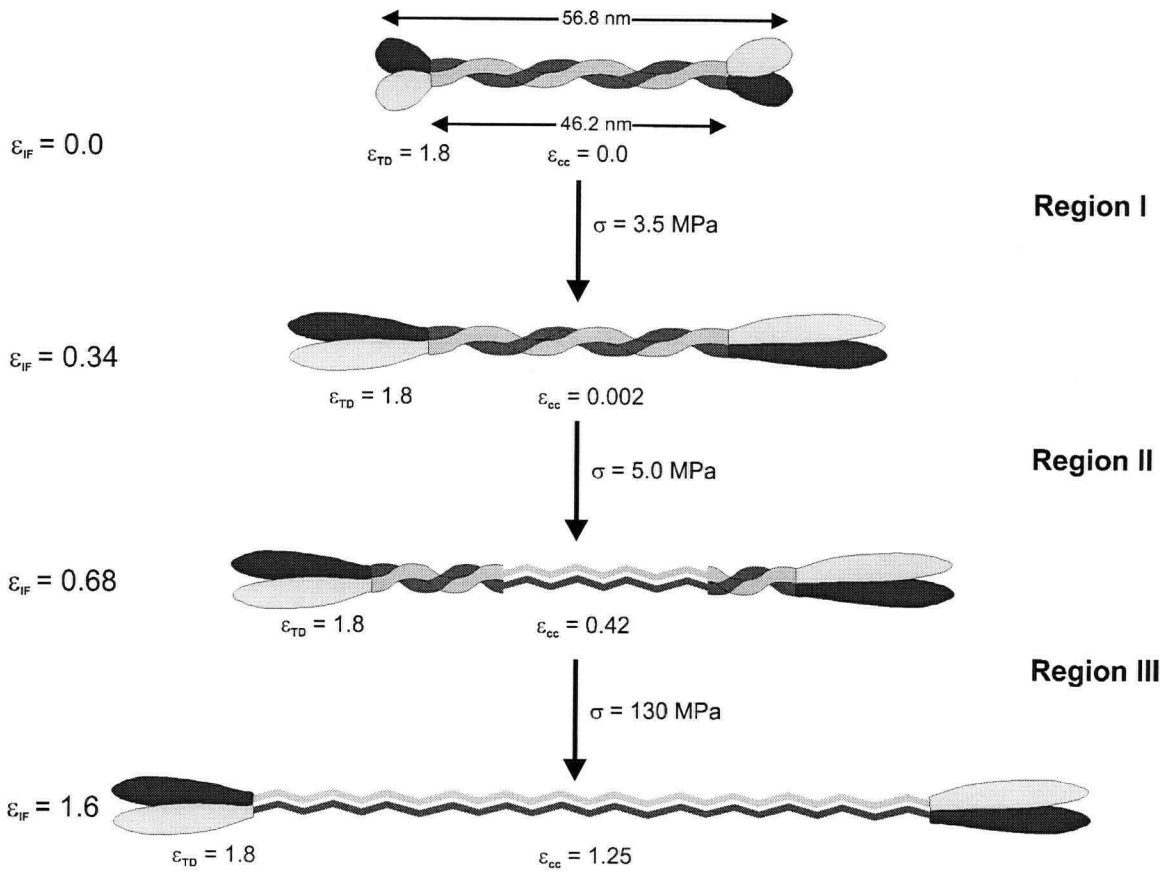

Fig. 2.12. Schematic of the proposed mechanical behavior of IF dimers in regions I-III. In region I, deformation occurs almost exclusively in the terminal domains. In region II, α-helices within the coiled coil motif begin to extend into β-sheets (denoted by the crimped lines). By the end of region III, all of the coiled coil α-helices have been extended to β-sheets. Note that this simple cartoon does not take into account the twists in the coiled coil which must somehow be relieved if the resulting β-sheets lack any helical character as depicted in the cartoon.

Feughelman (1979) and Wortmann and Zahn (1994), which claim that the stress at which α-helices are disrupted is not the same for the entire IF coiled coil. By the end of region III, coiled coils have been extended to their maximum theoretical strain of about 1.25. According to the model developed in Fig 2.12, the α→β transition should be complete by a strain of 1.4. The fact that it actually doesn't occur until a strain of 1.6 suggests that at these high stresses, some frictional sliding is occurring within and/or among the IFs. IV) At the end of region III, β-sheet and β-sheet crystal content are at their highest. Region IV therefore arises from the straining, slippage, and ultimate rupture of β-sheets and β-sheet crystals.

CONCLUSIONS

Experiments with slime threads suggest that intermediate filaments in water differ dramatically from hard α-keratins in their mechanical properties. Their low initial stiffness translates into an IF persistence length of 0.85 μm. These results confirm the low persistence lengths reported for IFs from light scattering, AFM, and TEM data, and do away with the need to invoke sub-filament sliding within IFs during bending. The low persistence length also suggests that IFs form entropic gels within cells. Unlike F-actin and microtubules, which are relatively rigid, IFs can extend reversibly up to strains of 0.34, suggesting that IFs could represent the stretchy tensile elements predicted by Tensegrity theory. At strains greater than 0.34, IF proteins undergo an irreversible α→β transition as suggested by congo red staining and x-ray diffraction. The appearance of β-sheet structure in cytoplasmic IFs after severe cell deformations may play a role in the onset of programs of cellular repair or even apoptosis. Lastly, the high strength and toughness of IFs helps explain why IF-deficient cells and tissues often exhibit mechanical fragility.

CHAPTER 3: HYDRATION EFFECTS ON SLIME THREAD MECHANICS: IMPLICATIONS FOR IFS IN α-KERATINS

INTRODUCTION

In this chapter, I use the hagfish slime thread model to illuminate the function of IFs within a vertebrate biomaterial known as keratin. The word "keratin" can be used to describe a group of materials, a type of IF, as well as individual proteins. From a biomaterials standpoint, *keratins* are insoluble, composite materials of epidermal origin in which fibrous proteins are embedded in an amorphous protein matrix (Fraser et al., 1972). Hair, nail, scale, horn, hoof, feather, and the outer layer of skin are all considered keratins. *Keratin IFs* are IFs within cells of ectodermal origin that consist of type I and type II IF proteins. Two types of keratin IFs are now recognized - those that are expressed in hard keratinizing tissues such as hair and nail, called *trichocyte* keratin IFs, and those that are expressed in epithelia, called *cytokeratin* IFs. The former are heteropolymers made up of type Ia and type IIa IF protein chains, whereas the latter are made up of type Ib and IIb chains (Langbein et al., 1999; Parry and Steinert, 1999). Lastly, in the textile literature, *keratin* can be used to describe any of the dozens of proteins that can be found within keratins, including both IF proteins and non-IF "matrix" proteins. In this thesis, the term *keratin* on its own will always refer to the composite material. Other uses of the word will always be followed by a descriptive term or terms as in *keratin IF* or *keratin matrix protein*.

Keratins make up important structures in terrestrial vertebrates

In vertebrates, the integument consists of two major layers, the dermis, which is of mesodermal origin, and the epidermis, which is of ectodermal origin (Fraser et al., 1972). Both layers consist of a mechanically tough network of protein filaments. The dermis is dominated by two extracellular proteins, collagen and elastin, that are maintained by cells known as fibroblasts. The epidermis expresses a large diversity of proteins that are laid down intracellularly in cells known as keratinocytes. Keratinocytes die after their final stage of differentiation, a process that usually involves covalent cross-linking of the fibrous and matrix components and massive water loss from the cell (Fraser et al., 1972). These keratinized cells, which end up in structures as varied as stratum corneum (the outer layer of the epidermis in terrestrial vertebrates), hair, and feather, are the ones that come into direct contact with the outside world, and so it is not surprising that they are mechanically tough (Fraser and MacRae, 1980). Keratinized cells may slough off gradually (as they do in skin) or may be lost

episodically, as they are during the molting of fur or feathers. In either case, cells in lower germinal layers usually divide, differentiate, and take their place.

While intermediate filaments probably appeared early in the evolution of the metazoa, type I and II keratin IFs arose more recently within the chordate lineage, with most of the gene duplications and divergence taking place in the vertebrates (Luke and Holland, 1999). It could be argued that the specialization of keratins by terrestrial vertebrates represents one of the most important events in vertebrate evolution. Indeed, one of the most fundamental differences among vertebrate groups has to do with how they sculpt their keratins – whether into scales, fur, or feathers. The vertebrate transition from life in water to life on land was made possible by the development of the nearly water-impermeable outer epidermal layer known as the stratum corneum, which allowed animals to withstand the desiccating forces of air exposure. Subsequent to their invasion of land, vertebrates molded keratins into a wide variety of epidermal appendages, many of which represent important milestones in vertebrate evolution. These structures were instrumental in the evolution of endothermy in mammals (fur), birds (feathers), and possibly dinosaurs (feathers). While feathers likely first evolved as insulation, they were later elaborated into structures that made possible the evolution of flight in birds. All terrestrial vertebrates use epidermal keratins as a rugged barrier that protects living tissues from the physical, chemical, and microbial insults of the external world. In contrast, keratinous epidermal appendages typically have more specific functions such as defense (horns and claws), food gathering (claws and beaks), reproduction (display feathers, fur, and horns), mechanoreception (whiskers), and locomotion (feathers) (Fraser et al., 1972; Pough et al., 1989).

Classification of keratins

Given the fantastic variety of keratinous structures, it is not surprising that attempts have been made to classify keratins into distinct groups. The terms "hard" and "soft" have been used to differentiate flexible keratins such as stratum corneum and the eponychium of nails, from more rigid keratins such as hair, nail, or feather. Aside from differences in stiffness, the main difference between the two groups is that the IFs in hard keratins possess a higher proportion of cysteine than the IFs in soft keratins, which tend to have a higher proportion of glycine (Fraser et al., 1972; Wang et al., 2000a).

Another system of classifying the keratins is based on their high angle x-ray diffraction patterns. **α-keratins** exhibit a distinctive *α-pattern* characterized by a

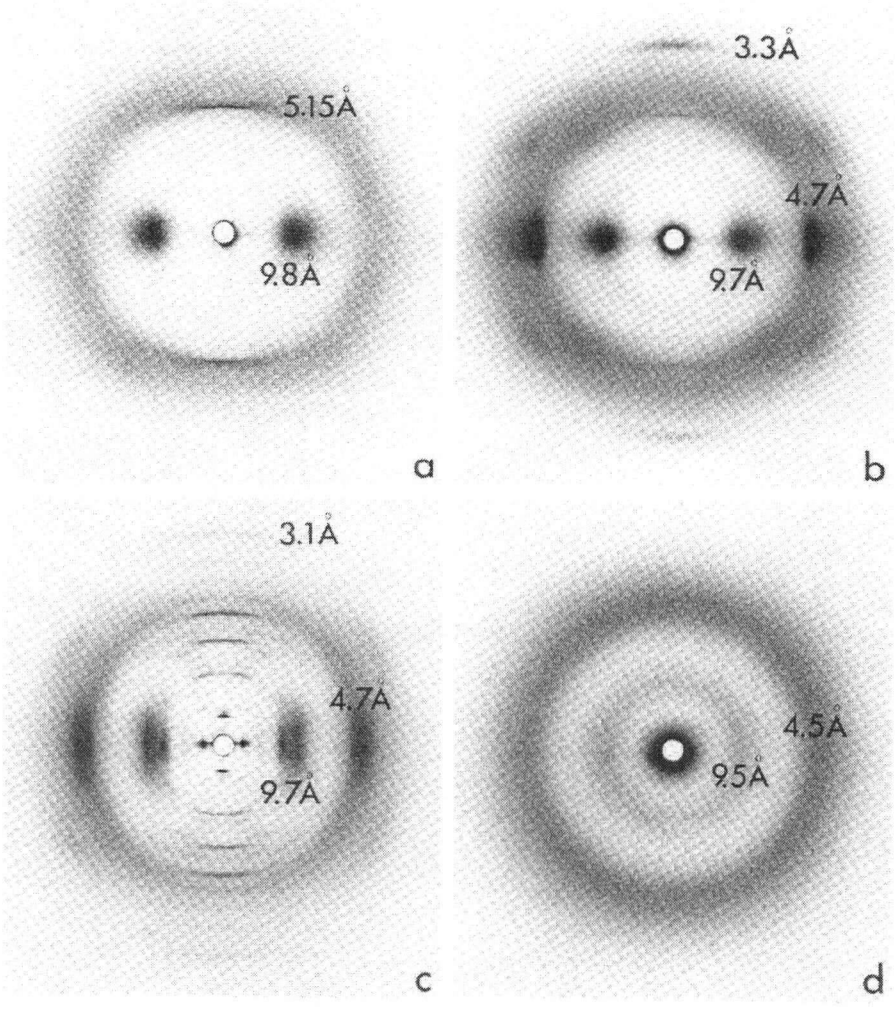

Fig. 3.1. Classification of keratins on the basis of their high-angle x-ray diffraction patterns. For panels, a-c, fibres are oriented vertically. a) α-pattern from porcupine quill. b) β-pattern from stretched porcupine quill. c) "feather" pattern from a β-keratin, seagull feather rachis. d) amorphous pattern from stratum corneum. Diffraction maxima (dark spots) are labeled according to the molecular spacing (in Angstroms, Å) to which they correspond. From Fraser and MacRae (1973).

meridional reflection of spacing 5.15 Angstroms (Å) and an equatorial reflection of spacing 9.8 Å (Fig. 3.1a). These reflections arise from the filamentous fraction of keratins (i.e. IFs) and correspond to the axial rise of IF α-helices and the spacing of α-helices within IF coiled coils, respectively. α-keratins include all mammalian keratins (both hard and soft, but in the latter, the diffraction pattern is not oriented), as well as soft keratins in reptiles and birds. Hard keratins in

reptiles and birds such as scale, claw, beak, and feather exhibit a distinct diffraction pattern that arises mainly from the β-sheet conformation of their fibrous component, and are thus termed **β-keratins** (Fig. 3.1c). IFs do not make up the fibrous component of β-keratins, as they do in α-keratins. The β-keratin diffraction pattern is characterized by a prominent equatorial reflection of spacing 4.7 Å, which corresponds to the inter-strand spacing within β-sheets, and is absent in the α-pattern. When hard α-keratins are slowly stretched in steam to a strain of about 0.8, they yield a diffraction pattern dominated by β-sheet secondary structure, and this pattern is known as the *β-pattern* (Fig. 3.1b). Both β-keratins and stretched α-keratins contain significant β-sheet structure, but their diffraction patterns are not identical. To avoid confusion, the β-keratin diffraction pattern is often referred to as the *feather pattern* (Fraser et al., 1972). Fig. 3.2 lays out the classification of keratins and the terms that will be used in this thesis.

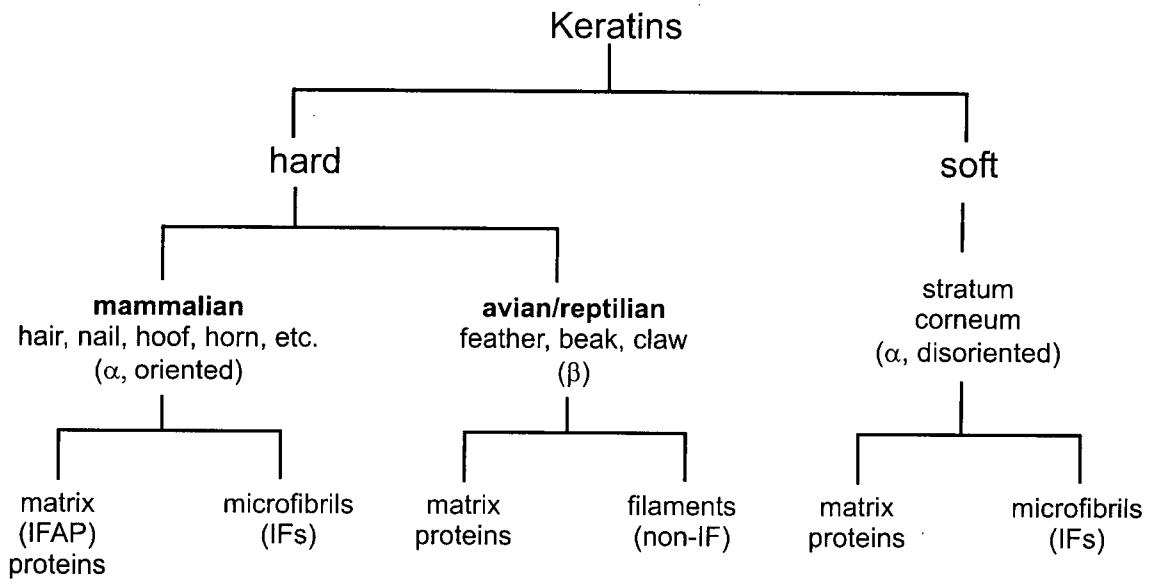

Fig. 3.2. Classification of keratins, modified from Fraser and MacRae (1980). IFAP = intermediate filament associated protein.

Two theories of keratin mechanics

In spite of the fact that scientists have been studying the structure and mechanics of hard α-keratins such as wool since the 1920s, a single dominant theory of keratin mechanics has yet to be established. Since 1959, there has been wide agreement that α-keratins are best described as a two-phase composite, with stiff IFs embedded in a softer, amorphous, high sulfur matrix (Feughelman, 1959).

However, the intimacy of the IF-matrix interaction makes it difficult to delineate which of the two components is responsible for which parts of the hard α-keratin stress-strain curve (Fig. 3.3), and this is where the current theories diverge.

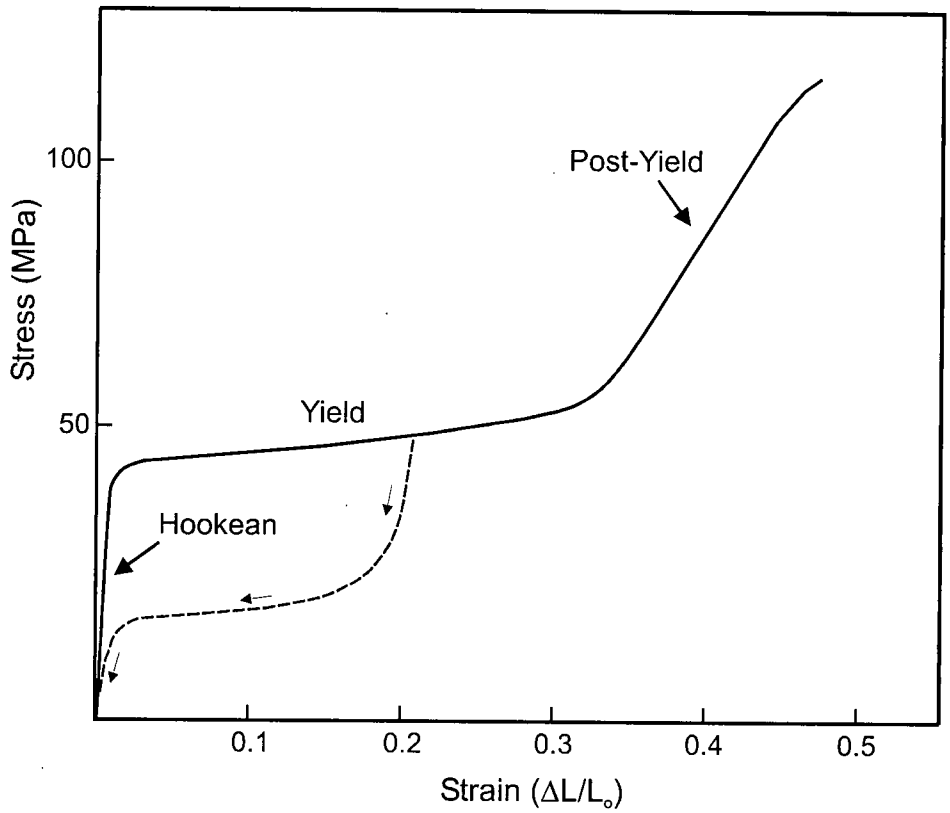

Fig. 3.3. Stress-strain curve for a hydrated hard α-keratin showing the three mechanical regions. The dashed line is the recovery curve for a fibre extended to a strain of 0.20 and unloaded.

There are currently two dominant theories of hard α-keratin mechanics, which differ in their interpretation of the hydrated keratin stress-strain curve. The keratin stress-strain curve shown in Fig. 3.3 is characterized by three distinct, approximately linear regions – an initial, high stiffness, "Hookean" region, a low stiffness "yield" region, and a terminal, high stiffness "post-yield" region. Both theories agree that the Hookean region arises mostly from the reversible deformation of bonds within and among IF α-helices (Feughelman and Druhala, 1976; Kreplak et al., 2001b; Pauling and Corey, 1950). They also agree that the sharp yield point that occurs between a strain of 0.02 and 0.03 arises from the opening of α-helices within IF coiled coils, ultimately leading to β-sheets and the

stacking of β-sheets into three-dimensional crystals in stretched fibres. The yield region corresponds to this α↔β transition (Feughelman, 1987).

Where the two theories part company is in their interpretation of the end of the yield region and the dramatic upturn of the stress-strain curve in the post-yield region. The first theory, proposed independently by Chapman (Chapman, 1969) and Hearle (Hearle, 1967) attributes the increase in stress and stiffness in the post-yield region to the keratin matrix, which it models as a cross-linked rubber-like elastomer with a J-shaped (i.e. rising stiffness) stress-strain curve. This theory, referred to by Hearle as the C/H theory, postulates that while IFs dominate the mechanics of α-keratin fibres in the Hookean and yield regions, the elastomeric matrix, which operates mechanically in parallel to the IFs, dominates at strains greater than 0.30. At a strain of 0.45 to 0.50, the matrix ruptures, leading to the rupture of the fibre as a whole.

Wortmann and Zahn, in a theory referred to as W/Z, propose that the post-yield region has nothing to do with the matrix, but rather to a continuation of the α↔β transition into more resistant zones of the IF α-helices (Wortmann and Zahn, 1994). This theory is an extension of Feughelman's original "series-zone" model (Feughelman, 1979), but incorporates more information about the structure of IF dimers. Specifically, W/Z postulates that the yield region corresponds to the extension of α-helices in segments 1A and 2A of the IF proteins, whereas the post-yield region is attributed to the extension of the 2B segments, which contain more cystine cross-links[3]. In the W/Z model, the matrix is modeled as a thixotropic gel that undergoes a dramatic yield at a strain of about 0.02, which is also referred to as a gel-sol transition. In this way, the matrix is proposed to make very little contribution to the mechanics of the keratin fibre.

In spite of their divergent interpretations of α-keratin molecular mechanics, it has been extremely difficult to experimentally distinguish the C/H and W/Z models, because to do so requires measuring the properties of the IFs and matrix independently. In the previous chapter I established hagfish slime threads as a model for exploring the mechanical properties of matrix-free IFs. Interestingly, the properties of hydrated IFs suggested by slime thread mechanics are radically different from the properties predicted by the C/H and W/Z models, which both postulate that the properties of the IFs in hard α-keratins are similar to the properties of the keratin itself. Hydrated slime threads are over 300 times less

[3] A more recent paper by Wang et al. (2000) suggests that in mouse trichocyte keratins, the cross-links occur in regions 1B and linker L1.

stiff and almost 5 times more extensible than hard α-keratins. They also yield at a stress that is about 10 times lower, and a strain that is about 10 times higher (Fig. 3.4 and Table 3.1)

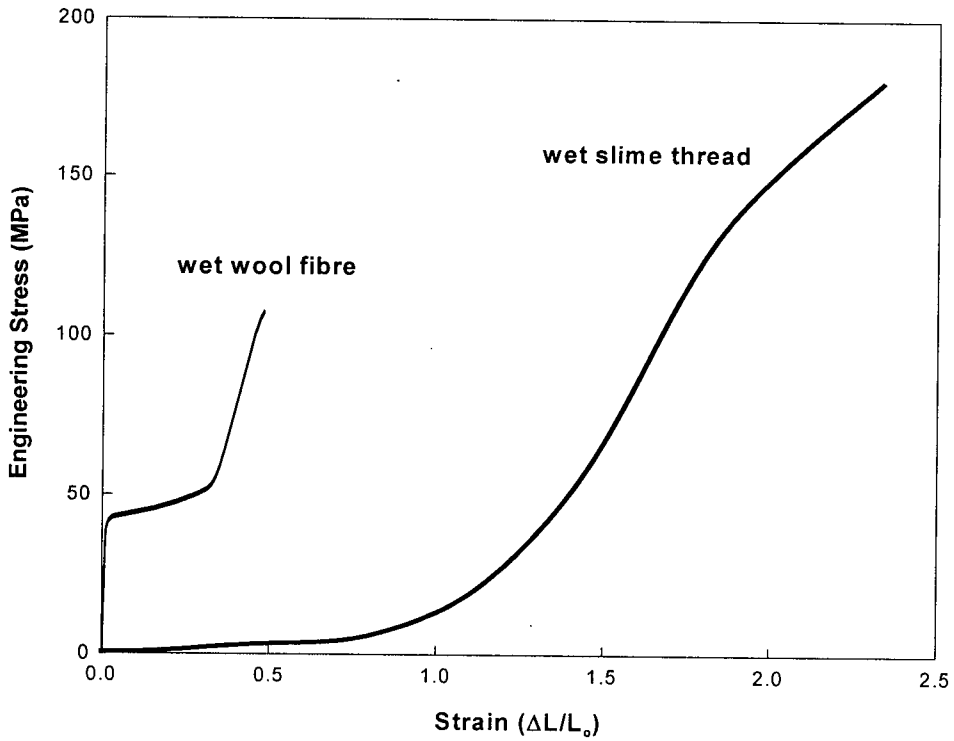

Fig. 3.4. Comparison of the tensile properties of slime threads in water (from Chapter 2) with hydrated hard α-keratins such as wool.

Table 3.1. Mechanical properties of hydrated hagfish slime threads and hydrated hard α-keratins such as wool.

	E_i (MPa)	Yield ε ($\Delta L/L_o$)	Yield σ (MPa)	Ultimate ε	Strength (MPa)
Wet slime threads	6.4 ± 0.9	0.34 ± 0.01	3.2 ± 0.4	2.2 ± 0.2	180 ± 20
Wet wool	2000	0.025	40	0.45	150

ε = strain, σ = stress.
Data for wet wool from Feughelman and Druhala (1976).

How can we explain such dramatic differences in properties? The most obvious candidate is covalent cross-linking. Whereas slime thread IF proteins possess almost no cysteine, hard keratin IFs are known to possess several disulfide (cystine) cross-links (Wang et al., 2000a). According to the model developed in Chapter 2, cystine cross-links between adjacent coiled coils within IFs would effectively bypass the soft terminal domain, giving the IFs an initial stiffness much closer to that of coiled coils, or about 2 GPa. This is consistent with the initial stiffness of hydrated hard α-keratins. However, covalent cross-linking cannot explain the high yield stress of hydrated hard α-keratins. Because the yield stress corresponds to disruption of the *weakest* region of the coiled coil, bridging adjacent coiled coils with cystine cross-links should have little effect on its value.

Increasing the yield stress of the IFs therefore requires stabilization of all portions of the coiled coils, and this can only be achieved by manipulating an agent that is distributed throughout the IF structure. Water is just such an agent, and it is a known plasticizer of proteins. Water molecules will have access all along IF proteins, and their removal should stiffen the elastomeric terminal domains and stabilize the α-helical structure of the coiled coils. Thus, dehydration should increase both the stiffness and the yield stress, and therefore hydration could be a key parameter in determining the properties of IFs in hard α-keratins. I hypothesized, therefore, that the IFs in hydrated hard α-keratins are dehydrated to some extent. This hypothesis makes two explicit predictions that can be tested using the slime thread model. The first is that hydrated slime threads should lose more water than hydrated hard α-keratins when they are dehydrated. The second prediction is that slime threads tested in air should exhibit mechanical properties that are similar to those of hydrated hard α-keratins.

Another major difference between the mechanical behavior of hydrated hard α-keratins and hydrated slime threads is that hard α-keratins recover fully from post-yield deformations, whereas slime threads do not (Fig. 2.6). The two theories of keratin mechanics explain the recovery of hard α-keratin fibres in two ways. The first is that deformation of IFs is inherently reversible. Both the C/H and W/Z models suggest that the α↔β transition is reversible and stress-dependent. At low stresses, the α←β direction is favored, whereas at higher stresses, the transition proceeds from α→β. Thus, unloading a fibre after deformation into the yield zone (i.e. decreasing the stress) shifts the equilibrium to the α←β direction, and the fibre eventually recovers its original length. The second mechanism (proposed only by the C/H model) is that recovery is aided by a recoil force provided by the elastomeric keratin matrix.

Post-yield deformation of hydrated slime threads is *not* inherently reversible, due to an irreversible α→β transition. This suggests that recovery in hydrated hard α-keratins is mediated primarily by recoil of the matrix, with the IFs contributing little. However, if IFs are maintained in a dehydrated state as suggested earlier, then the recovery behavior of wet slime threads may not be relevant. A recent paper by Kreplak et al. (2001) on the structural mechanics of hair suggests that the α↔β transition in keratins is hydration-dependent (Kreplak et al., 2001a). These results suggest that recovery may also be hydration-dependent. For these reasons, I investigated the recovery behavior of dry slime threads to answer the question of whether deformation of IFs is inherently reversible in the dry state.

In this chapter, I demonstrate that the swelling and mechanical properties of dry slime threads are consistent with the hypothesis that IFs in hydrated hard α-keratins are partially dry. Furthermore, I demonstrate that deformation of dry IFs is not inherently reversible, which suggests that the keratin matrix is critical for recovery.

MATERIALS AND METHODS

Slime thread swelling

Swelling behavior was quantified by measuring both the change in diameter and the change in length that occurs when slime threads are dehydrated. The change in diameter was estimated by measuring the maximum diameter of threads within intact slime thread skeins (i.e. mature GTCs without their plasma membranes) in distilled water and following alcohol dehydration. Measuring the swelling behavior of a given slime thread was prohibitively difficult due to the

tendency of the skeins to move during the introduction or removal of solvent under the cover slip. Fortunately, there is little variation among the skeins in their maximum thread diameter, making paired measurements unnecessary. Nevertheless, a large number of measurements (30) were made for both hydrated and dehydrated slime threads to reduce sampling error. For the measurement of hydrated slime thread diameter, stabilized skeins were placed on a glass slide and covered with a cover slip. Distilled water was introduced under the cover slip by placing a drop on one side and pulling it through with a piece of filter paper from the other side. This was repeated three times to insure removal of the stabilization buffer. Diameter was measured under high power (100x interference contrast oil immersion objective) on a Leitz Orthoplan-pol microscope (Ernst Leitz Canada, Midland, Ontario) using a 15x Filar-micrometer eyepiece. For the measurement of dehydrated slime thread diameter, stabilized skeins were first separated from stabilized slime mucin vesicles by filtering with 54 μm nitex mesh. The skeins were retained on the mesh during this procedure, and subsequently rinsed with anhydrous ethanol. Skeins were separated from the screen by placing the filter disk in a 50 mL capped centrifuge tube with 25 mL of anhydrous ethanol and shaking to dislodge the skeins from the mesh. A drop of skeins suspended in ethanol was next placed on a glass slide and the ethanol allowed to evaporate. The skeins were then covered with a drop of immersion oil (to prevent hydration from the air) and a cover slip. Maximum thread diameter was measured as described above.

Dehydration-induced length changes were measured by mounting 9-10 mm lengths of threads in distilled water using the TackiWax method described in Chapter 2. Thread length was measured by dialing the micrometer/traveler arm until the thread was just taut. The fibre was then slackened and the water in the 9 mL chamber serially replaced with ethanol via 50, 1.0 mL replacements (i.e. one mL of ethanol added, one mL of solution in chamber removed), resulting in a final water concentration of less than 1%, assuming perfect mixing. When the replacement was complete, thread length was measured again. Measuring both the change in diameter and length allowed calculation of the change in volume experienced by slime threads when they are dehydrated.

Mechanical measurements

Tensile properties of dry slime threads were measured using the glass microbeam apparatus described in Chapter 2 fitted with a thicker glass beam of diameter 124 μm. Preliminary tensile tests revealed that it is not possible to pull slime threads out of water directly into air without some of their proteins

undergoing an α→β transition. This effect can be attributed to the surface tension forces that resist pulling a slime thread through the air-water interface. In order to circumvent this problem, slime threads were unraveled and mounted in water, and the water gradually replaced with ethanol using the procedure described above, resulting in a final ethanol concentration of about 95% (i.e. 26 changes). The lower surface tension and the dehydrating/stiffening effect of the ethanol allowed the threads to pass through the ethanol/air interface without major deformation. Mechanical tests were conducted at room temperature (~20 °C) in air at ambient humidity, which was 40% on average, and varied little over the course of the experiments.

Slime thread diameter measurements

For each slime thread segment tested, the diameter of an adjacent piece of thread was measured using a Hitachi S-4700 scanning electron microscope (SEM). Samples were transferred to mirror-polished SEM grids, secured with a bead of epoxy at either end, and gold sputter coated under vacuum for 3.2 minutes, resulting in about a 10 nm gold coating. Digital images of threads were captured at an acceleration voltage of 5.0 kV at 18.0k times magnification (Fig. 3.5). Thread diameter was measured from calibrated digital images using Scion Image v. 3b analysis software (Scion Corp., Frederick, MD, USA).

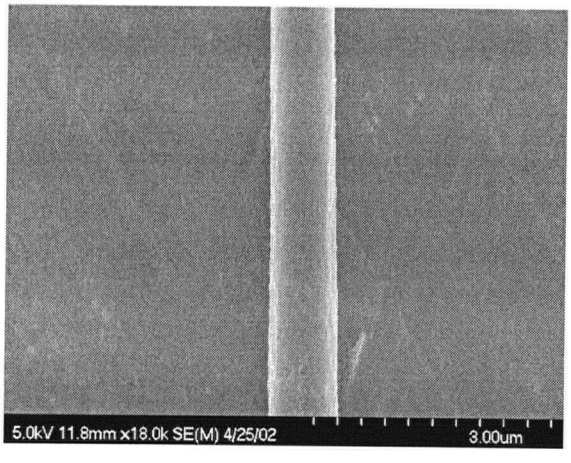

Fig. 3.5. Scanning electron micrograph of a gold sputter coated slime thread isolated into air via the ethanol dehydration technique.

Recovery behavior

Dry, untransformed threads were obtained as described above, and recovery behavior measured in air (R.H. = 40%) in a manner similar to that described in

Chapter 2 for hydrated threads. One difference in the methodologies was that recovery from a series of increasing strains was measured for each dry thread. In addition, between trials, threads were exposed to warm humid air so that the effect of hydration on recovery could be quantified. Seven threads were tested in total. The strains for which recovery was measured were: 0.05, 0.10, 0.20, 0.30, 0.40, 0.50, 0.60, 0.70, 0.80, 0.90, and 1.0. Threads were stretched to the desired strain, held for one minute, then allowed to recover for ten minutes at ambient humidity (40%) after which the recovered length was measured. Threads were then slackened and exposed to warm, humid air (i.e. they were breathed on) until their length remained constant over time (about 30 s), and their recovered length measured again.

Load-unload cycles were performed by conducting tensile tests as described above, and reversing the 72-rpm motor driving the traveler arm when the desired maximum strain was reached. For consecutive load cycles, a second video dimension analyzer tracked the movement of the traveler arm, which allowed simultaneous collection of both force and extension data.

RESULTS

Slime threads in water swell to over two times their dehydrated volume

Swelling experiments revealed that the diameter of dry slime threads increases by 45% (2.2 ± 0.1 μm vs. 3.2 ± 0.1 μm for dry and wet slime threads, respectively) when they are hydrated, and the length *decreases* by 2.1 ± 0.8%. These values correspond to a 110% increase in cross-sectional area and a 106% increase in volume caused by hydration.

Dry slime threads mechanics resemble hard α-keratins

Tensile tests on dry slime threads revealed a three-part, hard α-keratin-like stress-strain curve, with an initial stiff region, a yield and plateau, and a final rise to failure (Fig. 3.6A). Dry slime threads exhibited high initial stiffness (E_i = 7700 ± 500 MPa) and extensibility (ε_{max} = 1.0 ± 0.1), and yielded at a strain of 0.024 ± 0.001, and a stress of 150 ± 10 MPa. Strength was 530 ± 40 MPa, and toughness

was 240 ± 20 MJ/m^3. Mechanical data from tensile tests are summarized in Table 3.2.

Table 3.2. Mechanical properties of hagfish slime threads tested in air. Data for slime threads tested in water (from Chapter 2) are provided for comparison.

	E_i (MPa)	Yield ε ($\Delta L/L_o$)	Yield σ (MPa)	Ultimate ε	Strength (MPa)	Toughness (MJ/m^3)
Dry slime threads	7700 ± 500 (7)	0.024 ± 0.001 (13)	150 ± 10 (7)	1.0 ± 0.1 (13)	530 ± 40 (7)	240 ± 20 (7)
Wet slime threads	6.4 ± 0.9	0.34 ± 0.01	3.2 ± 0.4	2.2 ± 0.2	180 ± 20	130 ± 20

Values are mean ± SE. Sample size is in parentheses. ε = strain, σ = stress.

Recovery of dry slime threads

Recovery trials and load cycles show that dry slime threads possess little ability to recover from post-yield deformation in air. However, exposing the threads to warm, moist air during the recovery period resulted in considerable recovery (Fig. 3.7).

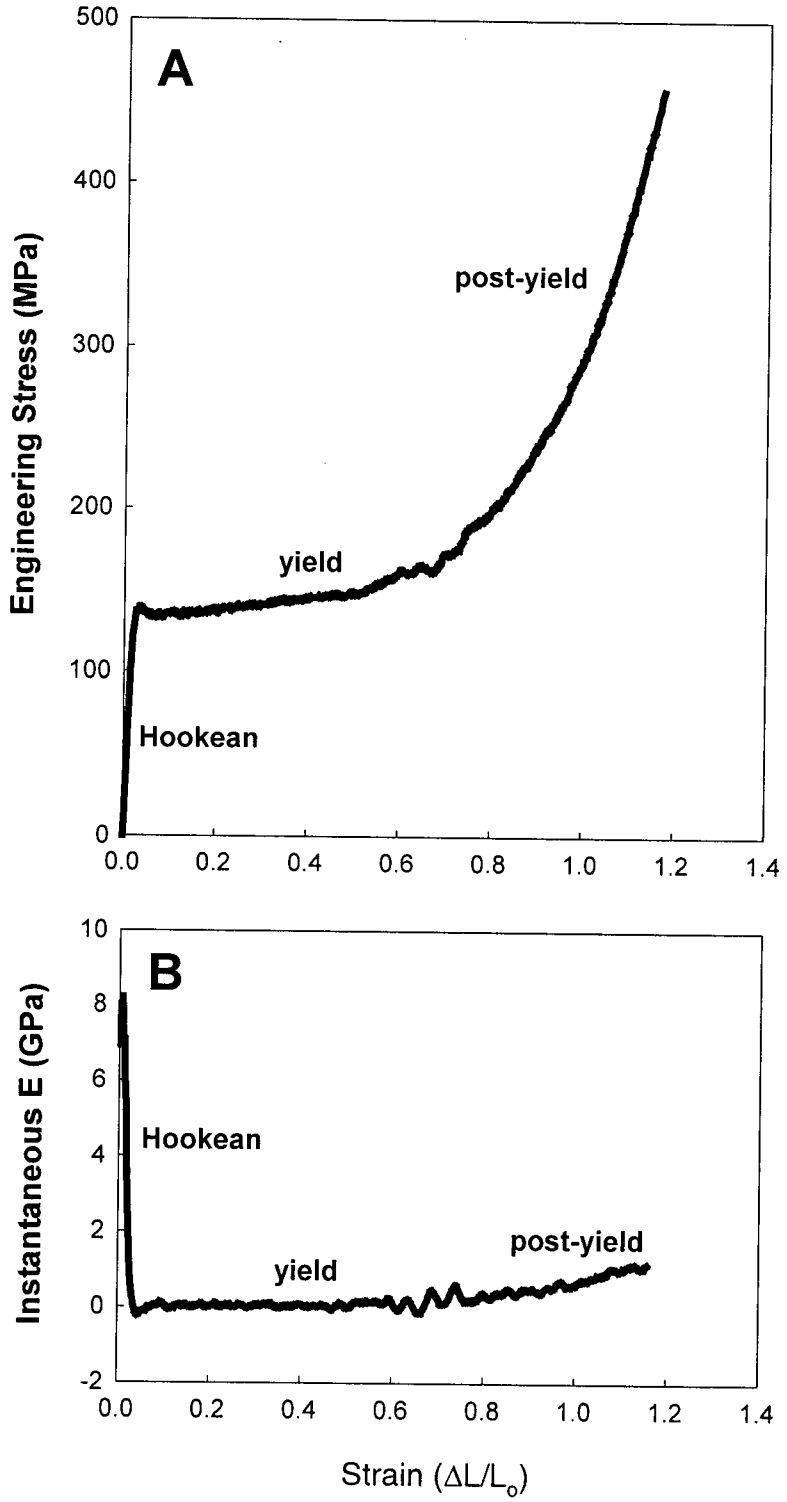

Fig. 3.6. Tensile mechanics of slime threads tested in air. A) Typical stress-strain curve showing the three mechanical regions discussed in the text. B) Instantaneous stiffness vs. strain from the same data set, also with the three regions indicated. The negative stiffness at the end of the Hookean region appeared repeatedly, and is therefore unlikely to be a result of noise.

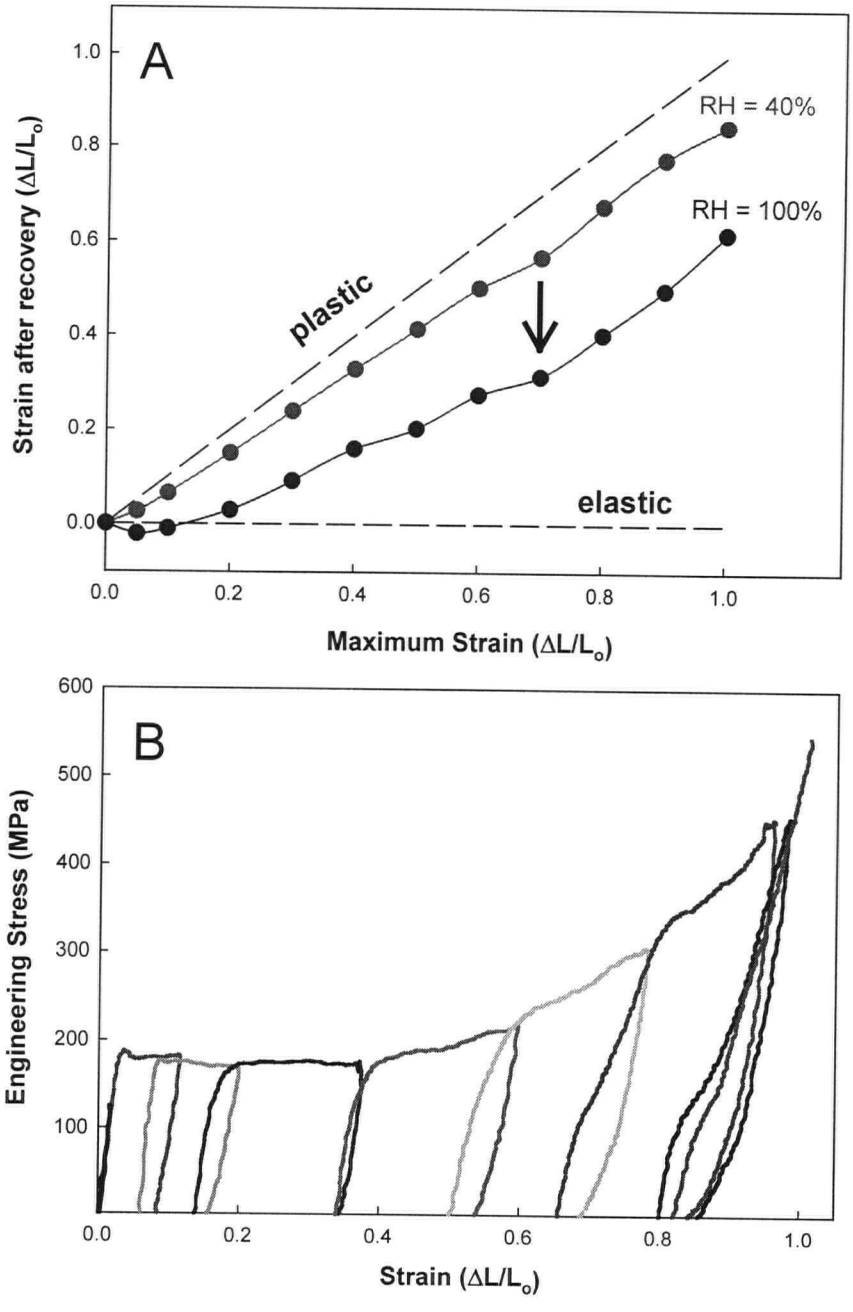

Fig. 3.7. Recovery of slime threads tested in air. A) Results from recovery trials in which threads were extended to a set strain, held for one minute, then allowed to recover for ten minutes in a slack state (red line). After recovery, threads were briefly exposed to warm, humid air and recovery measured again (blue line). Note that dry threads recover very little, but increasing humidity allows considerable recovery. B) Consecutive load cycles for a slime thread in air, which underscore the lack of recovery exhibited by dry slime threads.

DISCUSSION

Slime threads swell far more than hard α-keratins in water

The dehydration hypothesis put forth in the Introduction postulates that IFs in hydrated hard α-keratins are stiffer and have a higher yield stress than hydrated slime threads because they contain less water. This hypothesis predicts that hydrated hard α-keratins should therefore lose less water than slime threads when they are dehydrated, or should swell less when going from the dry to the wet state. The swelling data presented in Table 3.3 confirm this prediction; slime threads more than double in volume when hydrated, whereas hard α-keratins only increase by about 40%.

Table 3.3. Swelling of slime threads compared with hard and soft α-keratins.

	Swelling Ratio (wet:dry volume)	Reference	Notes
Slime threads	2.1	this thesis	
Hard α-keratin	1.43*	Fraser et al., 1972	human hair
	1.35	Feughelman, 1987	mammalian hair
Soft α-keratin	1.96*	Blank, 1952	human stratum corneum

*Calculated from water regain data assuming a dry keratin density of 1.4 g/cm^3.

Although a lack of data for the contribution of the matrix to swelling of α-keratins confounds precise interpretation of these numbers, the difference between slime threads and hard α-keratins is so large that it is nearly impossible to imagine a scenario where IFs in hard α-keratins take up as much water as they do in slime threads. Consider a typical hard α-keratin fibre in which 30% of the volume is occupied by matrix, and the other 70% by IFs (Gillespie and Frenkel, 1974). If the IFs were to double in volume (as they do in slime threads) and the matrix showed *no swelling at all*, the fibre would still exhibit a 75% increase in volume, instead of 40%. In fact, in order for the IFs to double in volume and still result in only 40% overall swelling, the matrix would not only have to exhibit *negative* swelling, but would have to disappear completely. Clearly this is not

possible, thus the water content of IFs in hydrated α-keratins is lower than in slime threads.

Dry slime threads exhibit a high yield stress

The other critical prediction of the dehydration hypothesis is that dry slime threads should possess a high yield stress, and this is indeed the case (Fig. 3.6 and Table 3.2). From Chapter 2 we know that the yield stress of hydrated IFs in slime threads, or the stress at which the α→β transition begins, is only about 7 MPa[4]. In wet wool, the yield stress is much higher at ~40 MPa. If 30% of the volume of a wool fibre is taken up by non-IF matrix proteins and the matrix contributes little to the yield stress, then IFs in wet wool yield at a stress of about 60 MPa. While this value is far higher than the stress at which they yield in slime threads, it is not as high as the yield stress of dry slime threads (150 MPa), which suggests that the IFs in hydrated hard α-keratins are only partially dehydrated.

The swelling and mechanical data discussed above strongly suggest that IFs in hard α-keratins are maintained in a partially dehydrated state. Other data in the literature point to a similar conclusion. Feughelman (1959) notes that the ratio of the tensile modulus (E) to the rigidity modulus (G) of wool fibres is highly hydration dependent. Dry wool fibres have an E/G ratio of 2.7:1 (Speakman, 1929), which is very close to the value expected for an isotropic material with a Poisson's ratio of 0.5. When wool fibres are hydrated, however, E drops by a factor of 2.6, whereas G drops by a factor of 15. The implication is that while the matrix properties are strongly hydration dependent, the IFs are hydration-resistant, which is what one would expect if the water content of IFs is somehow restricted.

The keratin matrix as regulator of IF hydration

The above conclusion about the hydration state of IFs in hard α-keratins raises obvious mechanistic questions. Namely, how is it that IFs are assembled in an aqueous environment in developing keratinocytes, yet are partially dehydrated when keratinization is complete, even when the cell is in equilibrium with water? One possibility is that the matrix forms a water-impenetrable barrier that simply keeps water away from the IFs. This is unlikely, however, because it is believed that the matrix itself is free to swell as hydration changes, and an impenetrable matrix would not allow the dehydration step that occurs at the end of the

[4] Because I am interested in the yield stress *per coiled coil*, I factored out the influence of swelling effects by multiplying the wet yield stress by the ratio of wet:dry cross-sectional areas (2.1).

keratinization process. Another possibility is that water is osmotically drawn away from the IFs by the matrix, leaving them in a partially dehydrated state. Such a mechanism is possible when a fibre is first placed in water, but as it approaches equilibrium, water will eventually reach the IFs no matter how strong the osmotic pull of the matrix. The last and most likely possibility is that the water potential in and around the IFs is decreased by pressure. If the matrix exerted an inward pressure on the IFs, the resultant decrease in water potential would reduce the hydration state of the IFs, even when the fibre is immersed in water.

Although an inward pressure exerted by the matrix is the most plausible mechanism whereby IFs in hard keratins could be dehydrated, how exactly would such a pressure develop? There are two possibilities. The first is that once the IFs and matrix are in place, dehydration occurs by simple air exposure, and subsequent covalent cross-linking of the matrix locks the IFs into a dehydrated state. When the fibre is placed in water, the IFs begin to hydrate, leading to an increase in pressure opposed by elastic deformation of the matrix. Hydration ensues until the pressure build-up halts the net influx of water into the IFs, and equilibrium is reached before the IFs are fully hydrated. The second possibility is that cross-linking of the matrix occurs in an aqueous environment, and actually *causes* dehydration of the IFs. It is well established that when covalent cross-links are introduced into an entangled polymer network, the network contracts to a smaller volume, forcing solvent out. In this scenario, cross-linking of the keratin matrix occurs in the hydrated state, causing a contraction of the matrix accompanied by water loss. Note that the result of both of the above mechanisms for the keratin composite in water is an outward pressure exerted by the IFs that is balanced by an inward pressure exerted by the matrix. It is also interesting to note that the first mechanism requires an air dehydration step, which could help explain why many fur-bearing aquatic mammals such as seals and sea lions confine their moults to brief bouts on land. In contrast, the development of continually wet keratinous structures such as whale baleen poses difficulties for this model, suggesting instead that cross-linking precedes and in fact causes dehydration, at least in these structures.

Regardless of the timing of cross-linking and dehydration in hard α-keratins, the concept that the matrix maintains the IFs in a partially dehydrated state is a powerful one. Not only does it explain the high stiffness and yield stress of hydrated hard α-keratins, but is also consistent with a peculiar relationship that exists between keratin matrix content and hydration. In an interspecies comparison, Bendit (1980) demonstrates an inverse relationship between the

matrix content of hard α-keratins and their ability to swell in water. In other words, dehydrated keratins with a high proportion of matrix take up less water than keratins with less matrix. This result is especially puzzling given the fact that most of the swelling in hard α-keratins is attributed to the matrix, and not the IFs. Fraser and MacRae (1980) explain the inverse relationship between matrix content and water uptake as a problem of space constraints. They postulate that keratins with more matrix have a higher concentration of matrix protein in the inter-IF spaces, which simply leaves less volume for water to enter. As evidence for this hypothesis, they cite data suggesting that the interfibrillar distance in various hydrated keratins is relatively constant across a range of matrix contents.

Following the line of logic established in this chapter, another explanation for this puzzling relationship emerges. If one of the roles of the keratin matrix is to exert an inward pressure on IFs that keeps them in a partially dehydrated state, then one would expect that a higher proportion of cross-linked matrix would be better able to do this. Keratins with less matrix would be less effective at opposing IF swelling, whereas keratins rich in matrix would be much more effective. While this theory is certainly consistent with the data, it hinges on the somewhat shocking premise that swelling in keratins is governed by the swelling of the IFs, and not the matrix. How can this be, given the current understanding that the matrix swells much more than the IFs?

The relative swelling of IFs and matrix in hard α-keratins is based on x-ray diffraction patterns from porcupine quill in the wet and dry state (Fraser et al., 1972). In this study, the authors show a 13% increase in the distance between IFs, and only a 6% increase in the IF diameter. They conclude that swelling in quill thus occurs mostly in the interfibrillar space, which they reasonably assume is occupied by matrix. However, more recent work on the diameter of IFs using scanning transmission electron microscopy (STEM) (Steven, 1990) suggests that some of this space may actually be occupied by IFs. Steven (1990) suggests that previous estimates of IF diameter (7.5 nm in hard α-keratins, 10 nm in cytoplasmic IFs) are in fact estimates of the diameter of the IF *backbone,* which ignores the presence of a low-density halo that gives IFs an outer diameter that is 50% larger. Structural models suggest that the backbone consists of aligned coiled coils, while the halo consists of terminal domains at the IF periphery. Given these insights, it is entirely possible that the increase in interfibrillar space measured by Fraser et al. is actually an increase in the distance between IF backbones caused mainly by swelling of the IF terminal domains, with far less swelling attributable to the matrix.

Slime thread volume increases by about 100% due to hydration, which is consistent with the above idea that IF swelling dominates the swelling behavior of α-keratins. Others have suggested that IF swelling should dominate the swelling of α-keratins, but the idea is not widely acknowledged in the literature. Based on an analysis of matrix and IF hydrophobicity, Zahn (1977) suggested that IFs should swell much more than the matrix, and even postulated that swelling of α-keratins is dominated by IF swelling. This idea has been abandoned, however, in favor of Fraser and MacRae's (1980) model in which water uptake is prevented in matrix-rich keratins by a lack of available space between the IFs.

The "matrix squeeze" hypothesis put forth here suggests a completely different interpretation, and does not require bizarre matrix swelling properties. As dry hard α-keratin is hydrated, water is taken up preferentially by the IF terminal domains, which mechanically strains the network of matrix proteins. As more water is taken up, further increases in volume are increasingly resisted by the matrix, and pressure rises. α-helices within the IFs are maintained in a partially dehydrated state because equilibrium is reached before they are fully penetrated by water. In this model, a greater volume fraction of matrix leads to less water uptake for two reasons – the low proportion of IFs, which tend to swell more than the matrix, and because the greater volume of matrix is better able to resist IF swelling.

If the matrix keeps the yield stress of α-keratins high in water by directly opposing IF swelling and limiting IF hydration, then one would expect that loosening of the matrix should allow for more swelling and therefore a reduction of the yield stress. Indeed, hydrated wool fibres show a progressive decrease in the yield stress as a function of cystine content (Feughelman, 1963). Repetitive loading and unloading of hydrated wool fibres also results in a progressive decrease in the yield stress (Feughelman, 1973). This phenomenon can be explained by the matrix squeeze hypothesis if axial deformation of the fibres results in an increase in their volume, and therefore a decrease in their internal pressure. An increase in fibre volume with elongation will occur in any material with a Poisson's ratio less than 0.5, i.e. most biological materials besides rubber. A decrease in internal pressure will tend to draw water into the fibre, thereby lowering the stiffness and yield stress.

Implications for soft keratins

While the properties of dehydrated IFs provide insight into the mechanics of

hard α-keratins such as hair and nail, how is it that soft keratins such as stratum corneum can be so much less stiff? Table 3.4 provides some basic mechanical data for hard and soft α-keratins tested both wet and dry. Note that the initial stiffness of stratum corneum decreases by about 300x when it is hydrated, whereas the stiffness of hair decreases by only 2.7x. The most plausible explanation is that the IFs in wet stratum corneum are fully hydrated, in contrast to the IFs hard α-keratins. If this is true, their mechanical properties should be closer to those of slime threads in seawater (Fig. 3.4) rather than those of slime threads in air (Fig. 3.6A). Fig. 3.8 demonstrates that the stress-strain behavior of hydrated stratum corneum is indeed not all that different from the behavior of slime threads in water, with differences in extensibility and stiffness that may be attributed to the stratum corneum matrix. Given its role as a flexible outer barrier, it should not be surprising that the IFs in the stratum corneum are extensible and resilient like slime threads. If the IFs were dehydrated as they are in hard α-keratins, this critical barrier would be awkwardly inflexible and prone to cracking.

Table 3.4. Effect of hydration on the tensile modulus of hagfish slime threads compared with hard and soft α-keratins (after Fraser and MacRae, 1980).

Material	Dry E (GPa)	Wet[a] E (GPa)	Ratio Dry:Wet	Reference	Notes
Slime threads	3.6[b]	0.006	560	1	
Hard α-keratin	2.6[c]	1.8	1.4	2	human nail
	2.3[c]	1.5	1.5	2	human hair
	5.6[d]	2.0	2.8	3	Cotswold wool
	6.8[e]	2.4	2.8	4	horsehair
	4.5[f]	2.5	1.8	5	Lincoln wool
Soft α-keratin	1.0	0.004	250	5	stratum corneum
	2.0	0.003	670	6	stratum corneum
			330	7	stratum corneum

E = initial stiffness

[a] Wet = in water or at 100% relative humidity

[b] Relative humidity (RH) ≈ 40%; calculated using the hydrated cross-sectional area for stress

[c] RH = 70%, [d] RH = 0%, [e] RH = 60%, [f] RH = 60%

1 This thesis, 2 Baden, Goldsmith, and Lee (1974), 3 Meredith (1956), 4 Bendit (1976), 5 Bendit, unpublished data, 6 Park and Baddiel (1972), 7 Kligman (1964).

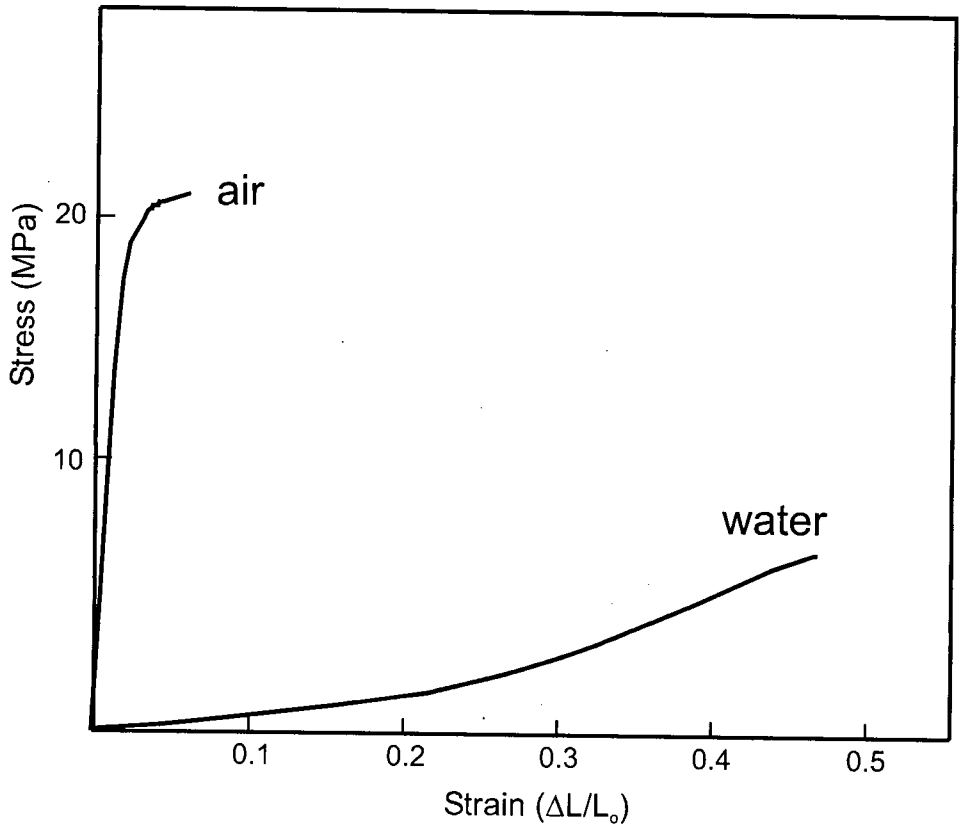

Fig. 3.8. Tensile stress-strain behavior of stratum corneum in water and air (65% relative humidity). After (Kligman, 1964) and (Park and Baddiel, 1972).

Recovery behavior

In Chapter 2 I showed that in contrast to hard α-keratins, slime threads in water exhibit very little post-yield recovery. Fig. 3.7A demonstrates that dry slime threads at a relative humidity of 40% also recover very little, but undergo considerable recovery when exposed to warm, humid air. How is it that exposure to water leads to substantial recovery of threads strained in air, but does not aid the recovery of threads strained in water? A recent x-ray diffraction study of hard α-keratins deformed in air may help to explain these peculiar results. In this study, Kreplak et al. (2001) demonstrate that coiled coils in hair IFs deformed at 30% relative humidity do not form β-sheets in the yield region, but rather melt and adopt a random coil conformation. This finding suggests that slime threads strained in water are prevented from recovering due to the formation of stable β-sheets that lock them into a new, longer resting length. In dry threads, β-sheets do not form, and therefore recovery is still possible as long as some water is available to allow for molecular mobility. Fig. 3.9 plots the

recovery data for both dry and wet slime threads with an emphasis on recovery from post-yield deformation, which corresponds to the unraveling of α–helices. From these plots it is clear that post-yield recovery of slime threads is increased by straining the threads in dry air and then allowing recovery at 100% humidity. It is interesting to note that even under these conditions, recovery is not complete, as it is in hard α-keratins. This may be due to the formation of stable β-sheets during recovery as the thread is exposed to water.

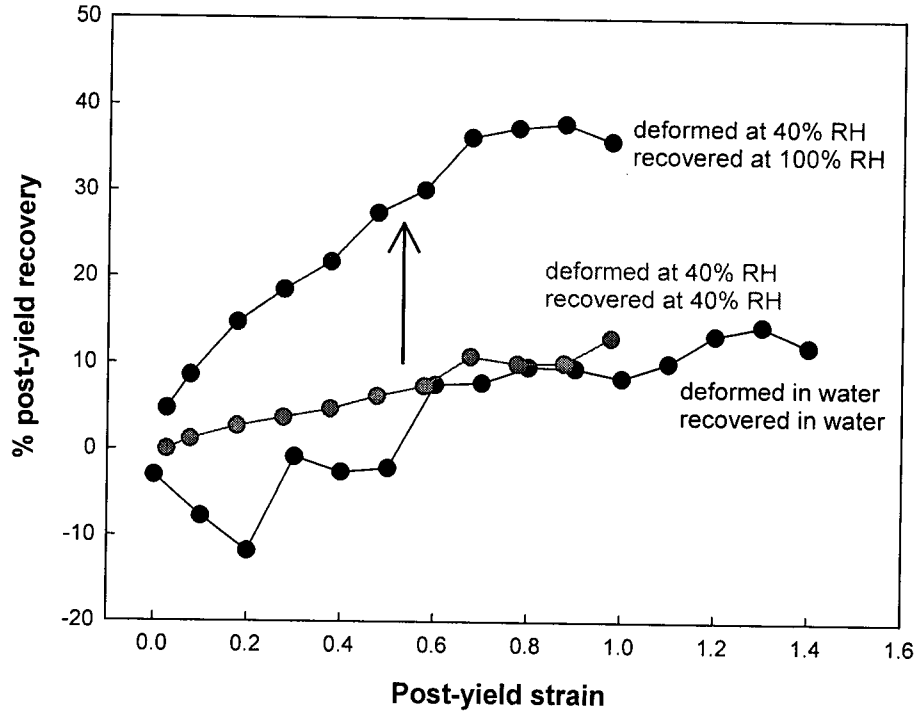

Fig. 3.9. Post-yield recovery of slime threads under different hydration regimes. Threads in water (black line) and air (red line) show little recovery from post-yield deformations, but threads that are strained in air and then exposed to warm, moist air (blue line) exhibit significant recovery. Data are the same as those presented in Figs. 3.7A, and 2.6A.

Previously in this chapter I suggested that an important role of the keratin matrix is to maintain the IFs in a partially dehydrated state. In light of the effects of hydration on IF recovery described above, it is possible that the matrix regulates IF hydration not only to keep IF stiffness and yield stress high, but also to maximize recovery. In other words, IF hydration must be kept low enough to keep stiffness and yield stress high and to inhibit the formation of stable β-sheets, but it must be high enough to provide the molecular mobility that is required for full recovery.

Implications for theories of hard α-keratin mechanics

If IFs in hard α-keratins are indeed partially dehydrated, then dry slime threads are an extremely useful tool for probing the mechanics of the keratin composite. Most importantly, they provide a means by which the mechanical properties of the IF fraction can be characterized in the absence of both matrix and disulfide cross-links. In this section, I will walk through the stress-strain curve for dry slime threads and discuss the implications for the current theories of keratin mechanics described in the Introduction of this chapter.

Hookean region

Both the C/H and W/Z theories agree that the Hookean region of the hard α-keratin stress-strain curve corresponds to a reversible straining of α-helices and coiled coils in the IF protein rod domains. X-ray diffraction of keratin fibres confirm that fibre strain in the Hookean region is accompanied by both axial stretching of the α-helices as well as an untwisting of the coiled coils (Kreplak et al., 2001a). In dry slime threads, this region is characterized by a stiffness of 7.7 ± 0.5 GPa, a yield stress of 150 ± 10 MPa and yield strain of 0.024 ± 0.001. The stiffness of dry slime threads is somewhat higher than the stiffness of dry α-keratins such as wool, which have a stiffness of 5-6 GPa. Although it is generally accepted that dry keratins are isotropic (Feughelman, 1959), these data suggest that dry IFs might actually be slightly stiffer than the dry matrix.

The high stiffness of dry slime threads also suggests that something dramatic happens to the IF protein terminal domains when they are dried out. Recall from Chapter 2 that in the wet state, the terminal domains dominate the low strain mechanics, and as a result, hydrated slime threads have a low stiffness of 6.4 MPa. In the dry state, slime threads are three orders of magnitude stiffer. There are two possible explanations for such a huge rise in stiffness. The first is that the terminal domains remain in series with the helical rod domains, but they become hard and glassy when they are dried out. The tensile modulus of polymers in the glassy state is typically three orders of magnitude higher than in the rubbery state (Lillie and Gosline, 2002), which is similar to the change in modulus seen in slime threads caused when they are dehydrated. The second possibility is that IF dehydration facilitates van der Waals and coulombic interactions (i.e. salt bridges) among adjacent coiled coils. In this way, force is transferred from one coiled coil to another via shear, resulting in at least partial bypassing of the terminal domains, with a large increase in stiffness.

A brief analysis of the above mechanisms suggests that both of them are likely to be relevant. The first possibility requires that the terminal domains be able to withstand the yield stress of 150 MPa, otherwise, the fibre would break or yield before the yield zone even began. Polymers in the glassy state typically yield or break at a stress of about 150 MPa (Lillie and Gosline, 2002), which is in the right range, but is not likely to be entirely sufficient. Coupling of adjacent coiled coils via shear is also not likely to be adequate. Composite theory predicts that the two most important parameters that determine whether loads can be effectively transferred from one fibril to another via shear are the aspect ratio of the fibrils (i.e. length:radius), and the shear modulus of the material between them. Fibres within effectively reinforced composites typically have aspect ratios of 10^2 to 10^3, whereas coiled coils have an aspect ratio of only about 45 (45nm/1nm), suggesting that they are too short for transfer of stress between them to be complete. Although neither of the above mechanisms appears to adequately explain stress transfer between coiled coils on their own, they are not mutually exclusive, and a combination of the two can account for both the high modulus and yield stress of dry slime threads. Specifically, glassy terminal domains act for the most part in series with coiled coils, but some transfer of stress between coiled coils via shear lowers the stress that must be borne by the terminal domains.

Yield region

Although the Hookean region of dry slime threads is quite similar to the corresponding part of the hard α-keratin stress-strain curve, the yield regions exhibit an important difference. In hard α-keratins, the yield region ends at a strain of about 0.30, whereas in dry slime threads the plateau often continues to a strain of about 0.70 to 0.80[5]. It is well-established that in hard α-keratins the disruption and extension of α-helices occurs in both the yield and post-yield regions, and ends at a fibre strain of about 0.80[6] (Bendit, 1960). This suggests the possibility that in dry slime threads, the entire α→β transition occurs in the yield region, and the post-yield region is governed by other processes.

Application of the analysis developed in Chapter 2 provides further insights. If we assume that the terminal domains in dry thread IF dimers are glassy with an

[5] I use the qualifier "often" because the variability in the length of the plateau region was substantial, which was most likely due to the pre-straining of some fibres during their isolation from water into air.

[6] Most hard ⍺-keratin fibres break at a strain of about 0.45 in water. Much higher extensibilities can be obtained by slowly stretching the fibres in steam. From these experiments it was shown that the α→β transition is complete by a strain of about 0.80 (Bendit, 1960).

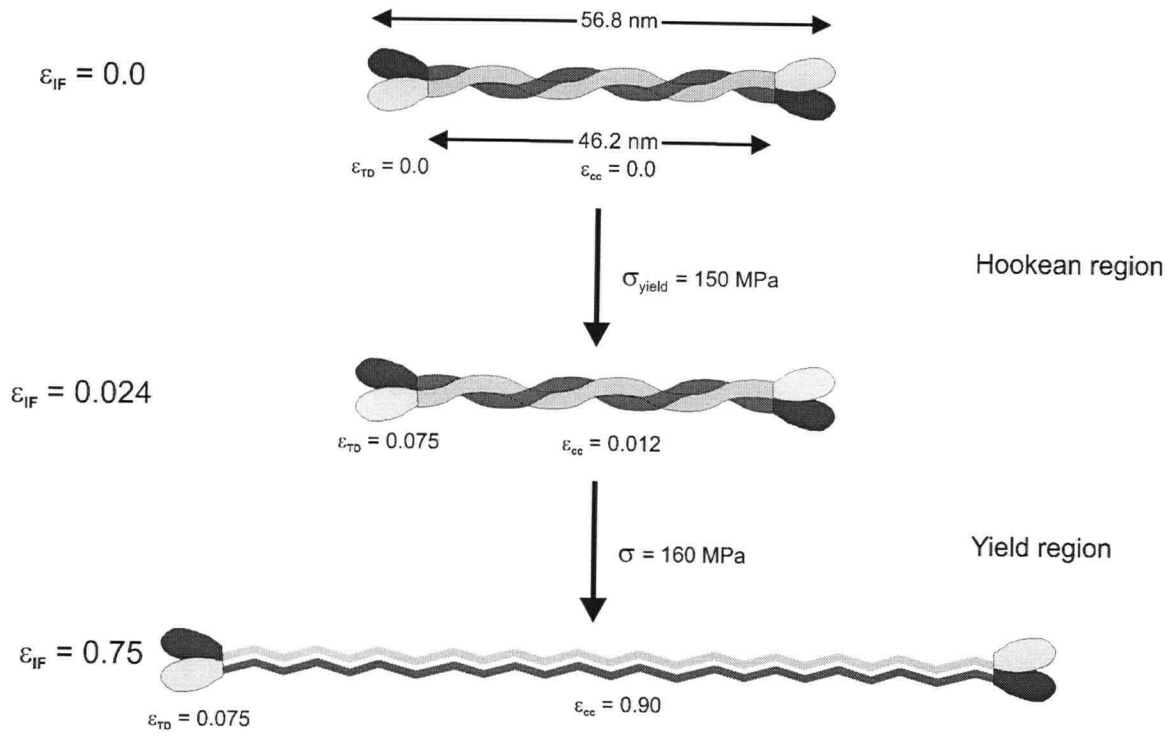

Fig. 3.10. Proposed mechanical behavior of IF dimers in dry slime threads in the Hookean and yield regions. The model is based on the dimer dimensions proposed in Chapter 2, and the assumption that in the dry state the terminal domains are glassy with a stiffness of 2 GPa. Based on these assumptions, the stiffness of the coiled coils in the dry state is about 12 GPa. Note that in contrast to hydrated dimers, the terminal domains are strained relatively little in the dry state. Note also that this two-dimensional depiction does not take into account the helical twists of the coiled coil, which must either be taken up by the terminal domains, or result in helical β-sheets.

initial stiffness of 2 GPa (i.e. 3 orders of magnitude higher than in the wet state), it is possible to estimate the coiled coil strain at which the yield region ends (Fig. 3.10). This analysis suggests that the coiled coil strain at the end of the yield region is about 0.90, which is a bit lower than the theoretical maximum of 1.25 calculated for an α→β transition (Hearle, 2000). While this discrepancy leaves open the possibility that the α→β transition continues on into the post-yield region in slime threads, as it does in hard α-keratins, it is equally likely that the theoretical strain is never achieved due to conformational constraints that arise from untwisting of the coiled coils.

The increased length of the yield zone in dry slime threads as compared to hard α-keratins unfortunately does not help distinguish the two theories of keratin mechanics, because they both predict such a result for cross-link and matrix-free keratins, albeit for different reasons. The C/H model, which emphasizes the role of an elastomeric matrix in the post-yield upturn, predicts a longer yield region in slime threads due to their lack of a matrix. The W/Z model, which denies any significant role of the matrix, attributes the post-yield upturn to the opening up of α-helical domains that are stabilized by cystine cross-links, and predicts a longer yield region in slime threads due to their lack of inter-dimer cross-links. Although the W/Z model is fairly explicit about the post-yield rise in stress being due to the opening of IF α-helical rod domains stabilized by cystine cross-links, previous so-called "series-zone" models were not so explicit, and simply attributed the rise in stiffness to regions of the IF α-helices that are more difficult to open. If IFs are involved in the post-yield rise in stress in hard α-keratins, it must be via cystine cross-links, because the yield zone in cross-link free IFs is fairly homogeneous from beginning to end, and shows no keratin-like upturn at a strain of 0.3.

Furthermore, if the dehydration hypothesis is correct, and the matrix is robust enough to resist swelling of the IFs and keep them largely dehydrated, then it must be robust enough to resist uniaxial extension of the IF-matrix composite as well. This implies that the matrix is not only capable of contributing to the recovery of the composite, but is also a likely candidate for the post-yield rise in stiffness.

Post-yield region

The above analysis makes it fairly clear that whereas the α↔β transition in hard α-keratins occurs in both the yield and post-yield regions, in dry slime threads, the transition occurs almost exclusively in the yield region with little increase in stress. What then is going on in the dry slime thread post-yield region? The C/H model predicts that when all of the IF α-helices are completely extended, stiffness rises abruptly to that of a β-sheet crystal, and remains constant until failure (Hearle, 2000). This behavior may actually be accurate for an individual IF, but is not completely consistent with what happens in dry slime threads, in which stiffness in the post-yield region is not constant, but rising (Fig. 3.6B). The most plausible explanation for this rising stiffness is a strain-induced ordering of β-sheet crystals in this region.

While providing a useful baseline for the mechanics of matrix and cross-link free

IFs, mechanical data from dry slime threads cannot fully distinguish between the two competing theories of hard α-keratin mechanics. One of the reasons for this is that the theories differ mostly in whether certain mechanical properties are attributed to the matrix or to intra-IF covalent cross-links. Dry slime threads lack both matrix and covalent cross-links, so it is difficult to assign mechanical differences conclusively to one or the other. Of course, the establishment of slime threads as a useful keratin model in this thesis will pave the way for experiments in which slime thread IFs are covalently cross-linked or even imbibed with a matrix, providing a means to evaluate the effects of the presence or absence of each.

Dry IFs are remarkably tough

The high breaking strength of dry slime threads ($\sigma_b = 530 \pm 40$ MPa) and their high extensibility ($\varepsilon_b = 1.0 \pm 0.1$) combine to make them one of the toughest biological materials known, with an energy to break of 240 ± 20 MJ/m^3 (Table 3.2). Such impressive properties for matrix-free IFs raise the question of why hard α-keratins have a matrix at all, when undiluted dry IFs are stiffer, stronger, tougher, and have a higher yield stress (Table 3.5). Based on the analysis presented in this chapter, one of the roles of the matrix is to keep the IFs from fully hydrating in water. Horse hooves made purely of IFs would be of little use for walking across a river or marsh if they swelled and softened in the manner of slime threads. Cystine cross-linking could be used to by-pass the soft terminal domains, but the yield stress would still be prohibitively low. Furthermore, without a matrix, deformations past the yield point would likely be permanent, which is not a problem for disposable structures such as slime threads, but would definitely be a problem in more permanent structures such as hooves, horns and claws.

The matrix is likely to be important in the dry state as well. One of the reasons why dry slime threads are so tough has to do with their small diameter, which make them extremely unlikely to possess flaws that are large enough to propagate. However, larger structures made completely of IFs would be increasingly susceptible to premature failure due to crack propagation along planes of weakness between IFs. Holding the IFs together with a softer matrix not only would allow the material to withstand compression loads better, but could also play a crack-blunting role at matrix-IF interfaces. These positive contributions to keratin mechanics likely balance the diluting effect that the matrix has on α-keratin toughness, strength, and stiffness.

Table 3.5. Mechanical properties of dry slime threads compared with dry wool (i.e. hard α-keratins), spider dragline silk, mussel byssal threads, and collagen.

	E_i (MPa)	Ultimate ε	Strength (MPa)	Toughness (MJ/m³)
Dry slime threads	7700 ± 500	1.0 ± 0.1	530 ± 40	240 ± 20
Dry wool[1]	5600	0.35	200	45
Spider dragline silk[2]	10000	0.3	1100	160
Mussel byssal threads, distal[3]	870	1.09	75	45
Collagen (tendon)[4]	1200	0.13	120	6

Data are from [1](Peters and Woods, 1955), [2]Denny (1976), [3](Bell and Gosline, 1996), and [4](Pollock and Shadwick, 1994).

CONCLUSIONS

Swelling and mechanical tests of dry hagfish slime threads support the hypothesis that IFs in hydrated hard α-keratins are maintained in a partially dehydrated state. Dehydration of the IFs not only increases their initial stiffness and yield stress, but may also inhibit formation of stable β-sheets, allowing for more effective recovery of IFs following post-yield deformation. These results suggest a novel function of the keratin matrix, which is to limit hydration of the keratin IFs. The results also suggest that the differences in the properties of hard and soft α-keratins can be attributed to the hydration state of the IFs in these materials.

CHAPTER 4: THE BIOMECHANICS OF HAGFISH SLIME

INTRODUCTION

Although the hagfishes possess several unique characteristics that set them apart from other animals, they are best known for their slime. In fact, many of their common names include the word slime, such as "slime eel" and "slime hag." The Atlantic hagfish, *Myxine glutinosa*, is twice named for its slime (*myx* = slime, mucus, *glutin* = glue). Many animals release slime under stress, but hagfish slime is unique because of the large volumes that are produced (up to several liters from a single hagfish), the incredible speed with which it appears, and the fact that it contains very fine fibres. The fibres lend strength to the slime, so much so that it can support its own weight when lifted out of water (Fig. 4.1). These fibres are of course the slime threads that I used as a model for understanding the mechanics of intermediate filaments in Chapters 2 and 3. In this chapter, I will explore the function of slime threads in the context in which they evolved – within one of the most unique materials produced by animals.

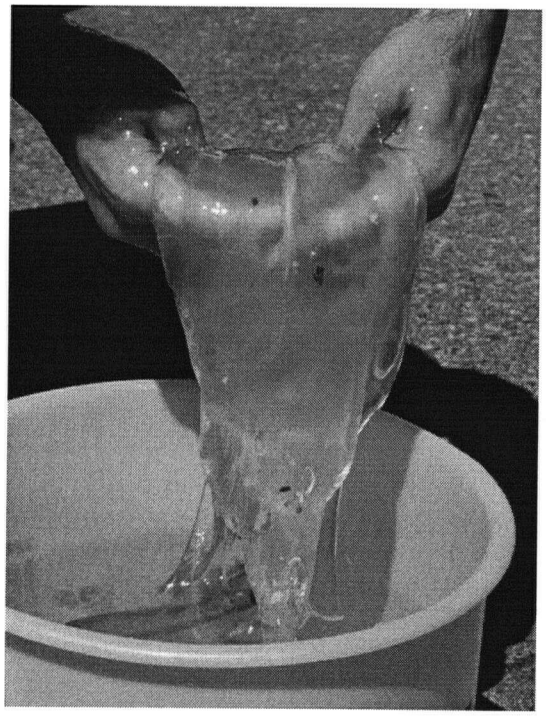

Fig. 4.1. Slime production by a hagfish in seawater. Note the large volume of slime produced and its strength, which allows it to be lifted out of water in a coherent mass.

Hagfish slime has attracted the attention of scientists throughout the ages. In the mid 18th century, Linnaeus wrote the following of hagfishes: "aquam in gluten mutat", or "transforms water into slime." Charles Darwin mentions hagfishes and their slime in his recounting of his time on the *H.M.S. Beagle* (Darwin, 1842), and the great German anatomist Johannes Műller (1845) described the structure of hagfish slime glands and their contents. For obvious reasons, older studies of hagfish slime tended to focus on morphology (Blomfield, 1882; Kolliker, 1860; Schreiner, 1916), while more recent work has focused on molecular aspects, with particular emphasis on the proteins that make up the fibrous component of the slime (Downing et al., 1981a; Downing et al., 1981b; Koch et al., 1995; Koch et al., 1994).

The hagfish slime gland

The slime originates within numerous slime glands located along both sides of the hagfish's body. *Eptatretus stoutii,* the species used in this study, typically possesses about 150 slime glands. The glands are dominated by two cell types, gland mucus cells (GMCs), and gland thread cells (GTCs), which are responsible for the mucus and fibrous components of the slime, respectively. GMCs and GTCs originate in the germinal layer of the gland and are pushed toward the gland lumen as they mature. The glands are approximately spherical in shape and are encased by a capsule of connective tissue, which is in turn surrounded by a thin layer of striated muscle fibres (Downing et al., 1984). When these muscle fibres contract, mature GMCs and GTCs are ejected from the gland via the holocrine mode into seawater through the gland pore (Downing et al., 1981b).

Gland mucus cells

The mucus component of hagfish slime originates in the GMCs, which are distinct from the small and large mucus cells (SMCs and LMCs) found in hagfish epidermis (Spitzer et al., 1979). The sole function of GMCs is to package collapsed mucins into membrane-bound vesicles that are 3 to 5 μm in diameter (Downing et al., 1981a). When mature GMCs are ejected from the slime gland, they lose their plasma membrane (even if ejection occurs in the absence of water) and release thousands of vesicles that swell and rupture upon contact with seawater, thus forming the mucus component of the slime.

Compared to GTCs, GMCs and their secretion products are poorly studied. The genes for the molecules that make up the mucus component of hagfish slime have yet to be characterized, but histological staining and immunolabeling suggest that they are mucins (Koch et al., 1991b). Mucins are very large (0.5 to 30

MDa), heavily glycosylated proteins, in which up to 85% of the dry weight is carbohydrate (Gum, 1995). Typically hundreds of oligosaccharides are linked to the mucin protein core via serine and threonine residues. Many of the terminal saccharides are ionized at physiological pH, which contributes to the highly hydrophilic nature of mucins, as well as their ability to swell rapidly from a collapsed state (Tam and Verdugo, 1981). SDS-PAGE of isolated hagfish slime vesicles demonstrates that they contain very high molecular weight molecules that are too large to enter a stacking gel. Hagfish slime mucins differ from other mucins in that their total carbohydrate content is only 12%, and they have lower serine and higher sulfate contents (Salo et al., 1983).

Luchtel et al. (1991) studied the osmotic properties of hagfish slime mucin vesicles and discovered that they are stable in solutions of impermeant ions greater than 800 mOsmol/L. The implication of this result is that the vesicle interior is actually hypo-osmotic to seawater (s.w. osmolarity ≈ 1000 mOsmol/L), which is surprising given the explosive nature of hagfish slime hydration. They also inferred that the vesicles are permeable to a variety of ions, including all cations and monovalent anions tested. This implies that vesicle swelling in seawater is driven first by an influx of ions down a concentration gradient (mostly Na^+ and Cl^-), rather than by a simple influx of water down an osmotic gradient (Luchtel et al., 1991). Because pure lipid bilayers are extremely impermeable to ions (Gennis, 1989), these results also imply that the vesicles possess at least two kinds of ion channels – one for cations and another for anions.

Gland thread cells

The fibrous component of hagfish slime originates in the GTCs. The function of these cells is to package keratin-like intermediate filaments into a single, continuous, intricately coiled protein thread that in mature cells occupies the vast majority of the cell volume (Downing et al., 1981b) (Fig. 1.4). GTCs are large and roughly ellipsoidal in shape, with distinctive blunt and pointed ends. The length of the GTC thread has never been measured directly, although most agree that when laid from end to end it is "several" centimeters long (Downing et al., 1981b; Fernholm, 1981; Ferry, 1941; Newby, 1946). Based on estimates of the number and length of the loops in a GTC, Fernholm gives an estimate of slime thread length of 6-11 cm. By modeling the GTC as an ellipsoid in which a slime thread with a diameter 1.0 μm is packed with a packing efficiency of 0.7, Downing et al. (1981b) estimate thread length to be 23.7 cm in average-sized GTCs, and up to 60 cm in larger GTCs. In this chapter, I will present data from experiments in which

thread length is measured in a more direct manner.

Although thread assembly is not well-understood, Downing et al. (1984) put forth a model for thread assembly and packaging within GTCs based on a detailed study of GTC maturation. In this model, a short "primal thread" arises near the blunt end of the cell near the nucleus. The primal thread is believed to be capped at one end and increases in length via the addition of IFs at the other. Thread diameter increases by the addition of IFs laterally. This model is consistent with the changes in thread morphology that occur as immature GTCs develop into mature thread cells, but does not explain how the cell regulates thread diameter and quality and achieves such exquisite packing.

The mechanism of assembly aside, simply describing the anatomy of the thread within mature GTCs is not trivial and has attracted the attention of several investigators (Downing et al., 1981b; Fernholm, 1981; Newby, 1946). The current understanding of thread packing is difficult to summarize in a few sentences, and the above references (especially Fernholm) should be consulted for a complete description. Briefly, the majority of the thread is organized as if it were laid down in staggered loops in an egg-shaped barrel. Within these loops, the thread takes on three main trajectories – an ascending trajectory toward the pointed end of the cell, a curved trajectory in which the thread winds circumferentially around the cell periphery for about 60°, and a descending trajectory toward the blunt end. Because of the 60° peripheral runs, the loops are staggered around the longitudinal axis of the cell, and about six of these three-dimensional loops define a cone-like structure that points toward the pointed end of the cell. Although it is meaningless to delineate the beginning of one cone and the end of another, for the purpose of this description, successive cones are neatly nested on top of each other, and occupy the majority of the cell volume. The packing of the loop segments in the peripheral runs gives a cabled appearance to the surface of intact slime thread skeins. Both Fernholm (1981) and Downing et al. (1981) demonstrate that the cabling effect is an illusion, which is sensible since twisting of the thread around itself would hinder effective unraveling. At the blunt end of the cell, the hollow space inside the cones is filled by a series of loops that are oriented parallel to the longitudinal axis of the cell. Fernholm (1981) compares the staggered loop packing of the thread within GTCs to the faked patterns created by sailors to prevent the fouling of lines as they are run out. In this chapter I examine the handedness of thread coiling within slime thread skeins, which has implications for the mechanism of thread packing in developing GTCs.

In addition to providing an estimate of thread length, Downing et al. (1981b) also reveal that threads within GTCs are tapered. In this and a subsequent publication (Downing et al., 1984), they claim that the thread is thickest near the pointed end of the cell, and thinnest near the blunt end. They base this conclusion on two pieces of evidence. The first is that longitudinal cross-sections of immature GTCs near the so-called "mitochondrial rich zone" exhibit numerous threads in cross-section, with those close to this zone having a relatively small diameter, and those distal or lateral having relatively large diameters. The second piece of evidence comes from transverse cross-sections of more mature cells that exhibit smaller diameter threads axially, and larger threads at the periphery. In light of the nested cone packing arrangement described above, this suggests that thread diameter decreases toward the blunt end of the cell. In this chapter, I present new data that suggest that the threads are in fact tapered at *both* ends, with the largest diameter occurring in the middle of the thread.

Slime formation, volume, and concentration

Little is known about the exact mechanism of slime formation, i.e. how a small amount of slime exudate can interact with seawater to form a large volume of fibrous slime. Koch et al. (1991) attempt to elucidate the steps of slime formation by studying the hydration of slime exudate stabilized in a high osmotic strength citrate buffer. Gradual dilution of stabilized slime with water allowed them to monitor both the gradual hydration of the mucin vesicles and the unraveling of the slime thread skeins, as well as interactions between them. They propose that the transformation from exudate to slime occurs in the following sequence: unraveling of the skeins, followed by aggregation of mucin vesicles along elongated slime threads, followed by rupture of the vesicles and release of mucin-like contents that adhere to the thread (Koch et al., 1991b). These observations are interesting, but their relevance to the process of slime formation by hagfishes in seawater is dubious at best considering all the differences (pH, ionic strength and composition, presence of chelators) between seawater and diluted stabilization buffer.

Estimates of the sliming capacity of a single hagfish vary widely in the literature. While most reports are anecdotal, Strahan (1959) applied a standardized approach to measuring the sliming abilities of *M. glutinosa* and concluded that a single 33 cm hagfish can produce about 540 mL of slime. Ferry (1941) states that in a given sliming event, a hagfish can produce "several times its own volume of slime." Although he does not state it explicitly, the implication is that this is just a

fraction of their total capacity. Koch et al. (1991) provide an estimate of over 8 L for *E. stoutii* based on their experiments with stabilized slime. Goode and Bean (1895) give a similar estimate of 7-8 L. Couch (1878) claims (somewhat outrageously) that a single *M. glutinosa* can produce 3 to 4 cubic feet of slime, or about 100 L.

Regardless of which of the above estimates is correct, hagfish slime must be more dilute than most mucus secretions, which typically are composed of about 30 mg mucin (dry wt.) per mL (Sellers and Allen, 1989). If we assume that Strahan's estimate of 540 mL is correct, and the slime is as concentrated as typical mucus secretions, then a hagfish must secrete over 16 g of mucins (dry wt.), which seems highly unlikely, especially since this estimate doesn't take the slime threads into account. Using Koch et al.'s estimate of 8 L, the figure rises to 240 g of dry mucins, which is greater than the mass of a typical hagfish! Clearly, the concentration of mucins in hagfish slime cannot be as high as it is in other mucus secretions, but how and why it is lower is not clear. In this chapter, I will present data on the concentration of both mucins and threads in naturally formed slime, and will provide new data for the maximum sliming capacity of *E. stoutii*.

Whole slime mechanics

The great polymer rheologist J.D. Ferry published a single paper on hagfish slime (Ferry, 1941), in which he concludes the following:

> The heterogeneity of the original slime and its irreversible contraction render it unsuitable for study of mechanical properties in relation to its composition and structure.

Ferry's words seem to have been taken to heart; not a single quantitative study of hagfish mechanics has been published to this day. Researchers have offered several qualitative descriptors of hagfish slime such as "viscous," "elastic," "tough," "stringy," and "gelatinous," but these are hardly satisfying or even consistent. Koch et al. (1991) mention that the viscosity of hagfish slime decreases in the presence of the reducing agent dithiothreitol, but do not provide any viscosity data in the paper. One aspect of the behavior of the slime that is fairly well documented is its tendency to contract, especially when it is agitated. Ferry (1941) estimates that over time, slime volume decreases by a factor of 50, resulting in a tough mat of fibres that are "soft and elastic" when wet, and "strong and flexible" when dry. In this chapter I present data for the mechanical properties of the mucus component of the slime, which together with the slime

thread mechanics presented in Chapter 2 can be integrated into a model of hagfish slime mechanics that takes into account the mechanical properties of the mucins and threads.

Mucin-thread interactions

Koch et al. (1991) conducted experiments in which stabilized mixtures of slime thread skeins and mucin vesicles were mixed into water, and the cohesiveness of the slime assayed by measuring the "removable mass," or the mass of slime that could be removed from the test beaker with a metal hook after stirring. Solutions of mucin vesicles or skeins alone resulted in dramatically less (by two orders of magnitude) removable mass than solutions in which both were present. These experiments demonstrate that the mucin and fibrous components of the slime act synergistically to organize water, and imply that the interaction between them is an important factor in determining the properties of the slime. In the same study, Koch et al. show that dithiothreitol decreases both the viscosity and removable mass of slime, suggesting that disulfide bonds (almost certainly among mucins) are also an important determinant of slime cohesion.

Is hagfish slime a fibre-reinforced composite?

One way to understand hagfish slime as a material is to model it as a fibre-reinforced composite, with discontinuous slime threads forming the reinforcing fibrils and mucins forming the soft matrix. When a composite material is strained, stress is transferred between the matrix and fibrils via shear at the fibril-matrix interface, with shear stress being highest at the fibril ends, and tensile stress highest in the middle of the fibril (Piggott, 1980). In order for the fibrils to strengthen the composite, they must be long and thin enough to allow for effective stress transfer from the matrix. If stress transfer is not effective, the fibril stress will never approach the fibril strength and the fibrils will provide little strength reinforcement (Trotter and Koob, 1989). The critical fibril aspect ratio (s_c = fibril length divided by radius) at which reinforcement is effective is determined by the ultimate stress (σ_{fu}) of the fibril divided by the yield stress of the matrix in shear (τ_{my}) or:

$$s_c = \sigma_{fu} / \tau_{my} \qquad \text{(Eq. 4.1)}$$

If the aspect ratio of the reinforcing fibrils is greater than s_c, then force transfer will be adequate to load the fibrils maximally, and they will strengthen the composite. If the aspect ratio is lower than s_c, the fibrils will not be loaded maximally, and they will be less effective at reinforcing the composite. In this

chapter, I will evaluate whether hagfish slime behaves as a fibre-reinforced composite using the slime thread mechanics reported in Chapter 2, as well as thread length and diameter measurements reported in this chapter. Specifically, these data include measurements of slime thread length and taper, as well as measurements of the concentration of mucins and threads in naturally formed slime. In addition, I present high speed video data of hagfish sliming that provide new insights into the sequence and timing of the events involved in slime dispersal and hydration.

MATERIALS AND METHODS

Scanning electron microscopy of slime thread skeins

SEM images were obtained from twenty different thread cells. To obtain clean thread cells free of mucin vesicles, slime exudate was first collected and stabilized in the aqueous stabilization buffer (ASB) described in Chapter 2. Stabilized slime was filtered through 54 μm nylon mesh, which retained the thread cells and allowed the mucin vesicles to pass through. After washing the filter disk with excess ASB, thread cells were removed from the disk by gentle shaking with 10 mL of ASB in a capped vial. Thread cells were fixed for two hours in 4% glutaraldehyde in ASB, rinsed with fresh ASB, and then rinsed with 0.2 M cacodylate buffer (pH 7.1). Thread cells were transferred onto a Nucleopore Track-Etch membrane (13 mm diameter, 6 μm pore size, Corning) in-line with a 5 mL syringe. The cells were dehydrated with an ethanol series consisting of 5 mL of the following ethanol solutions: 30%, 50%, 70%, 80%, 90%, 95%, 100%, 100%. While still wet with 100% ethanol, the filter disk was transferred into a Balzer CPD 020 critical point drying apparatus (Bal-Tec, Manchester, NH, USA). Before critical point drying, the ethanol was replaced by ten rinses with liquid carbon dioxide. Dried cells were immediately transferred into a Nanotech Semprep 2 gold sputter coater, and sputter coated under vacuum for 3.2 minutes.

Concentrations of threads and mucins in native slime

Hagfish were induced to produce a small mass of slime in their 200 L aquarium by giving them a pinch on the tail. Care was taken to insure that the slime was produced by hagfish swimming in the middle of the water column rather than close to the bottom or surface, which could have constrained slime hydration. The mass of slime was gently collected by scooping it into a plastic kitchen

colander lined with 54 μm nylon mesh. As the colander was lifted out of the aquarium, free water was allowed to run out of the bottom through the mesh, and the colander was tipped slightly to allow free water sitting on top of the slime to spill out. The contents of the colander were transferred to a bucket for the measurement of slime volume. Threads were removed from the slime by twirling them onto a glass rod until they collapsed and squeezed out most of the entrapped mucins and water. The threads were removed from the glass rod by simply sliding them off the end. This technique was very effective at collecting the vast majority of the threads in the slime, and concentrating them into a fibrous ring that could be easily handled for subsequent purification and drying. The ring of threads was placed back into the original slime solution to which a pinch of dithiothreitol (DTT) was added. Along with gentle heating of the slime (to about 60 °C), DTT helped in the removal of mucins that were still bound to the threads. The threads were treated in this way until they were no longer slippery to the touch (about 30 minutes), at which point they were removed, rinsed with several changes of distilled water, and dried in an oven at 80 °C for the determination of dry mass. Thread concentration was calculated by dividing the dry mass of threads by the total volume of the slime collected.

Mucin concentration was measured by dialysis of 50 mL of the remaining slime solution in Spectra/Por dialysis tubing (12-14 kDa cut-off, Spectrum Laboratories Inc., Rancho Dominguez, CA, USA). Mucin samples were dialysed against 5 L of distilled water in a chilled room (4 °C) for eight hours, after which the process was repeated three more times. Preliminary trials demonstrated that the above procedure was more than adequate to lower the concentration of salts to a negligible amount. Mucin dry weight was obtained by drying 25 mL of the dialyzed solution in a drying oven at 80 °C. Mucin concentration was obtained by dividing the mass of mucins by the volume of solution dried. Mucin concentrations were adjusted by subtracting out the concentration of material in the distilled water, which was measured by drying down 25 mL of the distilled water used for the dialyses. Mucin and thread concentrations were measured in this way for five independent slime masses.

The high ratio of salts to mucins in the slime made it technically challenging to accurately measure the mucin concentration. In contrast, because the slime threads are insoluble, they were easily separated from the slime and therefore their concentration could be measured with far less error. In order to confirm the mucin concentrations obtained via dialysis, I also measured the mucin concentration via a centrifugation technique I will refer to as "slimatocrit" due to its similarity to the measurement of hematocrit. The premise of this technique is

that the volume ratio of mucin vesicles to threads can be measured by spinning down stabilized slime in hematocrit tubes. From these data, the concentration of mucins in the slime can be calculated from the thread concentration data, which we know are reliable. Slime exudate was collected from anaesthetized hagfish and transferred into a 0.5% toluidine blue in aqueous stabilization buffer solution. Stained and stabilized slime exudate was drawn up into 75 mm microhematocrit capillary tubes, and spun for 10 minutes in a hematocrit centrifuge. Centrifugation resulted in two distinct layers, a GTC layer, and a Toluidine blue stained mucin vesicle layer topped by stabilization buffer (Fig. 4.2). The relative volume of the layers was calculated from their dimensions, which were measured under a dissecting scope with a Filar eyepiece micrometer. Sixteen slimatocrit measurements were made in total.

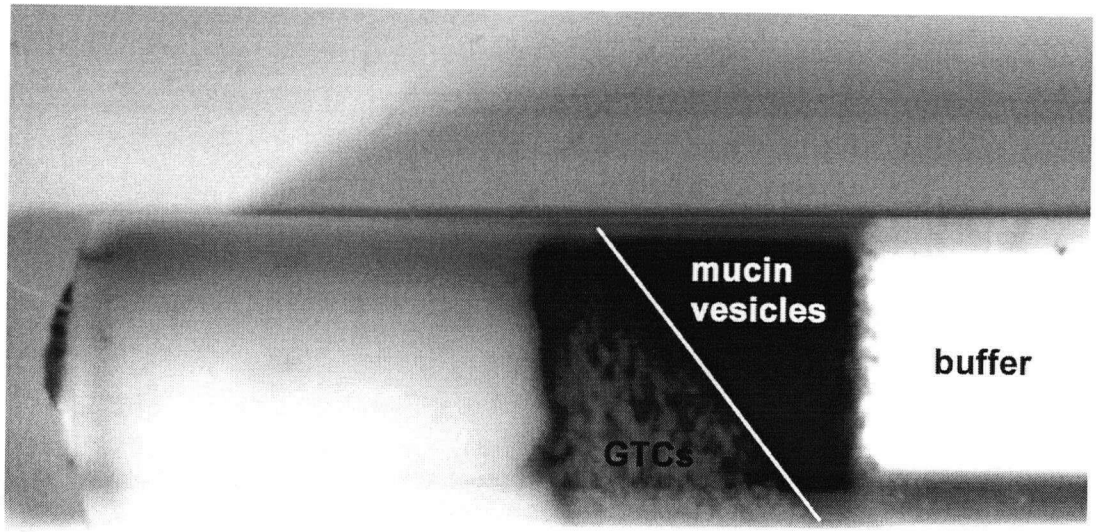

Fig. 4.2. Result of a typical "slimatocrit" trial, in which fresh slime exudate was stained with toluidine blue and spun in hematocrit tubes to measure the relative volume fractions of thread cells and mucin vesicles. Note that mucin vesicles (dark staining) and GTCs make up about equal amounts of the exudate volume.

Slime storage vs. hagfish mass

Measurement of the amount of exudate stored in slime glands was performed on hagfish that were anaesthetized as described in Chapter 2. Hagfish that released slime in the anesthesia bucket were rejected and placed back in the aquarium.

Immediately after losing touch sensitivity, hagfish were removed from the anesthesia bucket, blotted dry, and weighed. The animals were then placed on a chilled dissection tray where they were kept hydrated and cool, except for the area from which slime exudate was collected, which was rinsed with distilled water and blotted dry. Rather than trying to measure the mass of exudate expressed from every slime gland, five glands were chosen as representatives. Exudate was expressed from the glands via mild electrical stimulation. Exudate from all five glands was collected with a spatula and transferred to a capped, pre-weighed microcentrifuge tube. Glands were stimulated until exhausted of exudate. Wet and dry mass were measured using a Mettler H31 balance (Mettler Instruments, Zurich, Switzerland). Exudate samples were dried in a drying oven at 80 °C until the mass was stable over time. The total mass of stored exudate was calculated by multiplying the pooled exudate weight by the total number of glands and dividing by five.

Mucin viscosity

The viscosity of mucins from five different slime masses was measured using an Ostwald viscometer. For each slime mass, viscosity was measured three times, each using a different 7 mL sub-sample, and the values averaged. Transit times through the viscometer were measured with a stopwatch to the nearest 0.01 s. The viscometer was mounted in a water bath maintained at 9 °C, which was the temperature at which the hagfish were held. After introduction into the viscometer, mucin samples were allowed to equilibrate for twenty minutes before testing. Between trials, the viscometer was flushed with the following solvents: 10 mL dH_2O (3x), 10 mL 1 M HCl, 10 mL dH_2O, 5 mL acetone, 5 mL acetone, flushed until dry. Mucin samples were obtained by collecting slime masses from the 200 L hagfish tank using a mesh-lined colander. Slime threads were removed by twirling them out onto a glass rod. Mucins bound to the threads on the glass rod were removed by gently massaging the threads until they were no longer slippery to the touch. Before testing, mucin samples were filtered twice through 54 μm mesh to remove particulates that might have interfered with the viscosity measurements.

Slime thread length

Thread length was measured using an elongated version of the glass microbeam apparatus described in Chapter 2 (Fig. 4.3). A single stabilized slime thread skein was transferred to the seawater-filled test chamber and its respective ends attached to two glass rods as described in Chapter 2. The original intent of this

setup was to slide one rod away from the other until the thread was just taut; the distance between the two rods would then reveal the length of the thread. This plan was confounded by the tendency of the thread to unravel in stages, with the thread going taut at times when there were clearly large sections that had not yet unraveled. Because it was not possible to observe the glass rod under the microscope and simultaneously observe the entire length of the thread for clusters of thread loops, using tautness as an endpoint was abandoned. Instead, thread failure was used as an endpoint and the resting length calculated from the average failure strain of slime threads as reported in Chapter 2 ($\varepsilon_{max} = 2.2$). While the popping open of clusters of loops caused deflections of the glass rod, these were always transient and easily distinguished from the long steady deflection that occurred before failure of the thread. In essence, these length measurements were tensile tests of entire slime threads.

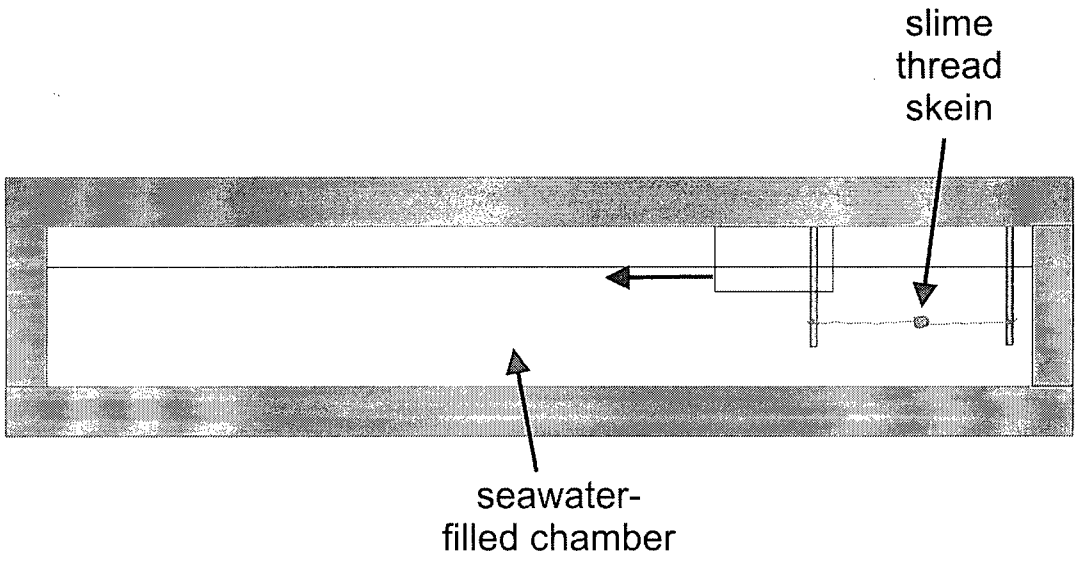

Fig. 4.3. Overhead view of the apparatus used for the measurement of the breaking length of slime threads. One end of the thread was attached to a stationary glass beam, and the other end to a rod mounted on a sliding platform. The breaking length of the thread was measured by observing the deflection of the glass beam as the sliding platform was pulled back. The original length of the thread was then estimated using the extensibility of shorter thread segments. Diagram is not to scale.

Slime thread taper

Diameter measurements were made at eleven approximately equispaced positions along the length of intact slime thread skeins in distilled water. While most slime thread skeins rupture and lose their coiled structure in water, some

remain mostly intact, and it was these that were used for diameter measurements. GTCs were visualized under high power (100x interference contrast oil immersion objective) on a Leitz polarizing microscope (Ernst Leitz Canada, Midland, Ontario) fitted with a Panasonic WV-BL600 video camera. Thread diameter was measured on captured images using Scion Image release v. 3b software (Scion Corp., Frederick, MD, USA).

Congo red staining

"Unperturbed" slime was gently collected from the aquarium in a shallow, mesh-lined colander with a glass slide on the bottom. The slime was allowed to drain and adhere to the mesh before being rinsed with a very gentle, continuous flow of tap water for fifteen minutes. The slime was then rinsed with distilled water, and allowed to completely dry onto the glass slide and the mesh. When dry, the glass slide was freed from the mesh by trimming the slime threads with a razor blade. The slime was stained for one hour, after which the stain was removed by soaking in distilled water for five minutes, followed by a gentle distilled water rinse. "Perturbed" samples were prepared in the manner described above, except a ruler was pushed into the slime and moved back and forth twenty times (to simulate thrashing of a fish) before the sample was collected into the colander.

High speed video

Hagfishes were transferred from their home aquarium to a 10 L aquarium filled with chilled (9 °C) seawater (34‰). Sliming was initiated by a pinch on the tail using long forceps. Digital video of the sliming event was captured at 250 fps using a Redlake MotionScope digital high speed video camera (Redlake-DuncanTech, Auburn, CA). Similar footage was obtained for the introduction of about 0.5 mL of fresh slime exudate into the aquarium using a spatula, or via injection with a syringe fitted with a shortened 18-gauge needle. The capture rate for these trials was 60 fps.

Ionic effects on slime cohesion

Solutions of varying composition were tested for their ability to combine with fresh exudate to form competent slime using a modification of a technique described in Koch et al. (1991). In this study, the authors evaluated slime cohesion by measuring the mass of slime that could be removed from the solution with a metal hook after the introduction of a small volume of stabilized

slime. In the present study, fresh slime exudate was used rather than stabilized slime so that the composition of the final solution could be more tightly controlled. The solutions tested were the following: distilled water, 34‰ artificial seawater (Instant Ocean, Aquarium Systems, Inc., Mentor, OH, USA), seawater + 2.5 mM EGTA, 2.5 mM EGTA, 0.5 M NaCl, 10 mM $CaCl_2$, 0.5 M NaCl + 10 mM $CaCl_2$, 0.33 M $CaCl_2$. All solutions were adjusted to a pH of 7.0, and tested at 20 °C.

Statistics

Removable mass data were analyzed with an ANOVA using SigmaStat v. 2.03. Post-hoc pairwise comparisons were made using the Tukey multiple comparisons test.

RESULTS

GTCs exhibit consistent handedness of thread coiling

All twenty thread cells examined under SEM exhibited the same direction of thread coiling (Fig. 4.4).

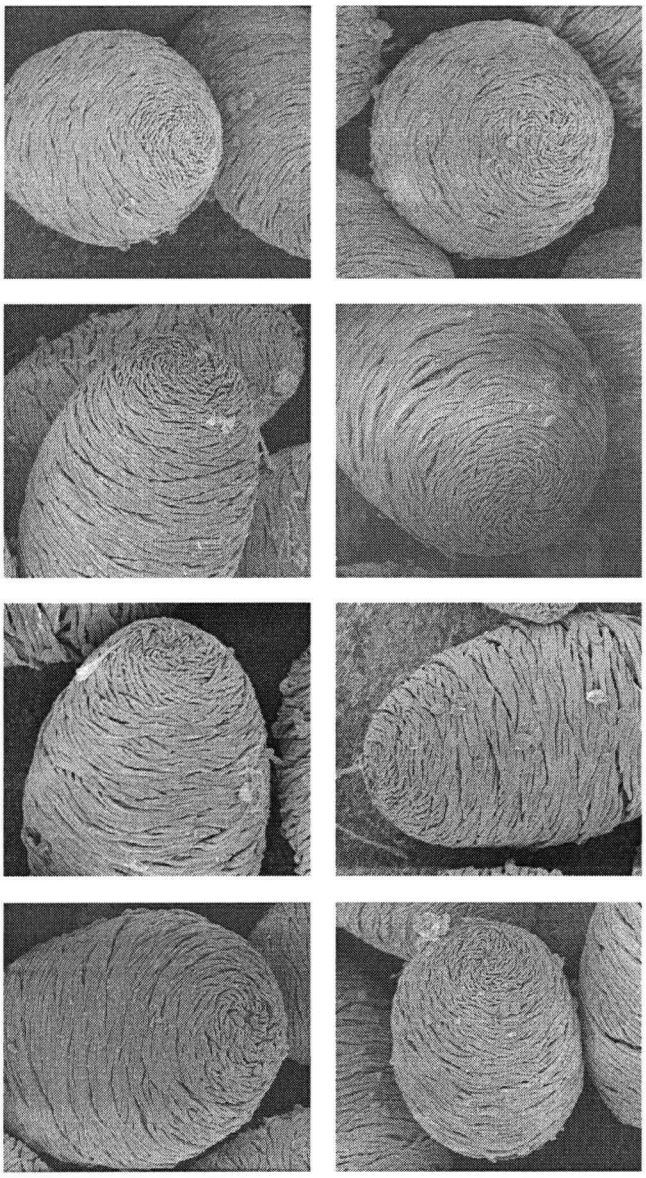

Fig. 4.4. The handedness of coiling was the same in all slime thread skeins examined, suggesting either a helical bias to the growing thread, or a cellular mechanism that regulates the direction of thread coiling.

Hagfish slime is 99.996% seawater, 0.0015% mucin and 0.002% threads

Dialysis and gravimetric analysis of naturally formed slime (minus the threads) revealed a concentration of molecules greater than 12-14 kDa of 15 ± 1 mg/L. Slime threads occur at a similar concentration of 20 ± 3 mg/L. The average volume of slime produced from a single pinch on the tail was 0.91 ± 0.17 L. For the sixteen slimatocrit measurements that were made, the average ratio of mucin vesicle to GTC volume was 1.15 ± 0.1, which predicts a mucin concentration of 17 ± 3 mg/L, assuming that GTCs and stabilized vesicles have the same density. Expressed as percentages (w/v), the mucin and thread concentrations are both about 0.002%.

Stored slime represents about 3.6% of hagfish body weight

Collection of slime exudate from eleven anaesthetized hagfish revealed a significant positive linear relationship with body size ($p = 0.014$, $r^2 = 0.50$), with a regression equation of $S = 0.036 \cdot M_b$, where S is the total mass of stored slime (g) and M_b is the hagfish mass (g). From this equation, one can conclude that slime exudate makes up about 3.6% of hagfish body weight (Fig. 4.5).

The mucin component behaves as a viscous fluid

The average kinematic viscosity of the native mucin solutions was 1.38×10^{-6} m^2/s (SE = 0.003×10^{-6} m^2/s), which is indistinguishable from the viscosity of the seawater controls. The density of the mucin solutions was 1.040 g/mL, making the dynamic viscosity 1.44×10^{-3} Pa-s.

Slime threads break at a length of 34 cm

The average length at failure for the ten slime threads tested was 34 ± 1 cm. Because a small length of thread at either end was used to attach the slime thread to mounting rods, this value is a slight underestimate of failure length.

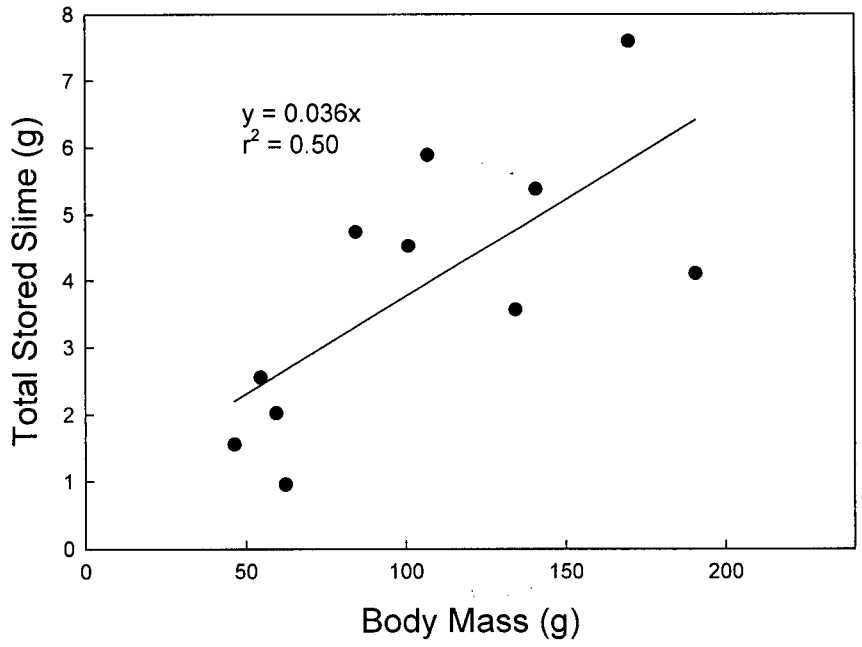

Fig. 4.5. Scaling of stored slime mass with body mass. The slope of the line suggests that stored slime represents 3-4% of the hagfish's mass.

Slime threads are bi-directionally tapered

Measurement of thread diameter within intact slime thread skeins using light microscopy revealed a distinct bi-directional taper (Figs 4.6). Hydrated threads within skeins exhibited a maximum diameter of 3.0 ± 0.4 μm, which occurred in the middle of the skeins. Thread diameter was 1.5 ± 0.2 at the pointed end, and 1.0 ± 0.2 at the blunt end. Inspection of thread diameter under SEM confirms this result (see composite SEM image below Fig. 4.6).

Slime perturbation induces an α→β transition in slime thread proteins

Slime threads from both unperturbed and perturbed slime bound congo red, but only threads from perturbed slime exhibited extensive congo red metachromasia (Fig. 4.7). The few threads that did exhibit congo red metachromasia in unperturbed samples were likely strained during collection or rinsing. Threads within perturbed slime also showed a tendency to form parallel bundles, whereas unperturbed samples did not.

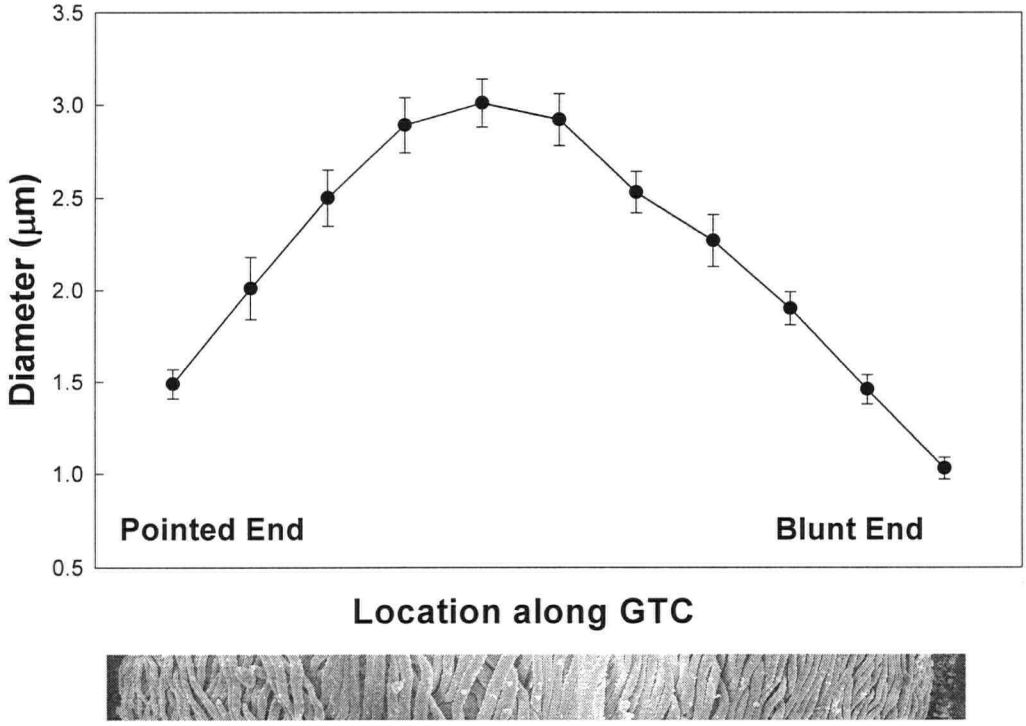

Fig. 4.6. The diameter of the thread on the outside of intact slime thread skeins as a function of position along their longitudinal axis. Note the strong bi-directional taper. Below the graph is a composite of four SEM images along a single thread cell that demonstrate how thread diameter tapers off at both ends of the cell and is largest in the middle.

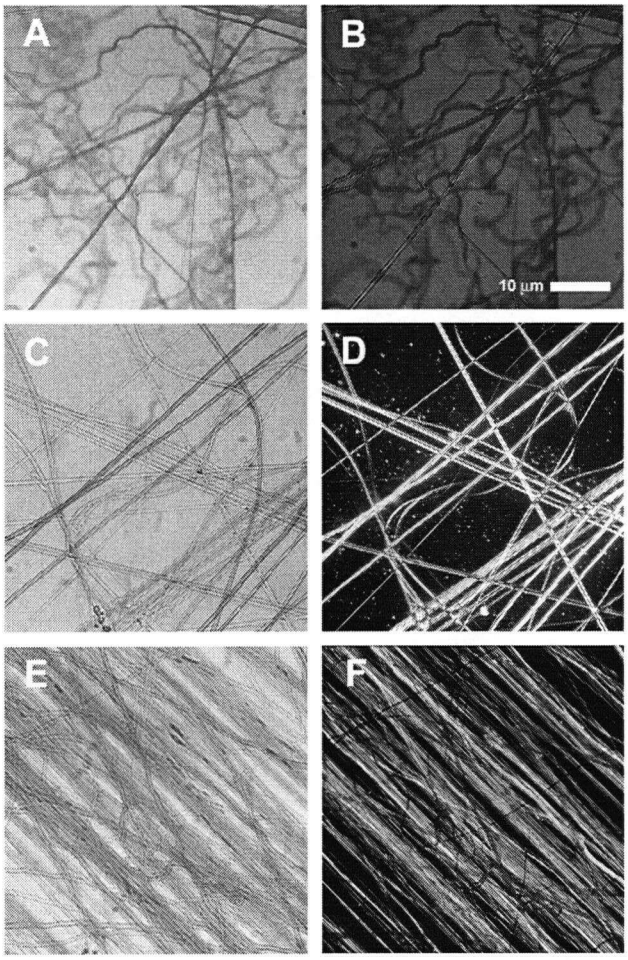

Fig. 4.7. Congo red staining of hagfish slime. Slime threads (but not mucins) bound congo red, but only threads from slime that was physically perturbed showed metachromasia. A) Bright field image of slime threads from unperturbed slime. B) Dark-field (polarizers crossed) image of same threads. Note the lack of congo red metachromasia in most of the threads. C) Bright field image of threads from perturbed slime. D) Same as C, dark field. E) Bright field image showing bundling of slime threads in perturbed slime. F) Same as E, dark field.

High speed video

High speed video of hagfish sliming provided new insights into the mechanism whereby slime exudate is released and interacts with seawater to form fully hydrated and functional slime. These trials confirmed that release of exudate from the slime glands occurs only from glands near the point of contact with the forceps, as opposed to global release from all of the glands (Fig. 4.8). It also became apparent from the video that exudate is forcefully ejected from the slime gland, as opposed to simply oozing out (Fig. 4.9). Some footage also suggested that release of exudate is often preceded by a puffing up of the body in the region from which the slime is released (Fig. 4.10). Because the exudate is opaque when it first exits the gland, and becomes more and more transparent as it disperses and hydrates, it was possible to monitor the rate of slime hydration. In one sliming event (portrayed in Fig. 4.11), the exudate was almost completely transparent about 80 ms after its release from the gland. Some trials suggested that whole body movements of the hagfish aided in the dispersal and hydration of the slime exudate after it was released. In one trial, a hagfish whipped its head through a cloud of exudate, which not only pushed it away from its head, but also greatly helped it to disperse (Fig. 4.12). In the same maneuver, it appeared that the hagfish "sneezed" a bolus of water from its nostril, which also aided in dispersal (Fig. 4.12, 48-60 ms frames). Introduction of freshly collected exudate into seawater using a spatula resulted in very little dispersal and hydration (Fig. 4.13). Similarly, exudate ejected from an 18-gauge needle (inner diameter = 1.07 mm) into seawater was also ineffective at producing normal slime (Fig. 4.14).

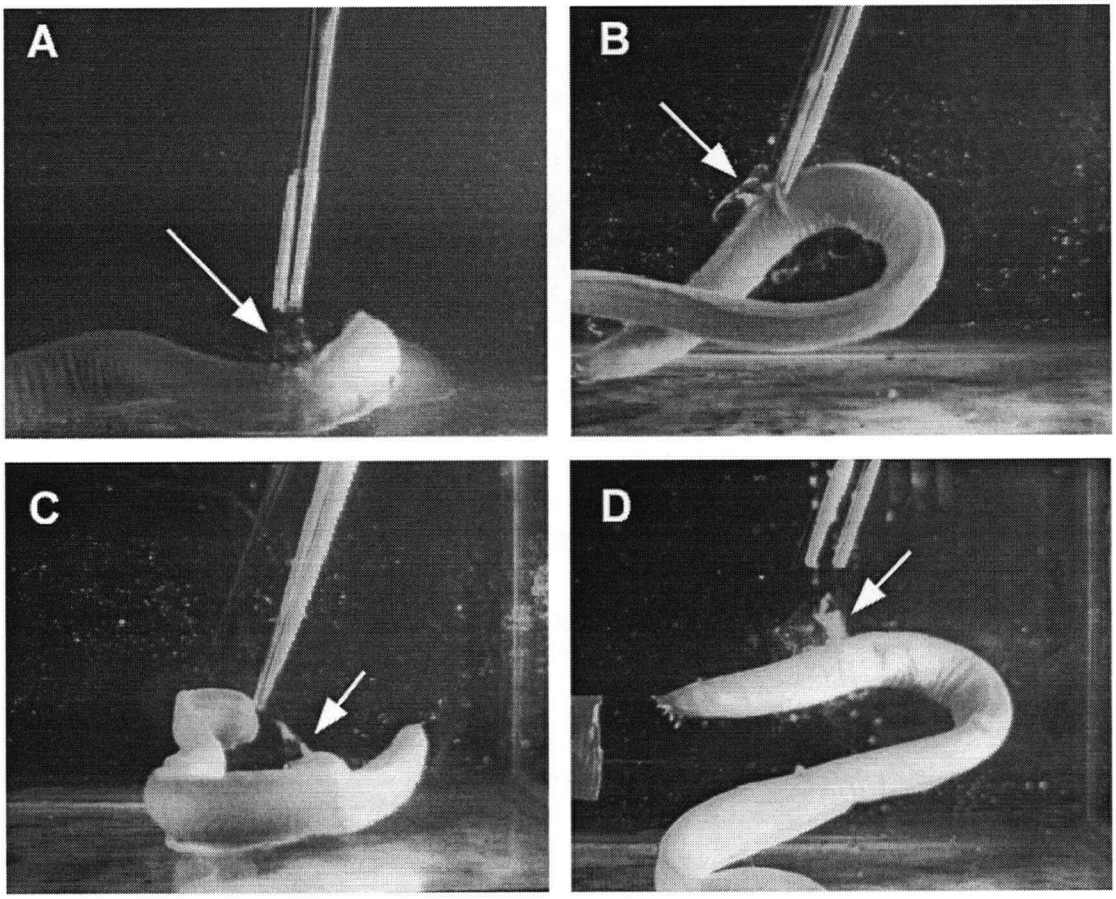

Fig. 4.8. Slime release after provocation was invariably from glands in the vicinity of the point of contact with the forceps, and rarely from other glands. Arrows indicate location of exudate release.

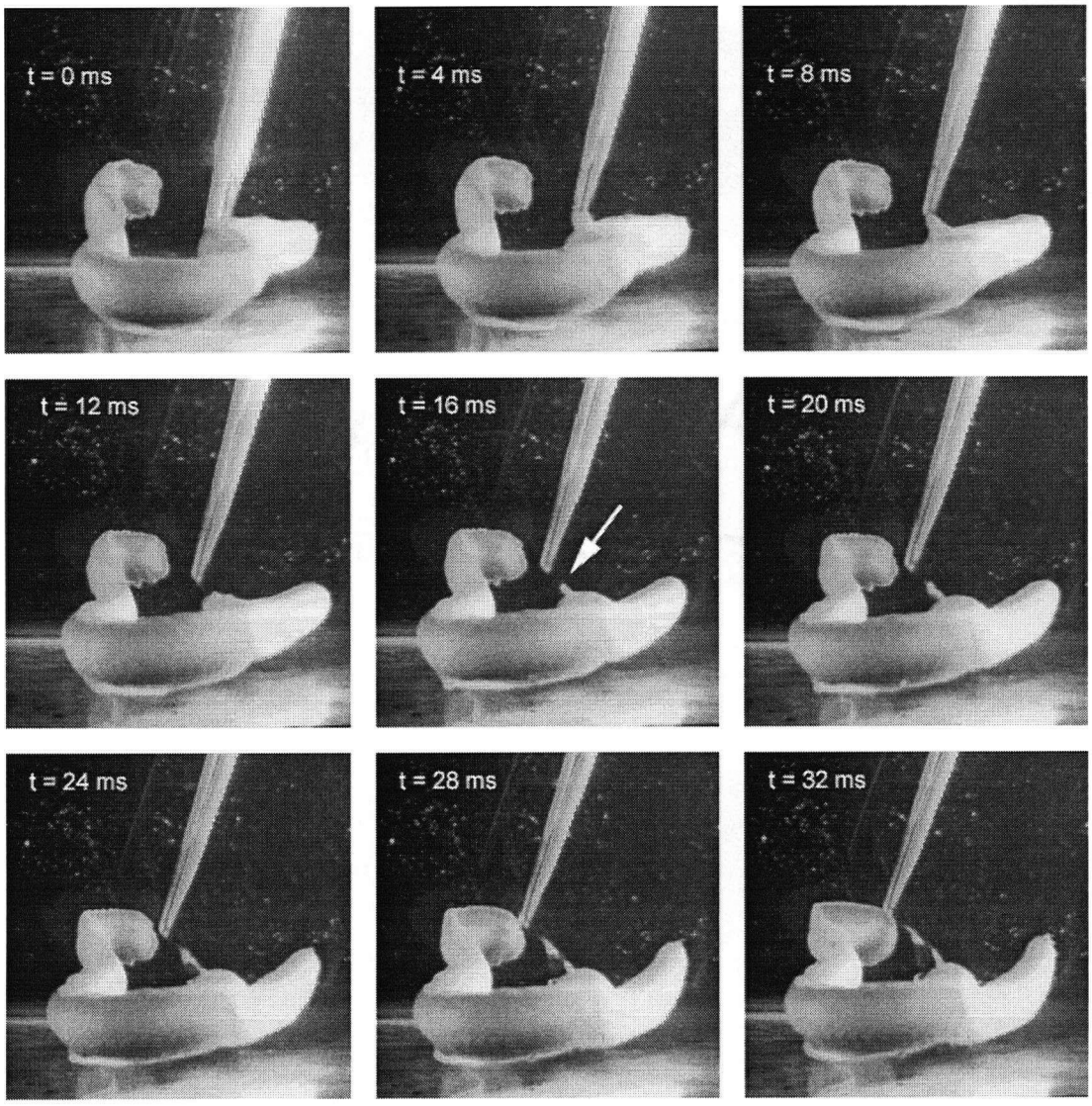

Fig. 4.9. High speed video frames of hagfish sliming reveal that slime exudate is forcefully ejected from slime glands. A jet of exudate is visible shortly after the forceps pull away (white arrow) and is followed by another jet that is probably from another gland.

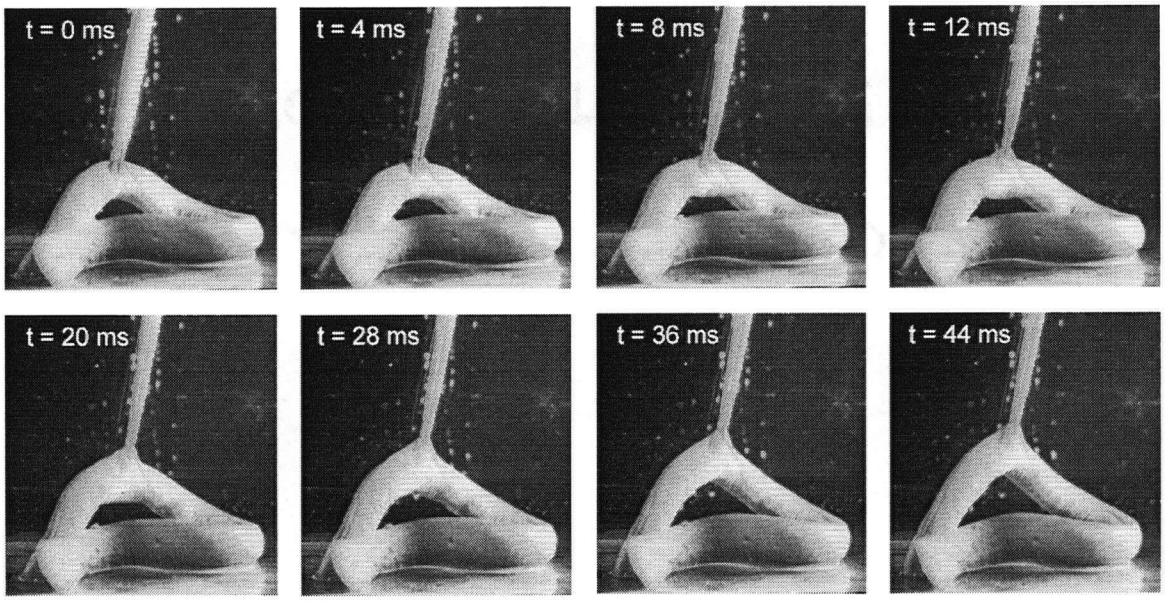

Fig. 4.10. Changes in body diameter in the vicinity of slime exudate release. Note the dramatic bulging in the 12 ms frame, which subsided after exudate was released. Exudate was released at about the 20 ms frame, but is not yet visible, and can begin to be seen in the 28 ms frame.

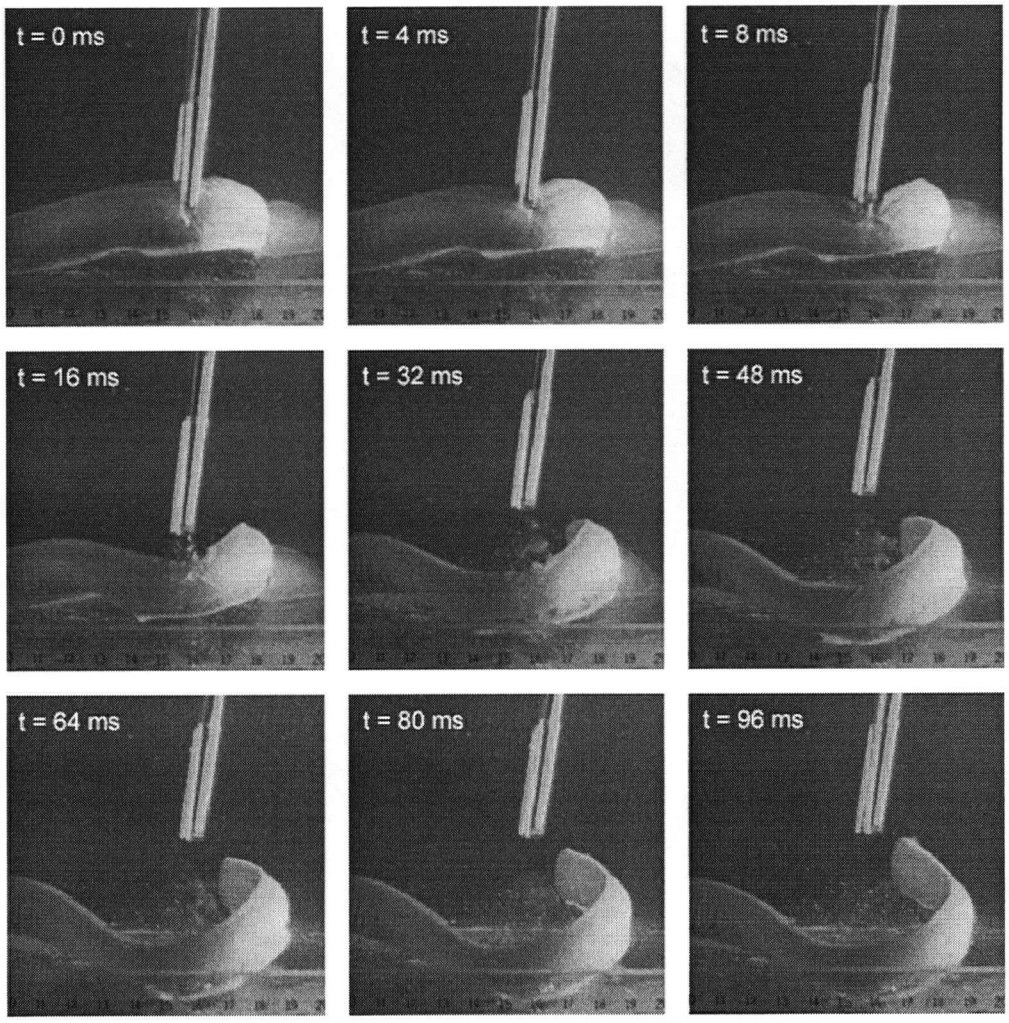

Fig. 4.11. High speed video frames of hagfish sliming reveal that slime hydration is complete in about 80 ms. Slime exudate (milky white substance) is first visible in the 16 ms frame near the forceps, and quickly disperses and hydrates. By 96 ms, the exudate is almost completely transparent. The small white particles are undissolved salt crystals that were kicked up as the hagfish started to struggle.

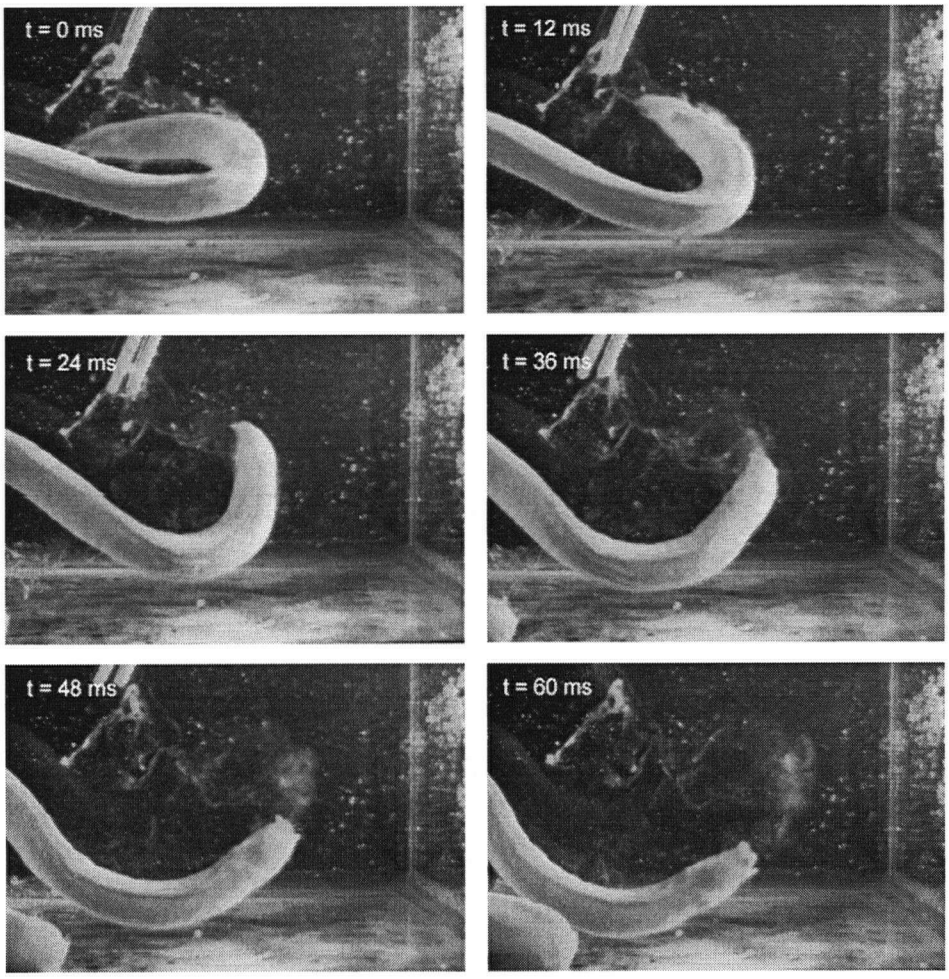

Fig. 4.12. Dispersal and hydration of slime exudate may be facilitated by movements of the hagfish's body. In the above frames, a hagfish whips its head through a cloud of undispersed slime exudate. The pictures also suggest that the hagfish may have "sneezed" water from its nostril as it passed through the exudate, further aiding in its dispersal.

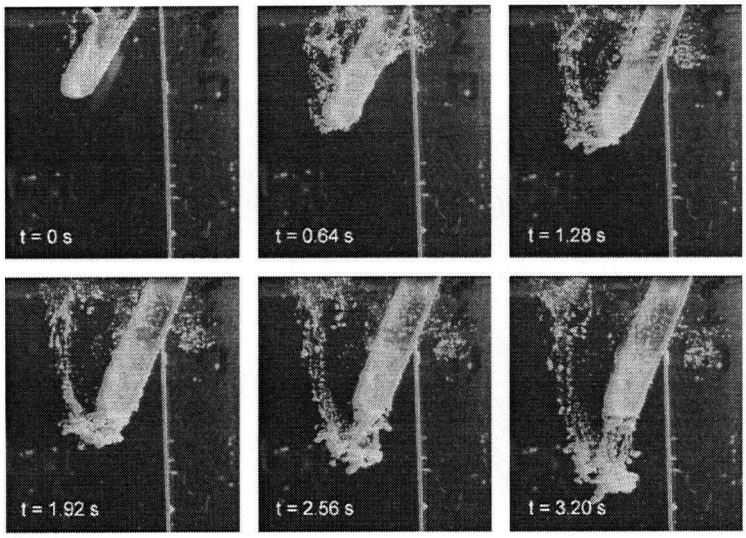

Fig. 4.13. High speed video frames of fresh slime exudate collected from an anaesthetised hagfish and placed directly into seawater. Note that in contrast to slime ejected from the slime glands, the slime undergoes little dispersal and hydration, even after several seconds.

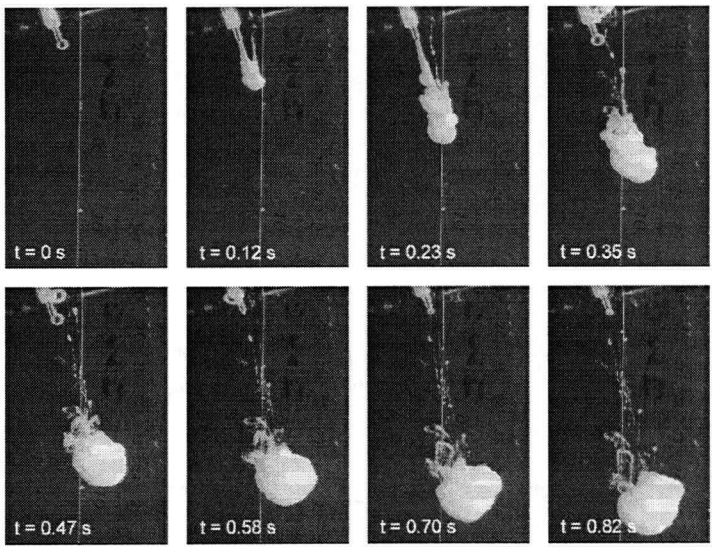

Fig. 4.14. High speed video frames of ejection of fresh slime exudate from an 18-gauge syringe into seawater. Slime volume was about 0.5 mL. Note how ineffective dispersal and hydration of the exudate are under these conditions.

Effective slime cohesion requires high ionic strength and calcium

The results presented in Fig. 4.15 demonstrate that both high ionic strength and calcium are required for effective slime cohesion. Solutions that lacked either exhibited dramatically lower slime cohesion as measured by removable mass. The removable mass for the 0.45 M NaCl, 10 mM $CaCl_2$ and 0.33 M $CaCl_2$ solutions were not significantly different from the seawater solutions ($p = 0.44$ and 0.32, respectively).

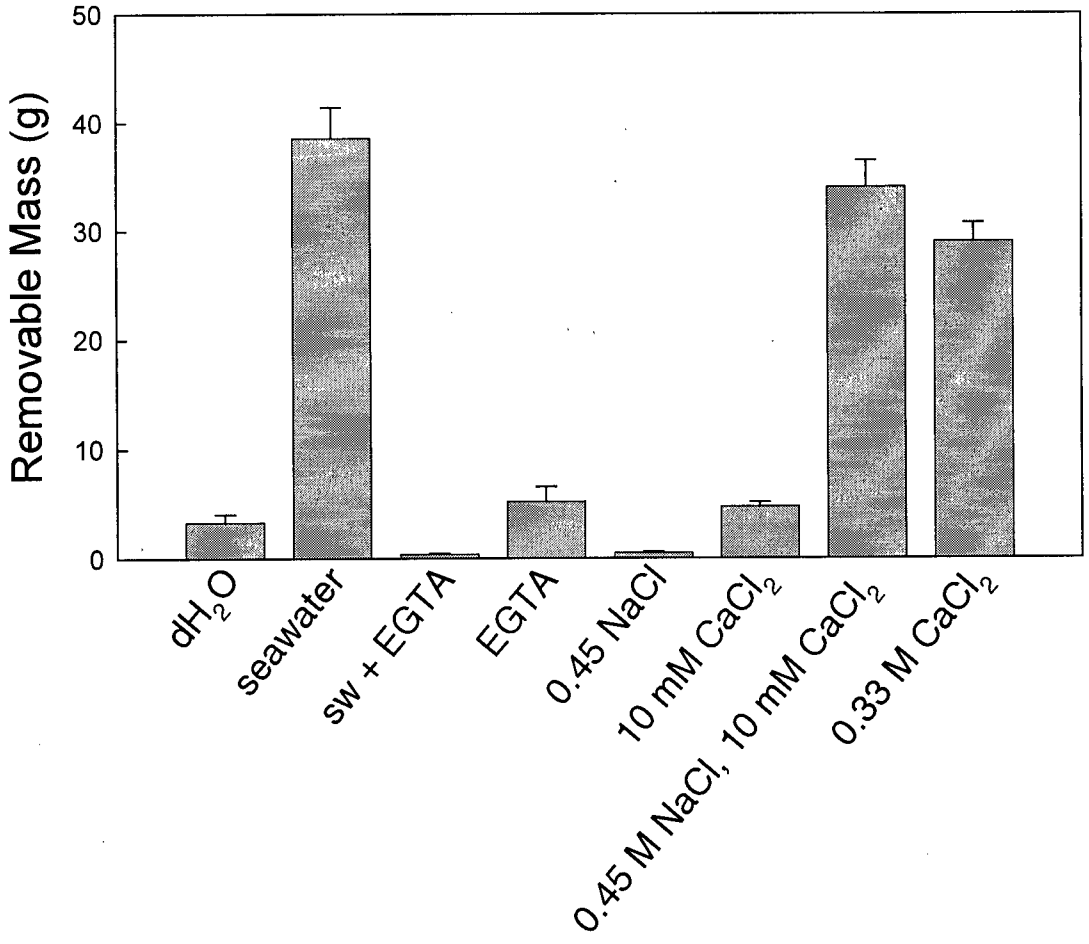

Fig. 4.15. Removable mass experiments with fresh slime exudate revealed that calcium and high ionic strength are both required for slime cohesion on par with that in seawater. Inhibition with EGTA, a calcium chelator, confirms that the effect is calcium specific, and not a more general divalent cation effect. The results for 0.33 M $CaCl_2$ suggests that the high ionic strength need not come from NaCl.

DISCUSSION

The results presented in this chapter provide new information about hagfish slime mechanics and structure at several levels of organization, from the size and shape of the slime threads, to the mechanism of slime formation and hagfish defensive behavior. Examination of slime thread skeins revealed a conservation of the handedness of thread packing as well as a strong bi-directional taper. During normal perturbation of the slime, slime thread IF proteins undergo an $\alpha \rightarrow \beta$ transition, and have a breaking length of about 34 cm. Mucins and threads were found to occur at remarkably low concentrations in whole slime, which helps explain how hagfishes can produce such large volumes of slime. Viscosity measurements of thread-free slime reveal that the mucin component alone has a viscosity that is indistinguishable from that of seawater, which should not be surprising given the vanishingly low concentration of mucins in whole slime. Experiments with fresh slime exudate revealed that proper slime formation requires both calcium as well as high ionic strength. High speed video footage of hagfish sliming revealed several new insights into this behavior. Most notably, slime release is local, rather than global, and occurs via forceful ejection of the exudate from the gland. In addition, hydration of the exudate is remarkably fast, and likely requires convective mixing.

Slime threads have a resting length of 10-17 cm

The breaking length of slime threads was found to be 34 cm. If we assume that the extensibility of entire slime threads is the same as the extensibility as the segments tested in Chapter 2 (i.e. $\varepsilon_{max} = 2.2$), then the resting length of slime threads is 10-11 cm. However, because whole slime threads are tapered, it is more likely that they will break at their narrowest point, with the thicker regions never reaching their maximum extensibility. Slime threads exhibit a three-fold difference in diameter from their thickest to thinnest points (Fig. 4.6), and therefore a nine-fold difference in cross-sectional area. This means that when the thinnest part of the thread is at the breaking stress (180 MPa), the stress in the thickest part will be only $1/9^{th}$ of that, or 20 MPa, which corresponds to a strain of only 1.0. This means that the overall strain of an entire thread will be somewhere between 1.0 and 2.2, giving a possible range of resting lengths of 10-17 cm.

Handedness of slime thread packing is regulated

Downing et al. (1984) propose that the slime thread originates in immature GTCs near the nucleus in an area they call the "zone of thread elongation." The thread elongates from one end and increases in diameter until it is densely packed and

occupies the majority of the cell volume. The implication of this model for thread assembly is that the packing of the thread is dictated by the constraints of the cell membrane, with the elongating thread packing into the pointed end of the cell wherever it can. The seemingly random packing observed in the pointed end is certainly consistent with this model (Fig. 4.16), but this pattern soon gives way to very regular packing as described in the Introduction of this chapter and depicted in Fig. 4.4. One explanation for the regular packing is that it simply arises from the constraints imposed by the shape of the cell and the diameter and flexural stiffness of the thread. In other words, once the thread starts the proper staggered loop pattern, it is self-propagating, and dominates the packing of the rest of the thread. The simplest version of this model predicts that the handedness of thread looping among GTCs should be randomly distributed, with some GTCs coiling to the left and some to the right. The complete conservation of coiling direction in all 20 skeins examined in this study suggests that the direction of thread coiling is regulated and does not arise randomly. Based on TEM images that show pitched striations and/or regularly spaced dots in tangential sections of developing slime threads, Downing et al. (1984) propose the existence of a filament-like helical component that wraps around the thread periphery. Such a helical component could impart the growing thread with a helical bias that would insure that coiling always proceeds with the same handedness.

From the initial stiffness data presented in Chapter 2, I concluded that slime thread IFs possess a persistence length of less than a micrometre. And yet, slime thread IFs are probably several micrometres in length, making it extremely unlikely that inidividual IFs could remain straight within a newly developing thread. From TEM data ((Downing et al., 1984) as well as the x-ray diffraction data presented in Chapter 2, however, we know that IFs within slime threads are highly axially aligned. How then does this axial alignment arise? Microtubules are likely to play a role, given their prominence within the developing thread, as well as their high persistence length of about 5 mm. Stabilization with rigid microtubules is most likely enhanced by bundling of adjacent IFs, which would serve to increase their collective persistence length. These mechanisms are likely to impart the developing thread with enough flexural stiffness to span from one end of the cell to the other.

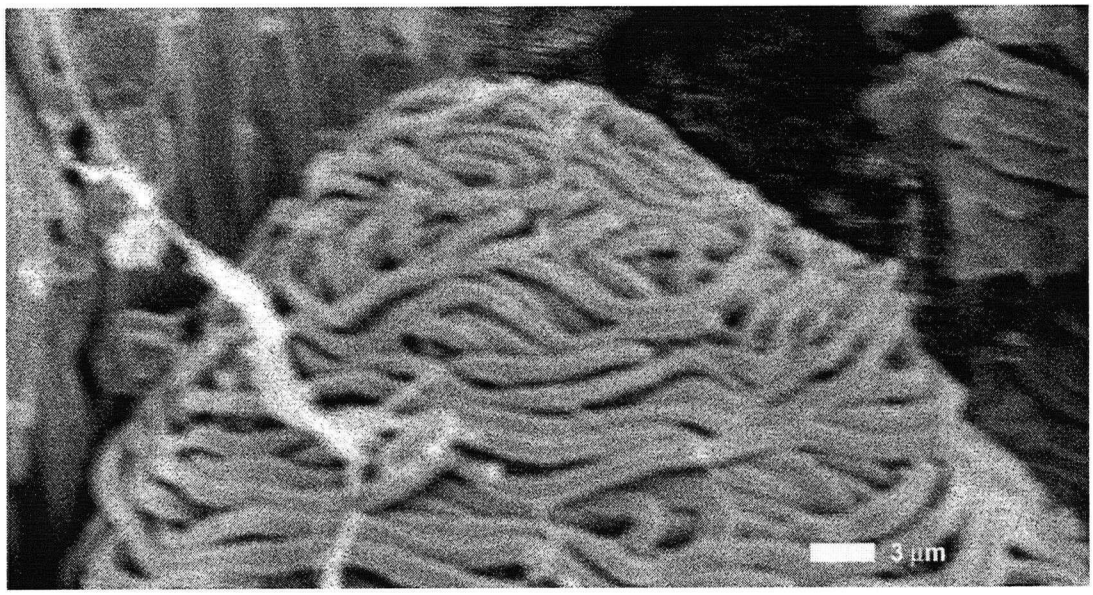

Fig. 4.16. SEM of the pointed end of a slime thread skein showing the relatively haphazard packing arrangement at this end in contrast to the ordered coiling that characterizes the rest of the cell.

Hagfish slime is 1000x more dilute than other mucus secretions

At a mucin concentration of only 15 mg/L, hagfish slime is over 1000 times more dilute than typical mammalian mucus secretions (Table 4.1). Along with the slime storage data reported in Fig. 4.5, the mucin concentration data can be used to calculate the maximum volume of slime that a typical hagfish can produce. An average sized *E. stoutii* is about 35 cm long and weighs about 60 g, so according to Fig. 4.5, it should have about 2.2 g of slime exudate in its arsenal. Of these 2.2 g, about 66% of the mass is water, leaving about 0.73 g of dry mucins and threads. The concentration data show that mucins and threads make up approximately equal amounts of the dry weight of the slime, which implies that about 0.36 g of the stored exudate is dry mucins. At a final mucin concentration of 15 mg/L, this amount of mucin could be used to make about 24 L of slime, or about 400 times the hagfish's own volume. Note that if the mucins in hagfish slime were as concentrated as they are in typical mammalian mucus (about 30 mg/mL), the hagfish would be able to produce only 12 mL of mucus.

Table 4.1. Concentration of mucins in a variety of mucus secretions.

Source	[mucin] mg/ml	Reference
Hagfish slime	0.02	this thesis
Gastric mucus	47	Sellers and Allen (1989)
Duodenal mucus	38	Sellers and Allen (1989)
Colon mucus	20	Sellers and Allen (1989)
Slug pedal mucus	1-32	Denny (1979)
Human salivary mucus	14	Veerman et al. (1989)
Human gastric mucus	30	Pain (1974)

The estimate of 24 L given above is far higher than Strahan's measurement of 0.5 L, but closer to the estimates of Koch et al. (1991) and Goode and Bean (1895) (about 7-8 L). Strahan's estimate can be dismissed due to some serious experimental flaws. In collecting slime for the measurement of mucin and thread concentration in the present study, the volume of an average slime mass produced after only a single pinch on the tail was 0.91 L. This surely is not even close to a hagfish's maximum capacity, and yet it already exceeds Strahan's estimate. The source of Strahan's underestimate can be traced to his method of collecting the slime, in which hagfish were placed in only 1 L of water. Because the vast majority of slime volume is seawater, holding them in such a low volume of water imposes an artificial ceiling on the maximum volume that can be measured.

Why is the mucin concentration so low? From an evolutionary standpoint, one would expect selection to favor hagfish that can produce functionally competent slime with as little energetic investment as possible. Because it is mostly water, mucus may not seem like an energetically expensive material to make, but for many marine organisms, mucus production represents a large portion of their energy budget. From 13-80% of the energy intake of gastropods and chitons is used in the production of mucus, and in the coral *Acropora acuminata*, about 40% of the energy budget goes to mucus production (Denny, 1989). In light of these data and the fact that 3-4% of a hagfish's wet mass is slime, it is not surprising that selection has favored hagfish that can produce slime as cheaply as possible.

It is clear that the concentration of mucins in hagfish slime is far lower than the concentration in typical mucus secretions, but how exactly does the hagfish produce such a strong, coherent mucus with so little material? The answer must lie in the slime threads. Koch et al. (1991) showed that the mucins and threads act

synergistically to produce a large volume of coherent slime. Without the mucins, the threads clump together in a very small fibrous clot, whereas without the threads, the mucins behave essentially as a viscous fluid with very little coherence. The viscosity measurements presented in this chapter for isolated mucins confirm the latter result. If the mucins in water behave as a fluid, then how exactly do the threads impart the whole with solid or gel-like properties?

The fluid-like properties of isolated slime mucins suggest that at the molecular level, interactions among mucins are transient, so that layers of the solution are free to shear past one another if acted on by a shear stress. When slime threads are present, however, shear is resisted with a greater elastic component. What exactly is the source of this elastic component? Using immunogold labeling of mucins, Koch et al. (1991) demonstrate that mucins bind preferably to the surface of slime threads. The data presented in Fig. 4.15 suggest that this mucin/thread interaction is mediated by calcium ions, since the absence of calcium or its chelation with EGTA dramatically reduces slime cohesion as measured by removable mass. Calcium binding to mucins is likely to be a non-specific electrostatic interaction between positively charged calcium ions and negatively charged mucin terminal saccharides. It is not clear whether the binding of calcium to slime threads is mediated by simple coulombic interactions or a more specific calcium-binding domain. At any rate, it is likely that the mucin/thread interaction is dominated by calcium bridges.

Given the affinity of mucins for slime threads, the simplest explanation for the mucin-slime synergy is that the threads immobilize the mucins, which would otherwise be freely diffusible. In this model, slime threads offer a large surface area for mucin binding, immobilizing enough of them (and their bound water molecules) that the slime mass behaves more like a gel than a fluid. One requirement of this model is that the surface area of the slime threads must be sufficient to bind a significant portion of the mucin molecules. From the thread concentration data, the mass of slime threads in a typical 1 L slime mass is about 20 mg. From the thread length and diameter data, it is possible to calculate the volume of a typical slime thread as about 5.5×10^5 μm^3, assuming that the thread is uniformly tapered with a middle diameter of 3.0 μm, and end diameters of 1.0 μm and 1.5 μm. If the thread has a hydrated density of 1.38 g/cm^3, then its mass is about 0.75 μg. At a concentration of 20 mg/L, this translates into about 27,000 slime threads in a 1 L mass of slime. Assuming a constant diameter of 2 μm and a length of 15 cm, each slime thread has a surface area of about 900,000 μm^2. The total length of slime threads in 1 L is therefore 400,000 cm, or 4 km, and the total surface area is 2.4×10^{10} μm^2, or about 240 cm^2.

The above estimate of thread surface area is not all that meaningful without knowing the total number of mucin molecules, which can be estimated assuming a reasonable molecular weight of 1 MDa (Gum, 1995). If one litre of slime contains 15 mg of mucins, this corresponds to about 9×10^{15} mucin molecules, yielding a ratio of mucin molecules per nm^2 of slime thread surface of about 0.37. In other words, if each mucin molecule were bound to the slime threads, there would be one mucin molecule bound per 3 nm^2 of thread surface area. Although not outrageously high, it is not likely that mucins could bind at such a high density to the threads and still have room to bind as much water as they do. This implies that at any given time a significant fraction of the mucins are not bound directly to a slime thread. This is a reasonable conclusion, because even if the mucins were completely elongated to their full length and oriented orthogonal to the thread axis, they would only protrude by about 2 μm from the thread surface, whereas from the above analysis we can calculate that the radius around each slime thread must be about 250 μm in order to account for 1 L of slime volume. Thus, if all of the mucins were bound to the thread surface, the vast majority of slime volume would be occupied by bulk water. This is unlikely given how different the properties of the whole slime are from bulk water.

The above analysis suggests that a large fraction of mucin molecules are not bound to the slime thread, but rather occupy the spaces in between. Carlstedt and Sheehan (Carlstedt and Sheehan, 1989) estimate the radius of gyration of cervical mucin molecules in water as about 200 nm, which corresponds to a volume of about 0.033 μm^3 per mucin. If we multiply this value by our estimate of the total number of mucin molecules in 1 L of slime, we get a volume of about 300 mL, which is not all that far off from 1 L. The conclusion from these analyses is that only a small fraction of mucins in the slime are directly bound to a slime thread, with the majority of mucins occupying the space in between.

Hagfish slime is not a fibre-reinforced composite

The bi-directional taper of the slime threads depicted in Fig. 4.6 is reminiscent of the taper exhibited by collagen fibrils in tendon, which is generally attributed to collagen's role as fibrous reinforcement in these structures (Trotter and Koob, 1989). Although quite long, the collagen fibrils do not span an entire tendon, and so stress must be transferred to adjacent fibrils via shearing of the soft proteoglycan matrix. Composite theory predicts that the tensile forces that must be borne by the fibrils decrease toward the fibril ends, and are highest in the middle. Thus, the most economical use of collagen protein is to make fibrils that

are tapered at both ends. Could this explain the taper of hagfish slime threads? The fibre-composite theory discussed in the Introduction assumes that the matrix in which the fibrous component is embedded behaves as an elastic solid. Hagfish slime mucins behave more as a fluid than a solid (with a viscosity of 1.44×10^{-3} Pa-s), which means that equation 4.1 is not useful for modeling hagfish slime as a composite material. Nonetheless, applying Eq. 4.1 using the data reported in this chapter yields some interesting insights. From Chapter 2 we know that the ultimate stress of slime threads in seawater is 180 MPa, and from this chapter we know that the aspect ratio of the threads (length/radius) is about 100,000 (10 cm/1 μm). From Eq. 4.1 we can calculate the magnitude of the matrix yield stress that would be required for the threads to be fully loaded in tension by stress transfer from an elastic matrix, which is about 1.8 kPa ($\tau_{my} = \sigma_{fu}/s_c = 180$ MPa/100,000). This value is over 3 orders of magnitude higher than the yield stress of conventional mucins such as gastric mucus ($\tau_{my} \approx 1$ Pa). The conclusion of this analysis is that even if hagfish slime mucus were as concentrated and elastic as gastric mucus, it still could not be effectively fibre-reinforced. Another way of expressing the same idea is that if the hagfish slime matrix had a yield stress of 1 Pa, slime threads could only be loaded to a tensile stress of 0.1 MPa, which is 1/30 of their yield stress, and only 1/1800 of their ultimate stress.

Of course it is meaningless to speak of a yield stress for hagfish slime mucus because it behaves not as a solid, but as a fluid characterized by a viscosity. The viscosity of a fluid is simply the slope of the shear stress vs. shear rate curve, and so provides information about how difficult it is to deform the fluid at a given shear rate. In Eq. 4.1, the yield stress of the matrix is used under the assumption that it is the highest stress that the matrix can resist elastically. A purely viscous matrix will also be able to transfer stress to the reinforcing fibres, although its ability to do this will be highly shear-rate dependent. Thus, the yield stress in Eq. 4.1 can be substituted with a fluid shear stress, and the relationship will still be valid. Eq. 4.1 predicts that the matrix must be able to exert a shear stress of 1.5 kPa in order for the threads to be fully loaded in the slime. From the viscosity of slime mucins provided in this chapter, we can calculate that the rate at which the mucins must be sheared to achieve this level of stress is about 10^6 strain units/s. This is an extremely high shear rate that could not possibly be experienced by hagfish slime under any natural conditions. Thus we must conclude (again) that hagfish slime does not behave as a fibre-reinforced composite. It therefore follows that there must be another explanation for the bi-directional taper of the threads besides fibre-reinforcement.

Although the above analysis predicts that the mucins will be ineffective at transferring significant loads to the slime threads, this does not mean that the threads will never be loaded. In fact, the congo red staining demonstrates that under "normal" deformations of the slime, as might occur while a fish thrashes within it, all of the threads are loaded to stresses higher than the yield stress (Fig. 4.7). Using the above analysis, the strain rate required for the mucins to load slime threads past their yield stress (3 MPa) is also absurdly high (about 15,000 s^{-1}). Thus, the loading of threads in the slime must occur via direct loading, which is not difficult to imagine, given the fact that they are long enough to span almost the entire diameter of a typical slime mass, and are likely to entangle with many other threads. Pulling on a slime thread will therefore result in its deformation due to the drag force that resists movement of the rest of the slime to which the thread is attached. In this way, the mucins do not directly transfer loads between slime threads, but their presence does greatly increase the volume of the slime, and therefore the drag forces that allow the threads to be transformed.

Hagfish slime is not a protective shroud

Because of the speed with which hagfishes release slime, it is extremely difficult to discern with the naked eye which glands release exudate in a given sliming event. When a hagfish is held out of water, exudate often oozes out of many glands, but it is not clear whether such a global release of slime also occurs in water. High speed video of slime release by hagfish revealed that exudate is typically released only from glands in the proximity of where the animal was touched (Fig. 4.8). These results suggest that the utility of predator-induced slime release is not to enshroud the entire hagfish in slime, but rather to direct slime at the predator making the attack.

Other evidence supports the idea that the slime is not simply a protective shroud. Release of slime is often followed immediately by an escape response, whereby the hagfish recoils from the attack, and swims vigorously to get away, leaving the slime behind it. If the hagfish's defensive strategy were to release slime and hide within it, one would not expect such behavior. Furthermore, exudate does not gently ooze out of the gland onto the hagfish's skin, but rather is forcefully ejected (Fig. 4.9). Again, if the slime were simply a barrier against further attacks, jetting the exudate away from the body could be counter-productive.

Given the fact that a layer of skeletal muscle surrounds each slime gland, it is not difficult to imagine the mechanism by which the slime exudate is ejected. However, some of the high speed video footage suggests that exudate release

may involve more than just the slime glands. In several trials, release of slime was preceded by a puffing up of the body in the vicinity of the attack, which subsided after the slime was released (Fig. 4.10). The increase in body diameter in the area of slime release is most likely due to a local contraction of the swimming muscles. The muscle layer surrounding the slime gland capsule is thin, so contraction of the relatively large swimming muscles presumably augments the pressure exerted on the gland and therefore the force with which the slime exudate is ejected. This conclusion is supported by observations of anaesthetized hagfish that are coaxed to release slime via electrical stimulation. At low stimulation frequencies and voltages, slime release is slow and appears to involve only the slime gland. However, with more intense stimulation that causes deeper contractions, the exudate is more likely to be forcefully ejected.

Dispersal is required for effective slime hydration

High speed video footage also suggests that effective slime hydration requires some form of convective mixing. Introduction of fresh slime exudate into seawater on a spatula without mixing resulted in very little slime dispersal and hydration (Fig. 4.13). Injection of exudate into seawater through an 18 gauge needle was just as ineffective (Fig. 4.14). How is it then that exudate released from the slime glands can disperse and hydrate in about 80 ms (Fig. 4.11)? The difference is that exudate ejected from a slime gland comes out in a fine stream, which has a much higher surface area to volume ratio than the samples introduced via spatula or syringe. The duct through which the slime exudate must pass as it is ejected from the slime gland is only about 100 μm in diameter (Downing et al., 1984), which forces the exudate to flow in a fine stream at high velocity and shear rate. Furthermore, it is probably not a coincidence that the diameter of the duct is about the same size as a GTC. In fact, the duct is wider than the width of a GTC, but smaller than its axial length, which implies not only that GTCs will pass through the duct singe-file, but also that they will be axially-aligned with the direction of flow. Ejecting the exudate in such a fine stream limits the volume that can be ejected in a given amount of time, but insures that the exudate has a high surface area to volume ratio, which is likely to be critical to efficient slime hydration. The surface area to volume concept may also help explain why hagfishes possess many glands (~150 in the case of *E. stoutii*) rather than fewer glands with greater storage capacity.

The utility of axially aligning the GTCs as they pass out of the gland is less obvious. Because the two free ends of the thread are at the distal ends of the cell, ejecting it in an aligned orientation makes it less likely that the ends of the

threads will tangle around each other when spooling out from the cell. If the cell were ejected in an orthogonal orientation to the direction of flow, the two free ends would be more likely to trail behind the cell and tangle together, which would decrease the length and surface area of the thread available for interaction with mucins. If it is indeed important to have the two free ends of the thread at the leading and trailing ends of the cell as it exits the gland, this may lend insight into the shape of the thread cells. If one were to design a cell that could pass through a narrow duct in an oriented manner, and pose little risk of clogging up the duct, an ellipsoid shape would surely be one of the best designs. Previously in this chapter I suggested that the bi-directional taper of the slime thread might be related to a fibre-reinforcement role of the threads, but this hypothesis was rejected. An alternative explanation for the slime thread taper is that it allows the developing thread cell to produce a bi-directionally tapered cell without having to continuously modify the packing geometry as the thread is laid down.

Dispersal and hydration of slime exudate ejected from the slime glands was clearly more effective than exudate introduced into seawater via a spatula or injected through a large-bore needle. However, some of the high speed video trials suggest that dispersal of exudate may be aided by movements of the hagfish's body in addition to its forceful ejection from the slime glands. Fig. 4.12 portrays the clearest case of this, in which a hagfish whipped its head through a cloud of undispersed exudate, resulting in increased convective mixing. In the same maneuver, it even appeared that the hagfish "sneezed" water out of its nostril as its head swept through the cloud of exudate. Clearly more observations of sliming behavior are needed to establish the role of convective mixing in the hydration of hagfish slime.

Ionic effects on slime formation and cohesion

Mucin vesicles exocytosed by mammalian goblet cells display fast and predictable swelling kinetics. Swelling of collapsed mucins is believed to be driven primarily by a "Jack-in-the-box" mechanism whereby charge-shielding ions such as calcium are exchanged for ions with little capacity for charge shielding such as sodium (Tam and Verdugo, 1981). Removal of charge shielding results in electrostatic repulsion among negatively charged mucin molecules and swelling kinetics that are much faster than can be explained by diffusional models alone. Swelling eventually slows as the average distance between adjacent mucin molecules increases (and repulsion decreases), and as the disulfide bonds that link mucins into a coherent, insoluble network are put into tension.

The explosive nature of hagfish slime formation suggests that hydration of the mucin vesicles in the slime may also occur via a Jack-in-the-box mechanism. Although one might think that the presence of calcium ions in seawater (at about 10 mM) could prevent such a mechanism from working, the concentration of sodium ions is far higher (about 450 mM), so an exchange of calcium for sodium is not unlikely, especially if calcium inside the vesicles is maintained at a high concentration. The cation channels predicted by the results of Luchtel et al. (1991) would facilitate the transmembrane cation traffic predicted by this model, with the monovalent anion channels allowing chloride ions to dissipate the electrical gradient resulting from the influx of sodium. However, charge shielding via calcium ions is not consistent with the removable mass data, which show that high concentrations of $CaCl_2$ (i.e. 0.33 M) are nearly as effective as seawater for the formation of competent slime. If mucin swelling were governed by Na^+/Ca^{2+} ion exchange, then solutions lacking Na^+ ions and possessing a high Ca^{2+} concentration should inhibit swelling, and this did not occur. These data clearly rule out Na^+/Ca^{2+} exchange as an important mechanism of hagfish slime vesicle swelling.

Summary of events leading to slime formation in seawater

Based on the results of this chapter and previous studies it is possible to sketch out some of the events involved in the formation of hagfish slime from slime gland exudate, as well as the molecular bases of its mechanical behavior. Sliming is initiated presumably via neural stimulation of the muscle fibres that surround the slime gland capsule, and usually occurs in the proximity of the stimulus that provoked the sliming response. Contraction of surrounding myotomal muscles may aid in the ejection of slime from the glands. Exudate is ejected from the slime gland through a narrow duct, in which GTCs most likely proceed single-file and axially-aligned to the direction of flow. As they pass through the duct, GTCs and GMCs lose their plasma membranes via shear. Slime exudate exits the duct in a fine stream, which facilitates its hydration. Swelling of mucin vesicles is initiated by a diffusional influx of ions (most likely Na^+ and Cl^-), presumably through ion channels in the vesicle membrane. Water follows the ions, leading to swelling and rupture of the vesicles. As the mucin vesicles swell, slime thread skeins loosen up and begin to unravel from both ends. Upon rupture of the mucin vesicles, calcium-mediated interactions begin to form between mucin molecules and slime threads. Post-rupture swelling of the mucins surrounding the thread cells leads to further unraveling and extension, so that when swelling is complete, the threads are completely spooled out and dispersed throughout the mass of slime.

Hagfish slime mechanics: a synthesis

In Chapter 2, I demonstrated that slime threads in seawater are soft and elastic up to a strain of about 0.34, and at greater strains, yield and undergo dramatic strain hardening and plastic deformation. In this chapter, I demonstrated that the mucus component of the slime behaves essentially as a low-viscosity fluid. Attempts to model the slime as a fibre-reinforced composite using these mechanical data fail due to the inability of the mucus component to effectively transfer stress to the threads. This of course raises the following question: if the slime isn't a composite material, what exactly is it?

The best place to begin to answer this question is with slime anatomy. In collecting slime for mucin and thread concentration measurements, the hagfish produced masses of slime that were typically about 900 mL in volume. If this volume of slime took on a spherical shape, it would have a diameter of about 12 cm, which is about the length of an unstretched slime thread, implying that slime threads span almost the full diameter of a typical slime mass. Analysis of total thread surface area suggests that it is unlikely that every mucin molecule can be bound to a slime thread, and a crude nearest-neighbor analysis suggests that the average distance between threads is about 250 μm. Assuming a radius of gyration of 200 nm for each mucin molecule, this corresponds to a distance of several hundred mucins between threads.

Ferry (1941) pointed out that hagfish slime contracts to about $1/50^{th}$ of its original volume when it is disturbed. Given the slime anatomy described above, it is now possible to explain how this occurs. From the viscosity measurements, we know that the mucins are not cross-linked together into an elastic network as they are in typical mucus secretions, suggesting that the mucins and water between slime threads behave as a fluid. As a slime mass is disturbed, slime threads come into contact and adhere to each other (Koch et al., 1991a), most likely with a number of mucin layers mediating the adhesion. The affinity of the mucin-coated slime threads for each other leads to an irreversible contraction of the slime, with the intervening mucin solution flowing out and dispersing into the surrounding seawater. What remains is a small, fibrous clot of mucin-coated slime threads.

The above model is supported by the fact that when slime is lifted out of water into air, it does not remain a coherent mass, but rather shrinks as water and mucins flow out of it. The implication of this is that the properties of hagfish slime are highly time-dependent due to its tendency to lose water and mucins as it is deformed. It is therefore difficult to provide a single description of hagfish

slime mechanics, because the composition and properties change as it is deformed. Future studies should attempt to quantify this time-dependent change in properties of whole slime.

Implications for the function of threads, mucins, and whole slime

The behavioral data presented in this chapter suggest that hagfish slime is not a simple defensive barrier in which a hagfish can take refuge from a predator. What then is its function? The most plausible hypothesis that has been suggested in the literature is that the slime acts as a deterrent specifically to gill-breathing predators (Fernholm, 1981). Anecdotal evidence suggests that fish that attack hagfishes risk clogging up their gills and suffocating (Fernholm, 1981). This idea is supported by the fact that there are no known fish species that rely on hagfishes for a significant part of their diet, whereas many air-breathing predators including seabirds, seals, and dolphins are known to prey regularly on hagfishes (Fudge, 2001; Martini, 1998)

The analysis of slime mechanics presented above is also consistent with the idea that the slime is not a protective shroud in which a hagfish can hide. The contraction behavior described above implies that a predator could make any adherent slime collapse if it were persistent enough in its attacks, after which it could consume both the hagfish and its thin envelope of mucus-coated slime threads. If fishes that approached the slime risked suffocation, however, the slime would perform an effective anti-predator function.

If the slime collapses and loses the vast majority of its water and mucins when it is disturbed, how can it effectively clog up gills? Shouldn't the fish be able to make the slime collapse by ventilating its gills? The answer is yes, the slime will collapse, but it will still be effective. Gas exchange at the gills is a diffusion-driven process, and for this reason is extremely sensitive to the thickness of the blood-water interface (i.e. the diffusional distance). While diffusion is effective for transport of molecules down a concentration gradient over very short distances, flux rates diminish with the square of the diffusional distance, making transport over large distances exceedingly slow. The diffusional (i.e. blood to water) distance of fish gills varies as function of fish lifestyle, but 1 μm is a typical value (Steen and Berg, 1966). If adherent hagfish slime added only 1 μm to this distance, the flux of respiratory gases across the gills would be reduced by 75%, and only 2 μm of slime would reduce gas exchange by 89%. From this analysis it is clear that even if most of the mucins dispersed from the original slime, the remaining threads and mucins could seriously disrupt gas exchange

across the gills, possibly suffocating the fish.

If primary function of the slime is protection against gill-breathing predators, the specific roles of the thread and mucin components become clearer. In this capacity, the function of the threads is to simply bind mucins and catch on the gills, thereby reducing their effectiveness. The impressive length of the threads (10-11 cm) can therefore be viewed as an adaptation for increasing the likelihood that they will catch on a gill filament or gill arch. It is interesting to speculate why selection didn't favor threads with an even greater aspect ratio. In other words, why make slime threads as a bundle of 1000 IFs instead of 10? Increasing the aspect ratio would make the threads even more likely to catch on the gills, and would also increase their surface area available to bind mucins. The answer may be that finer threads simply are not strong enough to resist attempts by the fish to dislodge the slime from the gills. Within this framework, the function of the mucins is to bind to the threads and participate in the thickening of the blood-water diffusional distance.

CONCLUSIONS

In this chapter, I provide data that increase our understanding of the mechanical properties of hagfish slime, its mechanism of formation, and some behavioral aspects of its release by the animal. Taken together, these results suggest that hagfish slime does not behave as a fibre-reinforced composite, but as a very dilute assemblage of protein threads and mucins that protects hagfishes from gill-breathing predators.

CHAPTER 5: GENERAL CONCLUSIONS

The 'design' of IF-based materials

IFs are remarkable in their mechanical versatility, forming structures as different as soft hagfish slime threads to hard nails and horns. How is it that natural selection has constructed such diverse materials from IF proteins that all share the same general domain structure? One of the keys to understanding this mechanical diversity is the fact that IF proteins contain both low-stiffness (terminal domains) and high stiffness (coiled coils) components. How these components interact to determine the mechanics of an IF depends on several factors that likely have been acted upon by selection to tune the mechanics of IFs to their function in life. These factors are: covalent cross-linking, hydration, composition of the protein matrix, draw processing, size and sequence of the terminal domains, the tendency of IFs to form bundles, and IF pre-strain.

Covalent cross-linking within and among IF protein chains

Hagfish slime thread IFs, which are very low in cysteine and therefore in potential cystine cross-links, represent the soft and extensible end of the spectrum with regard to the range of possible IF mechanical properties. Many cytoplasmic IFs such as desmin and vimentin are also low in cysteine suggesting that they are just as soft and extensible. Hard α-keratin IF proteins contain significant amounts of cystine cross-links that occur both within the terminal domains, and between adjacent alpha-helical segments (Fraser et al., 1988; Wang et al., 2000a). These hard and less extensible materials represent the opposite extreme of IF mechanical properties, underscoring the potential importance of covalent cross-linking to the mechanical properties of IF-based materials.

How exactly could cross-links contribute to IF mechanical properties? The mechanical models developed in Chapters 2 and 3 offer some insights into this question. In the fully hydrated state and in the absence of cross-links, IF protein terminal domains possess conformational freedom and therefore exhibit soft, rubber-like elasticity that dominates the low-strain behaviour of IFs. To understand why the soft terminal domains dominate, it is useful to consider the following macroscopic analogy of the series arrangement of coiled coils and terminal domains. If hard plastic rods (coiled coils) are connected in series by rubber bands (terminal domains) and a load applied to this structure, most of the strain will occur in the rubber bands, and the plastic rods will act virtually as rigid spacers.

One can also imagine that if the plastic rods and rubber bands are arranged *in parallel*, the mechanics will be dominated by the stiffer rods. This is likely what happens when covalent cross-links are introduced between adjacent coiled coils within IFs. This model predicts that IFs covalently cross-linked in this way (e.g. IFs in hard α-keratins) should exhibit an initial stiffness that is similar to the stiffness of coiled coils, and this is indeed the case. It is important to mention that if the IFs are hydrated, adding covalent cross-links will increase the initial stiffness, but the yield stress will still be low. Recall that the yield stress of α–helices in wet hagfish slime fibres is only about 3 MPa. In Chapter 3 I suggested that hard α-keratins achieve yield stresses about an order of magnitude higher than this by maintaining the IFs in a partially dehydrated state.

Introduction of cross-links into the terminal domains should also affect IF mechanics. The stiffness and extensibility of an elastomer varies as a function of the number of polymer chains per unit volume. Adding cross-links to the terminal domains will increase the effective number of chains, thereby increasing the stiffness and decreasing the extensibility of the terminal domains, and therefore the IFs. In the macroscopic analogy above, the effect would be similar to increasing the stiffness and decreasing the extensibility of the rubber bands. Of course, if extensive cross-linking already exists between coiled coil segments (as is the case in hard α-keratins), increasing the stiffness of the terminal domains will have little effect on the overall IF mechanics. The effects of introducing covalent cross-links in the terminal domains and between coiled coils on IF mechanics are summarized in Fig. 5.1.

Hydration

The initial stiffness of dry hagfish slime threads is three orders of magnitude higher than for wet threads. While such dramatic hydration dependence is typical for elastomeric protein materials such as elastin (Lillie and Gosline, 2002), hard α-keratins are relatively hydration insensitive, with stiffness rising only two to three times with dehydration (Feughelman, 1959). How can two IF-based materials show such differing degrees of susceptibility to water? In Chapter 3 I suggested that one of the key roles of the matrix in hard α-keratins is to exert an inward pressure on the IFs that acts to keep them in a partially dehydrated state. If this is true, then dehydration has a small effect on hard α-keratin mechanics because even at 100% relative humidity, the IFs are already partially dry. Another important factor to consider is the interaction between hydration and cross-linking. As mentioned in the section above, the mechanics of hydrated,

cross-link-free IFs are dominated by the terminal domains because of their series arrangement and low stiffness. When dried, it is likely that the terminal domains lose their conformational freedom (i.e. become glassy) with their stiffness rising by two to three orders of magnitude, causing IF stiffness to rise by a similar degree. In hard α-keratins, however, the more parallel arrangement of coiled coils and terminal domains means that changes in terminal domain stiffness have little effect on overall IF stiffness. The effects of hydration on IF mechanics are summarized in Fig. 5.1.

Protein matrix

From the above analysis, it is clear that IF-based materials that must possess both high stiffness and high yield stress in water cannot rely solely on covalent cross-links because the yield stress will still be low. In contrast, dehydration of IFs dramatically increases both the stiffness *and* the yield stress. This leads to the insight that while hard IF-based structures that function in water may possess cross-links, keeping the IFs in a dehydrated state is more important. In Chapter 3 I suggested that an important role of the matrix is to regulate IF hydration, which not only keeps the stiffness and yield stress high, but also may optimize recovery from post-yield deformation by inhibiting the formation of stable β-sheets. Furthermore, if the matrix can mechanically resist IF swelling, then it should also be robust enough to resist axial deformation, and therefore is a likely candidate for the post-yield rise in stress in hydrated hard α-keratins, as well as the full recovery exhibited by this material. In summary, changes in matrix content and composition have the potential to tune the stiffness, yield stress, extensibility, and recovery behavior of keratins.

IF terminal domains

The above analysis suggests that in hard α-keratins, in which adjacent coiled-coils are cross-linked, modifications of the terminal domains should have little effect on the properties of the IFs. However, in IFs that lack cross-links between their coiled coils, it should be possible to tune the mechanical properties of the IFs via modifications of the size and cross-linking of the terminal domains. Larger, more conformationally free terminal domains should yield IFs that are less stiff and more extensible than IFs with smaller or more highly cross-linked terminal domains. Furthermore, low stiffness IFs will have a lower persistence length, and therefore should be more competent at forming entropic gels in suspension.

Fig. 5.1. Summary schematic of the range of mechanical properties that can be achieved in intermediate filaments through variation in covalent cross-linking, hydration, and draw-processing. Grey bars represent coiled coils, squiggles terminal domains, black bars covalent cross-links, and crimped grey bars β-sheets. A) In the absence of cross-links, hydrated IFs behave like hagfish slime threads, i.e. they are soft and extensible with a low initial stiffness and yield stress. Inset is detail of curve at strains up to 0.5. B) Introduction of cross-links within the terminal domains increases their stiffness, and therefore the initial stiffness of the IFs. Extensibility is slightly reduced, but the yield and ultimate stresses are unaffected. Inset same as above. C) Cross-linking of adjacent coiled coils bypasses the soft terminal domains, dramatically increasing initial stiffness. Because the coiled coils are fully hydrated, however, yield stress is still very low. D) IFs in hard α–keratins are partially dehydrated by the keratin matrix, and therefore possess both high stiffness and yield stress. E) Dehydrated IFs in the absence of cross-links exhibit high stiffness, strength, and yield stress like slime threads tested in air. F) Draw-processed threads in air exhibit high stiffness, high strength, and low extensibility due to the extension of α-helices into β-sheets.

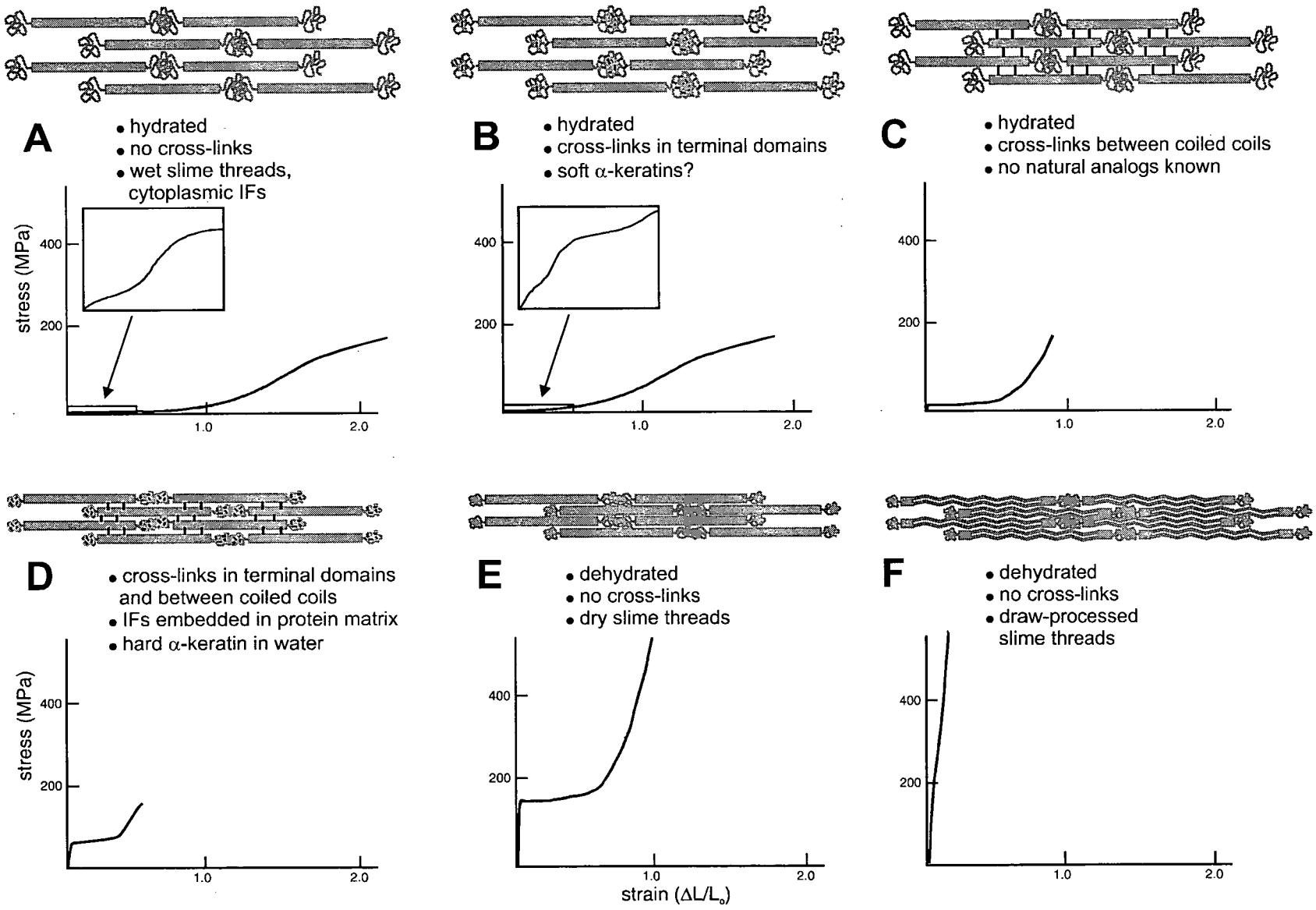
A
• hydrated
• no cross-links
• wet slime threads, cytoplasmic IFs
B
• hydrated
• cross-links in terminal domains
• soft α-keratins?
C
• hydrated
• cross-links between coiled coils
• no natural analogs known
D
• cross-links in terminal domains and between coiled coils
• IFs embedded in protein matrix
• hard α-keratin in water
E
• dehydrated
• no cross-links
• dry slime threads
F
• dehydrated
• no cross-links
• draw-processed slime threads
stress (MPa)
400
200
1.0
2.0
strain (ΔL/L$_o$)

IF bundling

If one of the functions of IFs in living animal cells is to impart entropic gel properties to the cytoplasm, one can imagine that in cells with different mechanical needs, selection might favour IFs that are more or less competent at gel formation. As suggested above, the terminal domains are an obvious target for this kind of selection, but bundling of IFs may also be relevant. Under physiological pH and ionic conditions, cytokeratin IFs tend to form bundles (Bousquet et al., 2001; Yamada et al., 2002). While an affinity of IFs for each other could conceivably strengthen an IF gel, excessive bundling could increase the persistence length of a bundle so much that the IFs no longer form an entropic gel. In contrast to cytokeratins, neurofilament IFs do not form bundles, and in fact appear to repel one another (Brown and Hoh, 1997). This repulsion could have opposite effects on the properties of entropic gels formed from neurofilaments.

IF pre-strain

Another mechanism by which the mechanical properties of IFs could be modified is via pre-strain. In the case of an IF entropic gel network, pre-staining of the network would increase its stiffness due to the positive relationship between stiffness and strain in IF gels (Janmey et al., 1991). Similarly, taut IFs in cells could be pre-strained in region I of the stress-strain curve without permanent alterations of their structure, which would also increase their stiffness (due to the approximate J-shape of the hydrated IF stress strain curve in region I (Fig. 2.6B)). Indeed, tensegrity theory rests on the assumption that F-actin and IFs in cells exist as a stable, pre-strained tensional network that is opposed by microtubules loaded in compression. The low stiffness elastic behavior I report for IFs in Chapter 2 is consistent with this idea.

IF draw-processing

It is possible that IFs could be pre-strained beyond region I of their stress-strain curve, which would irreversibly increase the β-sheet content of the IFs, increase their resting length, increase their stiffness, and decrease their extensibility. In Chapter 2 I suggested that the appearance of β-sheets in IFs may serve an important mechanosensory role that allows cells to detect large-scale deformations and respond appropriately. Is it also possible that certain cells *intentionally* transform their IFs in this way to increase stiffness and decrease extensibility? At this stage, the only cells in which draw-processing appears to be

part of their normal function are hagfish gland thread cells. In Chapter 4 I demonstrated that the slightest perturbation of hagfish slime leads to an $\alpha \rightarrow \beta$ transition in the slime thread IFs. In this case, extrinsic forces are used by the hagfish to draw-transform the IFs in the threads from a predominantly α-helical state to one in which β-sheets are prevalent. The possibility that other cells make use of draw-transformed IFs for mechanical reinforcement should not be overlooked.

Future directions for research

The model of IF mechanics developed in this thesis makes several predictions about the function of IFs under a variety of conditions (Fig. 5.1). One of these predictions is that IFs in living cells are soft and extensible, which contradicts the current belief that they are about as stiff as F-actin and microtubules. One way to test this prediction would be to do a tensile test on an individual IF in water. Atomic Force Microscopy (AFM) techniques have advanced so much over the past few years that mechanical testing of single (albeit very large) molecules such as titin (Fisher et al., 1999) is possible. Application of these techniques to individual IFs in water would represent an important test of the validity of the IF mechanical model proposed here. Furthermore, testing of different kinds of IFs may reveal that IF sequence diversity corresponds to mechanical diversity.

One of the more intriguing ideas that comes out of this thesis is that IFs in living cells may undergo an irreversible $\alpha \rightarrow \beta$ transition when cells are deformed. This prediction could be tested using the congo red methodology developed in Chapter 2. If IFs in living cells do in fact undergo an irreversible $\alpha \rightarrow \beta$ transition, one would expect them to test positive for congo red after appropriate strain regimes. A positive result would raise the possibility that draw-transformed IFs in cells act as mechanosensory cues used by cells to detect cytoskeletal damage. This idea could be tested by introducing draw-transformed IFs into cells (either via deformation of the cells or injection) and measuring changes in gene expression.

The molecular mechanics model developed in Chapter 2 attributes the low stiffness elasticity in region I of the stress strain curve to the IF terminal domains. Specifically, the model postulates that the terminal domains behave as elastomers, and therefore enjoy a certain degree of conformational freedom, at least in the hydrated state. If this is indeed the case, then slime threads strained in region I should exhibit thermoelastic behavior typical of rubber-like polymers such as elastin (Mistrali et al., 1971) or supercontracted spider dragline silk

(Gosline et al., 1984). In other words, increasing the temperature of a strained slime thread in water should increase the resultant stress. From this kind of experiment it is possible to tease apart the contributions of changes in conformational entropy and internal energy to the elastic modulus. If the entropic component is dominant, this would confirm that the terminal domains function as elastomers, but if the internal energy component dominates, region I elasticity arises mainly from the reversible straining of bonds.

The model developed in Chapter 3 for the mechanics of IFs in α-keratins also makes several testable predictions that should be pursued. One of the more important concepts to come out of Chapter 3 is that IFs in hard α-keratins are maintained in a partially dehydrated state by the keratin matrix. If this is true, it is unclear whether the matrix squeezes water out of fully hydrated IFs as it is cross-linked, or whether the IFs are dried during air exposure and subsequently locked into the dehydrated state by cross-linking of the matrix around them. Careful examination of the timing of chemical and histological changes during keratin biogenesis may be able to resolve this issue. If exposure to air does indeed play a role in hard α-keratin formation, then one would expect that hard α-keratins that are chronically wet, such as baleen or the oral filiform papillae in mammals, would exhibit unique composition (such as a higher proportion of matrix proteins) and/or mechanics.

If the IFs in hard α-keratins are maintained in a partially dehydrated state, then it is possible that modifications of the keratin matrix could result in changes in the properties of keratin by affecting the degree of IF dehydration. The data presented in Chapters 2 and 3 demonstrate that hagfish slime threads tested in water and at 40% relative humidity exhibit profoundly different mechanical properties. For example, the stiffness of slime threads in air is about 1000 times higher than the stiffness of threads in water. Quantification of slime thread mechanics as a function of relative humidity would allow one to estimate the degree to which IFs in hydrated hard α-keratins are dehydrated, or in other words, their effective relative humidity within the matrix.

The establishment of dry slime threads as a relevant model for the study of IFs in α-keratins also makes possible detailed studies of IF structural mechanics. Recent advances in x-ray diffraction techniques allow one to follow atomic-scale structural changes within very small fibres as they are deformed, almost in real time (Kreplak et al., 2002; Riekel et al., 2000). Application of these techniques to dry slime threads should yield further insights into the structural mechanics of IFs in hard α-keratins. Specifically, these types of experiments could explore the

roles that hydration, and therefore the matrix, play in IF recovery and β-sheet formation.

Dry slime threads could also be used to tease out the contribution that covalent cross-links make to α-keratin mechanics. By introducing cross-links at selected sites (between adjacent lysine or tyrosine residues, for example), effects of cross-linking on IF mechanics could be explored. It might also be possible to embed dry slime threads in matrices of various composition and properties to test more directly the effect of the keratin matrix on α-keratin mechanics.

The data presented in Chapter 4 represent a major leap forward in our understanding of hagfish slime mechanics and function, but many questions remain to be answered. Removable mass experiments with fresh slime established that calcium ions play an important role in slime hydration and/or cohesion, but the exact role that calcium plays is still unknown. Viscometry measurements of slime mucins as a function of calcium concentration would test the hypothesis that calcium is an important mediator of mucin-mucin interactions. Testing whether calcium mediates mucin-thread interactions will require more intricate experiments than simple viscometry.

Chapter 4 demonstrated that slime threads are critical to the structure and cohesion of hagfish slime; without them the slime is simply an extremely dilute mucin solution. Nonetheless, mucins make up about half of the dry weight of slime exudate, and so their contribution should not be overlooked. From the mechanics of slime threads in seawater (from Chapter 2) and the viscosity of slime mucins (from Chapter 4), one can speculate about the mechanical properties of the whole slime formed under natural conditions, as I've done in Chapter 4. However, a complete understanding of hagfish slime will include measurements of whole slime mechanics, such as the viscous and elastic components of the slime's stiffness at in vivo strain rates, as well a description of how the properties of the slime change over time.

Hydration and swelling of slime mucin vesicles also warrants further investigation. The rapid swelling of mucins released from mammalian goblet cells is believed to occur via a "Jack-in-the-box" mechanism in which the exchange of sodium ions for charge-shielding calcium ions results in repulsion among negatively charged mucins. Such a mechanism seems to be unlikely in hagfish slime mucins, which appear to hydrate just as well in solutions devoid of sodium and high in calcium. Experiments designed to probe the swelling of slime vesicles may elucidate a novel mechanism by which collapsed secretory

products swell and release their contents.

Practical applications of IF-based materials

Before relatively recent advances in chemistry and manufacturing allowed us to design and synthesize useful materials almost from scratch, humans made extensive use of biological materials such as wood, bone, shell, horn, silk, and tendon. Hard α-keratins were (and in some cases still are) conscripted for many uses because of their strength, flexibility, durability, and chemical resistance. Some of the more important hard α-keratins used include fur for clothing, insulation and bedding, wool and hair for textiles and fibre-reinforcement of pottery, horn for bows, and quills for writing.

But as fibrous tensile materials go, keratins are no match for silks. The domestication of the silkworm moth (*Bombyx mori*) was a major breakthrough in the history of human cultural and technological development, so much so that it led to the development of one of the most important trade routes to Asia, the Silk Road. The mechanical properties of certain silks from orb-weaver spiders are superior to silk moth silk, and even stronger than steel on a per-weight basis (Denny, 1976; Vollrath and Knight, 2001). Unfortunately, spiders have not lent themselves to domestication, and so the world will have to wait for another technological breakthrough before it sees textiles and other products spun from spider silk.

The explosion of biotechnology in the last few decades has kindled hopes that large scale production of spider silks for industry could come about via the cloning of spider silk genes into appropriate expression vectors. However, in spite of sizable infusions of research money from industrial and military sources into this problem, success has been modest at best. One of the main complications in the effort to produce biomimetic spider silk is that the silk genes are large and repetitive (Guerette et al., 1996), which makes their maintenance in expression vectors difficult. This obstacle was recently overcome by employing mammalian expression vectors, which have less trouble with large and repetitive inserts (Lazaris et al., 2002). The drawback of this approach is that mammalian expression systems are more costly than systems that employ bacteria, fungi, or plants.

Draw-transformed IF fibres for use in industry

Structural and mechanical studies of spider silks suggest that they owe much of

their outstanding properties to the presence of β-sheet crystals held together by kinetically-free amorphous domains (Gosline et al., 1999). The data presented in Chapter 2 demonstrate that slime threads can be transformed into stiff fibres dominated by β-sheet crystal structure by simply stretching them in water. Although draw-transformed slime threads in air are not as strong or tough as dragline silk (Fig. 5.2), they possess several attributes that make them worthy of biomimetic efforts to produce them in the lab, and possibly on an industrial scale (Fudge et al., 2002).

While domestication of hagfishes for the harvesting of slime is not likely to be embraced by industry, cloning IF genes into expression vectors is certainly feasible, and should be far simpler than it is for spider silk genes. IF genes are considerably smaller and far less repetitive than silk genes, and so their stability in conventional expression vectors should not be a problem. Furthermore, one of the major problems of spinning expressed silk protein into fibres is that it is difficult to keep the proteins in solution. In the past, this was overcome by using harsh and environmentally "unfriendly" solvents such as hexafluoroisopropanol (HFIP) (Fahnestock, 1994), which defeated the purpose of producing environmentally benign artificial silks. Fortunately, recent advances using larger gene inserts have eliminated the need to use solvents such as HFIP (Lazaris et al., 2002). The downside of this approach is that the larger gene inserts can only be handled by mammalian expression systems, precluding the use of cheaper, more conventional bacterial or yeast expression systems.

In contrast to spider silk fibroins, IF proteins are soluble in aqueous solutions and assemble readily into 10 nm filaments in vitro. These 10 nm filaments could represent an important intermediate structural stage that would allow for the spinning of soluble IFs into macroscopic fibres with high axial alignment. Drying and subsequent draw-processing would result in fibres not unlike transformed hagfish slime threads. A further advantage that these fibres have is that they are relatively hydration insensitive. One of the major drawbacks of using spider dragline silk for human uses is that it undergoes a process known as "supercontraction" when wet, in which length may decrease by up to 50% (Work, 1982). In contrast, draw-transformed slime threads exhibit only minor supercontraction on the order of 5-10%. For the above reasons, those interested in the industrial production of environmentally benign, high-performance protein-based fibres should consider the use of hagfish slime IFs or possibly other IFs.

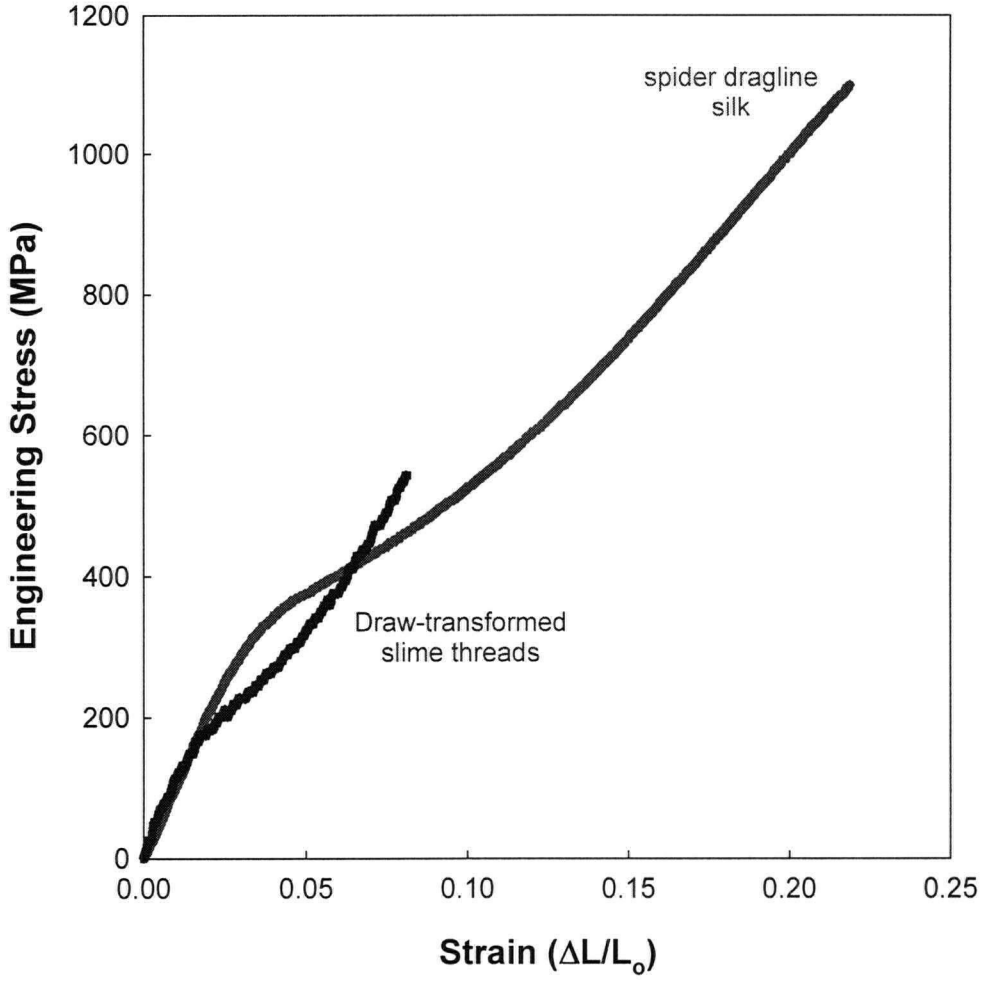

Fig. 5.2. Ultimate mechanics of spider dragline silk and draw-transformed hagfish slime threads tested in air. Although the transformed slime threads are not as strong or tough, they are equally stiff, and may be more amenable to artificial production on an industrial scale.

BIBLIOGRAPHY

Albers, K. and Fuchs, E. (1992). The molecular biology of intermediate filaments. *Int. Rev. Cytol.* 134, 243-79.

Alberts, B., Bray, D., Lewis, J., Raff, M., Roberts, K. and Watson, J. D. (1994). Molecular biology of the cell. New York: Garland, 1294 pp.

Baden, H. P., Goldsmith, L.A., Lee, L. (1974). The importance of understanding the comparative properties of hair and other keratinized tissues in studying disorders of hair. In *The first human hair symposium,* (eds. A. C. Brown), pp. 388-98. New York: Medcom Press.

Baribault, H., Penner, J., Iozzo, R. V. and Wilson, H. M. (1994). Colorectal hyperplasia and inflammation in keratin 8-deficient FVB/N mice. *Genes Dev.* 8, 2964-73.

Baribault, H., Price, J., Miyai, K. and Oshima, R. G. (1993). Mid-gestational lethality in mice lacking keratin 8. *Genes Dev.* 7, 1191-202.

Beckwith, T. G., Marangoni, R. D. and Lienhard, J. H. (1993). Mechanical Measurements. New York: Addison-Wesley, 876 pp.

Bell, E. and Gosline, J. M. (1996).

Bendit, E. G. (1960). A quantitative x-ray diffraction study of the alpha-beta transformation in wool keratin. *Text. Res. J.* 30, 547-55.

Blank, I. H. (1952). Factors which influence the water content of the stratum corneum. *J. Invest. Derm.* 18, 433-9.

Blomfield, J. E. (1882). The thread cells and epidermis of Myxine. *Quart. J. microsc. Sci.* 22, 355-61.

Bousquet, O. and Coulombe, P. A. (1996). Cytoskeleton: missing links found? *Curr. Biol.* 6, 1563-6.

Bousquet, O., Ma, L. L., Yamada, S., Gu, C. H., Idei, T., Takahashi, K., Wirtz, D. and Coulombe, P. A. (2001). The nonhelical tail domain of keratin 14 promotes filament bundling and enhances the mechanical properties of keratin intermediate filaments in vitro. *J. Cell Biol.* 155, 747-53.

Bovenschulte, M., Riemer, D. and Weber, K. (1995). The sequence of a cytoplasmic intermediate filament (IF) protein from the annelid Lumbricus terrestris emphasizes a distinctive feature of protostomic IF proteins. *FEBS Letters* 360, 223-6.

Bray, D. (2001). Cell Movements: From Molecules to Motility. New York: Garland, 372 pp.

Brown, H. G. and Hoh, J. H. (1997). Entropic exclusion by neurofilament sidearms: a mechanism for maintaining interfilament spacing. *Biochemistry* 36, 15035-40.

Carlstedt, I. and Sheehan, J. K. (1989). Structure and macromolecular properties of cervical mucus glycoproteins. In *Mucus and Related Topics,* (eds. E. Chantler and

N. A. Ratcliffe), pp. 289-316. Cambridge, UK: The Company of Biologists Limited.

Chapman, B. M. (1969). A mechanical model for wool and other keratin fibers. *Text. Res. J.* 39, 1102-9.

Colucci-Guyon, E., Portier, M. M., Dunia, I., Paulin, D., Pournin, S. and Babinet, C. (1994). Mice lacking vimentin develop and reproduce without an obvious phenotype. *Cell* 79, 679-94.

Couch. (1878). A History of the Fishes of the British Islandsp. 410 pp.

Cusack, S., Belrhali, H., Bram, A., Burghammer, M., Perrakis, A. and Riekel, C. (1998). Small is beautiful: protein micro-crystallography. *Nature Structural Biology* 5, 634-637.

Darwin, C. (1842). The zoology of the voyage of the H.M.S. Beagle under the command of captain Fitzroy, R.N. during the years 1832-1836. Londonpp.

Denny, M. (1976). The physical properties of spiders silk and their role in the design of orb webs. *J. Exp. Biol.* 65, 483-506.

Denny, M. (1979). The role of mucus in the locomotion and adhesion of the pulmonate slug, Ariolomax columbianus. In *Zoology*. Vancouver: University of British Columbia.

Denny, M. (1989). Invertebrate mucus secretions: functional alternatives to vertebrate paradigms. In *Mucus and Related Topics*, (eds. E. Chantler and N. A. Ratcliffe), pp. 337-66. Cambridge, UK: Company of Biologists Limited.

Downing, S. W., Salo, W. L., Spitzer, R. H. and Koch, E. A. (1981a). The hagfish slime gland: a model system for studying the biology of mucus. *Science* 214, 1143-5.

Downing, S. W., Spitzer, R. H., Koch, E. A. and Salo, W. L. (1984). The hagfish slime gland thread cell. I. A unique cellular system for the study of intermediate filaments and intermediate filament-microtubule interactions. *J. Cell Biol.* 98, 653-69.

Downing, S. W., Spitzer, R. H., Salo, W. L., Downing, S. D., Saidel, L. J. and Koch, E. A. (1981b). Hagfish slime gland thread cells: organization, biochemical features, and length. *Science* 212, 326-27.

Elder, G. A., Friedrich, V. L., Bosco, P., Kang, C., Gourov, A., Tu, P. H., Lee, V. M. and Lazzarini, R. A. (1998). Absence of the mid-sized neurofilament subunit decreases axonal calibes, levels of light neurofilament (NF-L), and neurofilament content. *J. Cell Biol.* 141.

Fahnestock, S. R. (1994). Novel, recombinantly produced spider silk analogs. US Patent #WO 94/29450.

Felgner, H., Frank, R. and Schliwa, M. (1996). Flexural rigidity of microtubules measured with the use of optical tweezers. *J. Cell Sci.* 109, 509-16.

Fernholm, B. (1981). Thread cells from the slime glands of hagfish (Myxinidae). *Acta Zoologica* 62, 137-45.

Ferry, J. D. (1941). A fibrous protein from the slime of the hagfish. *J. Biol. Chem.* 138, 263-68.

Feughelman, M. (1959). A two-phase structure for keratin fibers. *Text. Res. J.* 29, 223-8.

Feughelman, M. (1963). The mechanical properties of permanently set and cystine reduced wool fibers at various relative humidities and the structure of wool. *Text. Res. J.* 33, 1013-22.

Feughelman, M. (1973). Mechanical hysteresis in wool keratin fibers. *J. Macromol. Sci. Phys.* B7, 569-82.

Feughelman, M. (1979). A note on the role of the microfibrils in the mechanical properties of alpha-keratins. *J. Macromol. Sci. Phys.* B16, 155-62.

Feughelman, M. (1987). Keratin. In *Encyclopedia of Polymer Science and Engineering,* vol. 8. New York: Wiley.

Feughelman, M. and Druhala, M. (1976). The lateral mechanical properties of alpha-keratin. In *Proceedings of the 5th International Wool Textile Research Conference Aachen, 1975,* vol. 2, pp. 340-9. Aachen: Deutsches Wollforschungsinstitut.

Fisher, T. E., Oberhauser, A. F., Carrion-Vazquez, M., Marszalek, P. E. and Fernandez, J. M. (1999). The study of protein mechanics with the atomic force microscope. *Trends Biochem. Sci.* 24, 379-84.

Fraser, R. D. and MacRae, T. P. (1973). Conformation in Fibrous Proteins and Related Synthetic Polypeptides. New York: Academic Press, 628 pp.

Fraser, R. D. and MacRae, T. P. (1980). Molecular structure and mechanical properties of keratins. In *The Mechanical Properties of Biological Materials,* (eds. J. F. Vincent and J. D. Currey), pp. 211-46. Cambridge, UK: Cambridge University Press.

Fraser, R. D., MacRae, T. P. and Rogers, G. E. (1972). Keratins: Their Composition, Structure, and Biosynthesis. Springfield, IL: Charles C. Thomas, 304 pp.

Fraser, R. D. B., MacRae, T. P., Sparrow, L. G. and Parry, D. A. D. (1988). Disulphide bonding in alpha-keratin. *Int. J. Biol. Macromol.* 10, 106-12.

Fuchs, E. and Cleveland, D. W. (1998). A structural scaffolding of intermediate filaments in health and disease. *Science* 279, 514-9.

Fudge, D. (2001). Hagfishes: champions of slime. *Nature Australia* 27, 60-9.

Fudge, D., Gosline, J. M. and Guerette, P. A. (2002). Method for the production of high-performance intermediate filament based materials. US patent office, provisional patent #60/356,144.

Geisler, N., Schunemann, J., Weber, K., Haner, M. and Aebi, U. (1998). Assembly and architecture of invertebrate cytoplasmic intermediate filaments reconcile

features of vertebrate cytoplasmic and nuclear lamin-type intermediate filaments. *J. Mol. Biol.* 282, 601-17.

Gennis, R. B. (1989). Biomembranes: Molecular Structure and Function. New York: Springer-Verlag, 533 pp.

Gillespie, J. M. and Frenkel, M. J. (1974). Teh macroheterogeneity of type I tyrosine-rich proteins of Merino wool. *Australian J. of Biol. Sci.* 27, 617-27.

Gittes, F., Mickey, B., Nettleton, J. and Howard, J. (1993). Flexural rigidity of microtubules and actin filaments measured from thermal fluctuations in shape. *J. Cell Biol.* 120, 923-34.

Goode and Beane. (1895). *U.S. Nat. Mus. Spec. Bull.* 3.

Gosline, J. M., Denny, M. W. and DeMont, M. E. (1984). Spider silk as rubber. *Nature* 309, 551-2.

Gosline, J. M., Guerette, P. A., Ortlepp, C. S. and Savage, K. N. (1999). The mechanical design of spider silks: From fibroin sequence to mechanical function. *J. Exp. Biol.* 202, 3295-303.

Gosline, J. M., Pollak, C. C., Guerette, P. A., Cheng, A., DeMont, M. E. and Denny, M. W. (1994). Elastomeric network models for the frame and viscid silks from the orb web of the spider *Araneus diadematus*. In *Silk Polymers*, pp. 329-40. Washington, D.C.: American Chemical Society.

Guerette, P. A., Ginzinger, D. G., Weber, B. H. F. and Gosline, J. M. (1996). Silk properties determined by gland-specific expression of a spider fibroin gene family. *Science* 272, 112-5.

Gum, J. R. (1995). Mucins: their structure and biology. *Biochem. Soc. Trans.* 23, 795-9.

Hearle, J. W. (2000). A critical review of the structural mechanics of wool and hair fibres. *Int. J. Biol. Macromol.* 27, 123-38.

Hearle, J. W. S. (1967). *J. Polymer Science Part C* 20, 215.

Heidemann, S. R., Kaech, S., Buxbaum, R. E. and Matus, A. (1999). Direct observations of the mechanical behaviors of the cytoskeleton in living fibroblasts. *J. Cell Biol.* 145, 109-22.

Heidemann, S. R., Lamoureaux, P. and Buxbaum, R. E. (2000). Opposing views on tensegrity as a structural framework for understanding cell mechanics. *J. Appl. Physiol.* 89, 1670-78.

Heins, S., Wong, P., Muller, S., Goldie, K., Cleveland, D. W. and Aebi, U. (1993). The rod domain of NF-L determines neurofilament architecture, whereas the end domains specify filament assembly and network formation. *J. Cell. Biol.* 123, 1517-33.

Helmke, B. P., Goldman, R. D. and Davies, P. F. (2000). Rapid displacement of vimentin intermediate filaments in living endothelial cells exposed to flow. *Circ. Res.* 86, 745–52.

Henrion, D., Terzi, F., Matrougui, K., Duriez, M., Boulanger, C. M., Colluci, G. E., Babinet, C., Briand, P., Friedlander, G., Poitevin, P. et al. (1997). Impaired flow-induced dilation in mesenteric resistance arteries from mice lacking vimentin. *J. Clin. Invest.* 100, 2909-14.

Hesse, M., Magin, T. M. and Weber, K. (2001). Genes for intermediate filament proteins. *J. Cell Sci.* 114, 2569-2575.

Hofmann, I. and Franke, W. W. (1997). Heterotypic interactions and filament assembly of type I and type II cytokeratins in vitro: Viscometry and determinations of relative affinities. *European Journal of Cell Biology* 72, 122-32.

Hofmann, I., Herrmann, H. and Franke, W. W. (1991). Assembly and structure of calcium-induced thick vimentin filaments. *European Journal of Cell Biology* 56, 328-41.

Hohenadl, M., Storz, T., Kirpal, H., Kroy, K. and Merkel, R. (1999). Desmin filaments studied by quasi-elastic light scattering. *Biophys. J.* 77, 2199-209.

Holmes, K. C., Popp, D., Gebhard, W. and Kabsch, W. (1990). Atomic model of the actin filament. *Nature* 347, 44-9.

Howard, J. (2001). Mechanics of Motor Proteins and the Cytoskeleton. Sunderland, Massachusetts: Sinauer Associates, 367 pp.

Ingber, D. E. (1993). Cellular tensegrity: defining new rules of biological design that govern the cytoskeleton. *J. Cell Sci.* 104, 613-27.

Ingber, D. E. and Jamieson, J. D. (1985). Cells as tensegrity structures: architectural regulation of histodifferentiation by physical forces transduced over basement membrane. In *Gene Expression During Normal and Malignant Differentiation*, (eds. L. C. Anderson G. C. Gahmberg and P. Ekblom), pp. 13-32. Orlando, FL: Academic Press.

Janmey, P. A., Euteneuer, U., Traub, P. and Schliwa, M. (1991). Viscoelastic properties of vimentin compared with other filamentous biopolymer networks. *J. Cell Biol.* 113, 155-60.

Kishino, A. and Yanagida, T. (1988). Force measurements by micromanipulation of a single actin filament by glass needles. *Nature* 334, 74-6.

Kligman, A. M. (1964). The biology of the stratum corneum. In *The Epidermis*, (eds. W. Montagna and W. C. Lobitz), pp. 387-433. New York: Academic Press.

Knight, D. P., Knight, M. M. and Vollrath, F. (2000). Beta transition and stress-induced phase separation in the spinning of spider dragline silk. *Int. J. Biol. Macromol.* 27, 205-10.

Koch, E. A., Spitzer, R. H. and Pithawalla, R. B. (1991a). Structural forms and possible roles of alinged cytoskeletal biopolymers in hagfish (slime eel) mucus. *J. Struct. Biol.* 106, 205-10.

Koch, E. A., Spitzer, R. H., Pithawalla, R. B., Castillos, F. A., 3rd and Parry, D. A. (1995). Hagfish biopolymer: a type I/type II homologue of epidermal keratin intermediate filaments. *Int. J. Biol. Macromol.* 17, 283-92.

Koch, E. A., Spitzer, R. H., Pithawalla, R. B. and Downing, S. W. (1991b). Keratin-like components of gland thread cells modulate the properties of mucus from hagfish (Eptatretus stouti). *Cell Tissue Res.* 264, 79-86.

Koch, E. A., Spitzer, R. H., Pithawalla, R. B. and Parry, D. A. (1994). An unusual intermediate filament subunit from the cytoskeletal biopolymer released extracellularly into seawater by the primitive hagfish (*Eptatretus stoutii*). *J. Cell Sci.* 107, 3133-44.

Kojima, H., Ishijima, A. and Yanagida, T. (1994). Direct measurement of stiffness of single actin filaments with and without tropomyosin by in vitro nanomanipulation. *PNAS USA* 91, 12962-6.

Kolliker, A. (1860). Myxinoiden und die Epidermis der Neunaugen. *Wurzburg. naturwiss. Zeitschr.* 1, 1-10.

Kreplak, L., Doucet, J. and Briki, F. (2001a). Unraveling double stranded alpha-helical coiled coils: An x-ray diffraction study on hard alpha-keratin fibers. *Biopolymers* 58, 526-33.

Kreplak, L., Franbourg, A., Briki, F., Leroy, F., Dalle, D. and Doucet, J. (2002). A new deformation model of hard alpha-keratin fibers at the nanometer scale: implications for hard alpha-keratin intermediate filament mechanical properties. *Biophys. J.* 82, 2265-74.

Kreplak, L., Merigoux, C., Briki, F., Flot, D. and Doucet, J. (2001b). Investigation of human hair cuticle structure by microdiffraction: direct observation of cell membrane complex swelling. *Biochimica Et Biophysica Acta-Protein Structure and Molecular Enzymology* 1547, 268-274.

Kurachi, M., Hoshi, M. and Tashiro, H. (1995). Buckling of a single microtubule by optical trapping forces: direct measurement of microtubule rigidity. *Cell Motil. Cytoskel.* 30, 221-8.

Langbein, L., Rogers, M. A., Winter, H., Praetzel, S., Beckhaus, U., Rackwitz, H. R. and Schweitzer, J. (1999). The cataolog of human hair keratins. I. expression of the nine type I members in the hair follicle. *J. Biol. Chem.* 274, 19874-84.

Lazarides, E. (1980). Intermediate filaments as mechanical integrators of cellular space. *Nature* 283, 249-56.

Lazaris, A., Arcidiacono, S., Huang, Y., Zhou, J. F., Duguay, F., Chretien, N., Welsh, E. A., Soares, J. W. and Karatzas, C. N. (2002). Spider silk fibers spun from soluble recombinant silk produced in mammalian cells. *Science* 295, 472-76.

Li, Z., Colluci, G. E., Pincon, R. M., Mericskay, M., Pournin, S., Paulin, D. and Babinet, C. (1996). Cardiovascular lesions and skeletal myopathy in mice lacking desmin. *Dev. Biol.* 175, 362-66.

Lillie, M. A. and Gosline, J. M. (2002). The viscoelastic basis for the tensile strength of elastin. *Int. J. Biol. Macromol.* 30, 119-27.

Luchtel, D. L., Martin, A. W. and Deyrup-Olson, I. (1991). Ultrastructure and permeability characteristics of the membranes of mucous granules of the hagfish. *Tissue & Cell* 23, 939-48.

Luke, G. N. and Holland, P. W. (1999). Amphioxus type I keratin cDNA and the evolution of intermediate filament genes. *J. Exp. Zool.* 285, 50-6.

Ma, L., Xu, J., Coulombe, P. A. and Wirtz, D. (1999). Keratin filament suspensions show unique micromechanical properties. *J. Biol. Chem.* 274, 19145-51.

Magin, T. M., Hesse, M. and Schroder, R. (2000). Novel insights into intermediate-filament function from studies of transgenic and knockout mice. *Protoplasma* 211, 140-50.

Maniotis, A. J., Chen, C. S. and Ingber, D. E. (1997). Demonstration of mechanical connections between integrins, cytoskeletal filaments, and nucleoplasm that stabilize nuclear structure. *PNAS USA* 94, 849-54.

Martini, F. H. (1998). The ecology of hagfishes. In *The Biology of Hagfishes,* (eds. H. Malte), pp. 57-77. New York: Chapman and Hall.

Mistrali, F., Volpin, D., Garibaldo, G. B. and Ciferri, A. (1971). Thermodynamics of elasticity in open systems: Elastin. *Journal of Physical Chemistry* 75, 142-50.

Muecke, N. and Aebi, U. (2002). Characterization of vimentin assembly and filament properties by analytical ultracentrifugation and scanning force microscopy. In *Gordon Conference on Intermediate Filaments*. Roger Williams University.

Muller, J. (1845). Vergleichende Anatomie der Myxinoiden. Untersuchungen uber die Eingeweide der Fische. *Abh. K. Akad. Wissensch. Berlin* 1843, 109-170.

Newby, W. W. (1946). The slime glands and thread cells of the hagfish Polistotrema stouti. *J. Morph.* 78, 397-409.

Nogales, E., Whittaker, M., Milligan, R. A. and Downing, K. H. (1999). High-resolution model of the microtubule. *Cell* 96, 79-88.

Pain, R. H. (1980). The viscoelasticity of mucus: a molecular model. In *The mechanical properties of biological materials,* (eds. J. F. Vincent and J. D. Currey), pp. 359-376. Cambridge, UK: Cambridge University Press.

Park, A. C. and Baddiel, C. B. (1972). Rheology of the stratum corneum: a molecular interpretation of the stress-strain curve. *J. Soc. Cosmet. Chem.* 23, 3-12.

Parry, D. A. and North, A. C. T. (1998). Hard alpha-keratin intermediate filament chains : substructure of the N- and C-terminal domains and the predicted

structure and function of the C-terminal domains of Type I and Type II chains. *J. Struct. Biol.* 122, 67-75.

Parry, D. A. and Steinert, P. M. (1995). Intermediate Filament Structure. New York: Springer-Verlag, 195 pp.

Parry, D. A. and Steinert, P. M. (1999). Intermediate filaments: molecular architecture, assembly, dynamics and polymorphism. *Quart. Rev. Biophys.* 32, 99-187.

Pauling, L. and Corey, R. B. (1950). Two hydrogen-bonded spiral configurations of the polypeptide chain. *J. Am. Chem. Soc.* 72, 5349.

Peters, L. and Woods, H. J. (1955). Protein fibres. In *The Mechanical Properties of Textile Fibres*, (eds. R. Merideth), pp. 151-244. Amsterdam: North Holland Publishing Company.

Pickett-Heaps, J. D., Forer, A. and Spurck, T. (1997). Traction fibre:toward a "tensegral" model of the spindle. *Cell Motil. Cytoskel.* 37, 1-6.

Piggott, M. R. (1980). Load-Bearing Fibre Composites. Toronto: Pergamon Press, 277 pp.

Pollak, C. C. (1991). Mechanical and optical analyses provide a network model for spiral silk from the orb web of the spider *Araneus diadematus*. M.Sc. thesis, Dept. of Zoology, University of British Columbia, Vancouver, BC, Canada, 116 pp.

Pollock, C. M. and Shadwick, R. E. (1994). Allometry of muscle, tendon, and elastic energy storage capacity in mammals. *Am. J. Physiol.* 266, R1022-31.

Porter, R. M., Hutcheson, A. M., Rugg, E. L., Quinlan, R. A. and Lane, E. B. (1998). cDNA cloning, expression, and assembly characteristics of mouse keratin 16. *J. Biol. Chem.* 273, 32265-72.

Pough, F. H., Heiser, J. B. and McFarland, W. N. (1989). Vertebrate Life. New York: Macmillan, 904 pp.

Puchtler, H., Waldrop, F. S. and Meloan, S. N. (1985). A review of light, polarization and fluorescence microscopic methods for amyloid. *Appl. Pathol.* 3, 5-17.

Riekel, C., Madsen, B., Knight, D. and Vollrath, F. (2000). X-ray diffraction on spider silk during controlled extrusion under a synchrotron radiation X-ray beam. *Biomacromol.* 1, 622-26.

Salo, W. L., Downing, S. W., Lidinsky, W. A., Gallagher, W. H., Spitzer, R. H. and Koch, E. A. (1983). Fractionation of hagfish slime gland secretions: partial characterization of the mucous vesicle fraction. *Prep. Biochem.* 13, 103-35.

Schreiner, K. E. (1916). Zur Kenntnis der Zellgranula. Untersuchungen uber den feineren Bau der Haut von Myxine glutinosa. *ARch. Mikrosk. Anat. EntwMech.* 87, 79-188.

Sellers, L. A. and Allen, A. (1989). Gastrointestinal mucus gel rheology. In *Mucus and Related Topics*, (eds. E. Chantler and N. A. Ratcliffe), pp. 65-71. Cambridge, UK: Company of Biologists Limited.

Speakman, J. B. (1929). The rigidity of wool and its change with adsorption of water vapour. *Trans.Faraday Soc.* 25, 92.

Spitzer, R. H., Downing, S. W. and Koch, E. A. (1979). Metabolic-morphologic events in the integument of the Pacific hagfish (*Eptatretus stoutii*). *Cell Tissue Res.* 197, 235-55.

Spitzer, R. H., Koch, E. A. and Downing, S. W. (1988). Maturation of hagfish gland thread cells: composition and characterization of intermediate filament polypeptides. *Cell Motil. Cytoskel.* 11, 31-45.

Steen, J. B. and Berg, T. (1966). The gills of two species of hemoglobin-free fishes compared to those of other teleosts, with a note on severe anaemia in an eel. *Comp. Biochem. Physiol.* 18, 517-27.

Steven, A. C. (1990). Intermediate filament structure: diversity, polymporphism, and analogy to myosin. In *Cellular and Molecular Biology of Intermediate Filaments*, (eds. R. D. Goldman and P. M. Steinert), pp. 233-63. New York: Plenum Press.

Strahan, R. (1959). Slime production in *Myxine glutinosa* Linnaeus. *Copeia* 2, 165-166.

Strelkov, S. V., Herrmann, H., Geisler, N., Lustig, A., Ivaninskii, S., Zimbelmann, R., Burkhard, P. and Aebi, U. (2001). Divide-and-conquer crystallographic approach towards an atomic structure of intermediate filaments. *J. Molec. Biol.* 306, 773-81.

Tam, P. Y. and Verdugo, P. (1981). Control of mucus hydration as a Donnan equilibrium process. *Nature* 292, 340-42.

Terzi, F., Henrion, D., Colluci, G. E., Federici, P., Babinet, C., Levy, B. I., Briand, P. and Friedlander, G. (1997). Reduction of renal mass is lethal in mice lacking vimentin: role of endothelin-nitric oxide imbalance. *J. Clin. Invest.* 100, 1520-28.

Trotter, J. A. and Koob, T. J. (1989). Collagen and proteoglycan in a sea-urchin ligament with mutable mechanical properties. *Cell Tissue Res.* 258, 527-39.

Tsuda, Y., Yasutake, H., Ishijima, A. and Yanagida, T. (1996). Torsional rigidity of single actin filaments and actin-actin bond breaking force under torsion measured directly by in vitro micromanipulation. *PNAS USA* 93, 12937-42.

Veerman, E. C., Valentijn-Benz, M. and Nieuw Amerongen, A. V. (1989). Viscosity of human salivary mucins: effect of pH and ionic strength and role of sialic acid. *J. de Biologie Buccale* 17, 297-306.

Vollrath, F. and Knight, D. P. (2001). Liquid crystalline spinning of spider silk. *Nature* 410, 541-8.

Wang, H., Parry, D. A. D., Jones, L. N., Idler, W. W., Marekov, L. N. and Steinert, P. M. (2000a). In vitro assembly and structure of trichocyte keratin intermediate filaments: A novel role for stabilization by disulfide bonding. *J. Cell Biol.* 151, 1459-68.

Wang, J., Karabinos, A., Schunemann, J., Riemer, D. and Weber, K. (2000b). The epidermal intermediate filament proteins of tunicates are distant keratins; a polymerisation-competent hetero coiled coil of the Styela D protein and Xenopus keratin 8. *European Journal of Cell Biology* 79, 478-87.

Wang, N., Naruse, K., Stamenovic, D., Fredberg, J. J., Mijailovich, S. M., Tolic-Norrelykke, I. M., Polte, T., Mannix, R. and Ingber, D. E. (2001). Mechanical behavior in living cells consistent with the tensegrity model. *PNAS USA* 98, 7765-70.

Weber, K. (1999). Evolutionary aspects of IF proteins. In *Guidebook to the Cytoskeletal and Motor Proteins,* (eds. T. Kreis and R. Vale), pp. 291-3. Oxford: Oxford University Press.

Work, R. W. (1982). A physico-chemical study of the supercontraction of spider major ampullate fibers. *Text. Res. J.* 59, 349-56.

Wortmann, F.-J. and Zahn, H. (1994). The stress/strain curve of alpha-keratin fibers and the structure of the intermediate filament. *Text. Res. J.* 64, 737-43.

Yamada, S., Wirtz, D. and Coulombe, P. A. (2002). Pairwise assembly determines the intrinsic potential for self- organization and mechanical properties of keratin filaments. *Mol. Biol. Cell* 13, 382-91.

Zubay, G. L. (1998). Biochemistry. Dubuque, IA: Wm. C. Brown Publishers, 990 pp.